TAMPEREEN TEKNILLINEN YLIOPISTO
TAMPERE UNIVERSITY OF TECHNOLOGY

KAHO

JAN SERVOTTE

THE IMPACT OF A DISTRIBUTED BATTERY ENERGY STORAGE SYSTEM ON TRANSMISSION AND DISTRIBUTION POWER GRIDS

Master of Science Thesis

Examiners: Professor Enrique Acha
The examiners and the topic were approved in the Faculty of Computing and Electrical Engineering Council meeting on 08.05.2013

ABSTRACT

TAMPERE UNIVERSITY OF TECHNOLOGY
Master's Degree Programme in Electrical Energy Engineering
SERVOTTE, JAN: The Impact of a Distributed Battery Energy Storage System on Transmission and Distribution Power Grids
Master of Science Thesis, 81 pages
July 2013
Major: Electrical Energy Engineering
Examiner: Dr. Prof. Enrique Acha
Keywords: Batteries, Voltage Stabilisation, Frequency Stabilisation, Li-ion, Converters, Load Demand Curve, Voltage Support

This thesis reports on an investigation of the impact of battery energy storage systems (BESS) on the voltage and frequency stability of a transmission system. It also explores an application of a BESS into an active distribution system which delves the realm of smart grids.

Power quality and system stability are two major concerns in the transportation and distribution of electrical energy. It has long been recognised that energy storage is a possible way forward to improve on these parameters; but the battery technology and the ancillary power electronics had not been developed sufficiently, until quite recently; to meet such expectations. Current battery energy storage challenges the paradigm of instantaneous usage of electrical energy. Intermittent renewable energy production has the potential to improve the quality and efficiency of energy production.

The thesis gives an explanation of the battery working principles and includes a comparative study of battery technologies and the main advantages and disadvantages of batteries in comparison to other electrochemical energy storage technologies. Besides, the thesis addresses the all-important issue of power electronic converters. Battery converters are responsible for controlling the power exchange between the grid and the BESS. The link between the battery and the DC bus, i.e., DC-DC converter, and the link between the DC bus and the grid, i.e., DC-AC converter, are covered in depth.

It has been found that using a BESS in a transmission system significantly improves frequency stability. The damping of oscillations following a transient event is much improved. The BESS can be seen as additional spinning reserve in the system. On the other hand, when a BESS is applied in an active distribution system, the power, delivered by an intermittent energy source is of much higher quality. In particular, it is shown that the BESS has the potential for turning a part of the distribution system with intermittent generation, self-reliable from the energy perspective.

In brief, the outcome of this thesis shows the positive influence of the BESS in electrical powers grid. Further research is required to develop a more detailed model of the battery which would include battery ageing and temperature dependency.

PREFACE

This Master of Science thesis was written at the Department of Electrical Energy Engineering at Tampere University of Technology (TUT). My supervisor was Professor Enrique Acha.

First of all, I will like to show my sincere gratitude to Professor Enrique Acha for his indispensable guidance and never-ending interest during my research and writing process. His unique personality has made my stay in TUT enjoyable and full of challenges.

I would like to thank my friends, at home and abroad with whom I shared so many amazing moments. I also want to thank my colleagues in TUT - which I actually count among my friends – for the pleasant atmosphere in and outside the university. I would like to thank Luis Castro, in special, for being such an amazing friend and for all his support and sharing ideas during many productive discussions.

I would like to thank TUT for the remarkable hospitality and my home university KAHO Sint-Lieven for giving me all these opportunities.

Most of all, I would like to thank my family for their support and love during the joyful and though moments. I would never have got this far without them.

Table of contents

ABBREVIATIONS AND NOTATION

NOTATION

A	Ampère (unit of current)
B	Exponential zone time constant inverse $(Ah)^{-1}$
δ	Pulse width / duty cycle
E	Output voltage (V)
E_0	Battery constant voltage (V)
f_1	Fundamental frequency (Hz)
$f_{switching}$	Switching frequency (Hz)
i	Battery current (A)
i^*	Filtered current (A)
$it = \int idt$	Actual battery charge (Ah)
K	Polarisation constant (V/(Ah)) or polarisation resistance (Ω)
m_a	Amplitude modulation (-)
m_f	Frequency modulation (-)
Q	Battery capacity (Ah)
Q_{Ah}	Actual battery charge (Ah)
R_{in}	Internal resistance (Ω) (whole document)
R and C	Components of the RC circuit, used in battery models
V	Volts (unit of voltage)
V_{Batt}	Battery voltage (V) (only in Matlab model)
$\hat{V}_{control}$	Peak amplitude of the control signal in a PWM controlled Inverter (V)
$\hat{V}_{triangle}$	Amplitude of the triangular signal in a PWM controlled inverter (V)

ABBREVIATIONS

AC	Alternating Current
BESS	Battery Energy Storage System
CSI	Current Source Inverter
DC	Direct Current
DOD	Depth Of Discharge
HVDC	High Voltage Direct Current
Li-ion	Lithium-ion
LFC	Load Frequency Control
PWM	Pulse Width Modulation

SES	Secondary Energy Storage
SOC	State of Charge
SOH	State of Health
STATCOM	Static Synchronous Compensator
VSI	Voltage Source Inverter
VSC	Voltage Source Converter

1 INTRODUCTION

Energy consumption continues to increase unabated, following on a sustained path with the onset of industrialization in the latter half of the 19th century (*Figure 1. 1*). However, the largest increase (more than 2/3) of the total consumption has taken place in the past 50 years along with most of the energy coming from non-renewable sources, which are of a finite nature. Therefore, there is growing interest in the use of renewable energy.

Most of the energy we consume today comes from the sun, most of it in indirect form, since this has been first stored. There are many ways in which the solar energy is naturally stored at the macro level (organic fuel, wind, water evaporation). This enables energy concentration in huge quantities which we may consume long after it has been stored. Today, oil-based fuel seems to be the most convenient form of energy storage. The storage of oil is relatively easy, cheap and the storage time is in human hands. [1]

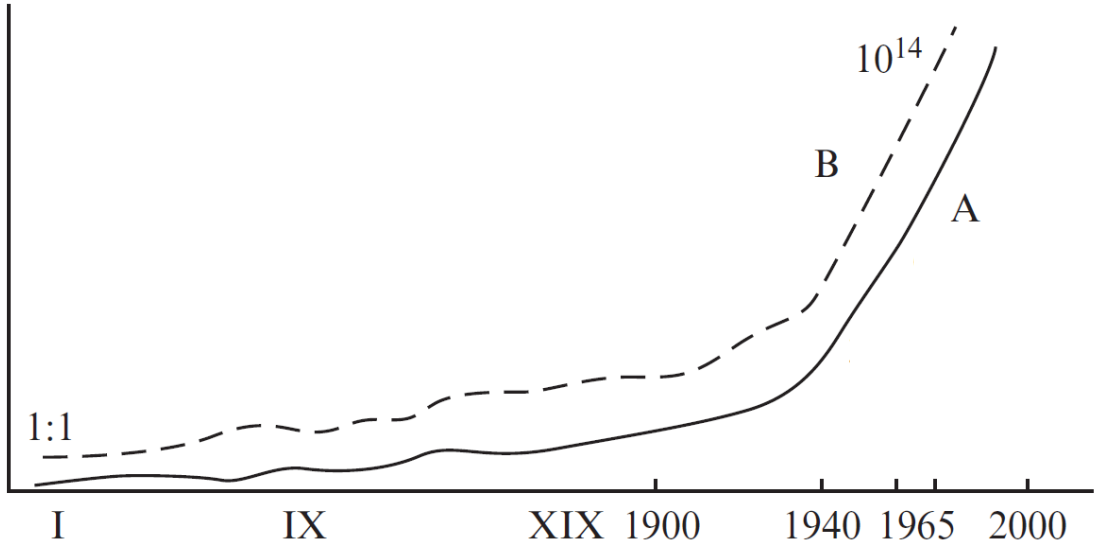

Figure 1. 1. (A): Total amount of energy consumption of humankind is 106 GW. (B): Total amount of stored information is 1014 bits. From prehistoric times to present days [1]

Renewable energy sources are not constant but highly dependent on the time of day, weather conditions and the season. The electrical energy demand is not constant either and its peak, more often than not, takes place at a time of day or season when the renewable energy resources are at their lowest. Owing to this time shift in renewable generation and consumption patterns, energy storage becomes an accentuated necessity.

Transportation of energy is an important part of getting the energy from source to consumer. Oil is a widely used carrier of energy. It is relatively cheap and easy to transport from the refinery to the gas stations.

Electrical energy has some exceptional advantages with respect to other carriers of energy between producers and consumers:

- Electromechanical machinery has existed for more than a century and during its existence the technology has been perfected to be robust and efficient, even though improvements continue to be made. For instance, with the introduction of power electronics, the torque and speed control of these machines has become highly controllable.
- Overhead transmission lines carry electricity at high voltages and underground cables are designed in such a way that power losses, dielectric losses and reflections in the lines are reduced to a minimum.
- It is economically more advantageous to deliver the energy to the end user in electrical form because of its higher quality than when delivered in liquid or solid form. The reason for this is the low efficiency of the Carnot cycle when converting the fuel into mechanical energy.

However, a major drawback of electricity has been our inability to store it in large quantities. Except for the hydro pumped storage that a handful of hydro power stations around the word can provide.

One credible option to overcome such a problem is to store the energy in so-called Secondary Energy Storage systems. This would enable us to store and release energy with low power losses, significantly improving the efficiency of the overall system, because it would flatten the load demand curve [1]. There is not a single best storage option, it all depends on requirements. Important parameters in the storage selection are the amount of power, the energy to be stored and the time scales in which this energy is going to be used.
Figure 1. 2 shows the most frequently used forms of energy storage. It is clear that some of them are more appropriate for delivering large amounts of power for a rather short period of time whereas other forms are more suitable for storing large amounts of energy.

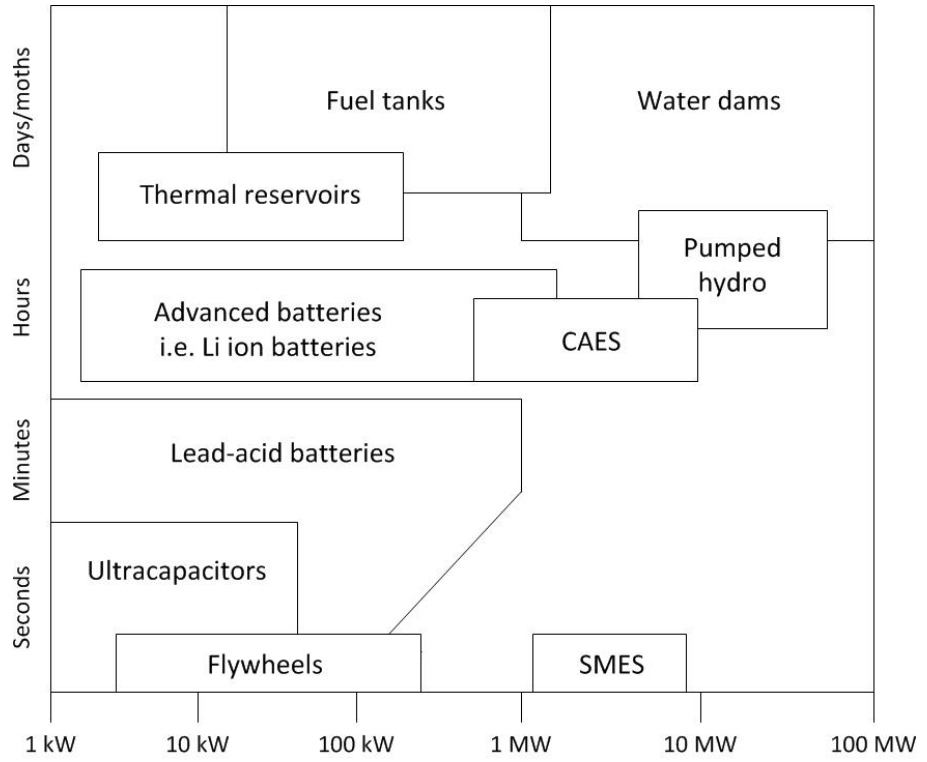

Figure 1. 2. Energy management, power quality and ride-through storage applications [2]

Other parameters that influence the choice of a specific technology are capacity, specific energy, energy density, specific power, efficiency, recharge rate, self- discharge, lifetime, capital cost and operating cost. For more information about the technologies presented in *Figure 1. 2*, read [2].

1.1 State-of-the-art of battery energy storage technology

The combination of a Voltage Source Converter (VSC) with a DC power source results in significant improvements over the traditional Static Synchronous Compensator (STATCOM) technology. The conventional STATCOM is able to control the flow of reactive power by adjusting the amplitude modulation ratio of the converter. *Figure 1. 3*(a) shows the schematic diagram of a STATCOM [3]. When the DC power source to be integrated with the STATCOM, is a battery pack; the arrangement is termed Battery Energy Storage System (BESS), is illustrated schematically in *Figure 1. 3*(b).

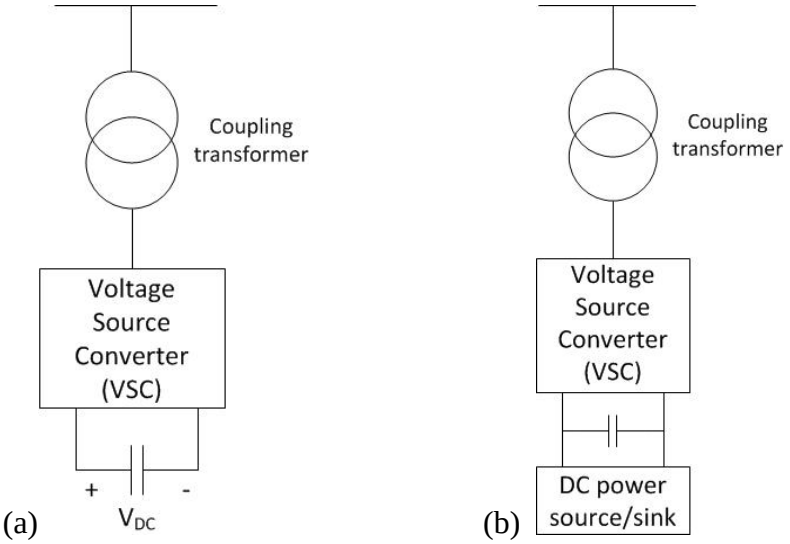

Figure 1. 3. (a) STATCOM connected to a transmission point; (b) Battery Energy Storage System [3]

The lithium-ion battery technology has emerged as a credible response to the growing need for reliable batteries. They were first put in the market by Sony Co. in 1991. Despite its high cost, the lithium-ion battery was accepted immediately because of its high-energy density, good performance and lack of memory effect. *Figure 1. 4* shows the rapid evolution of Li-ion batteries in the short time span of 15 years. It is fair to say that the development of new high-energy lithium systems has been a difficult road. The early rechargeable batteries were plagued with safety problems, such as explosions, occurring during overcharging. These were solved by introducing the Li-Al alloy anode for greater safety in coin cell batteries. However, this was insufficient for the larger AA-size cells. The Tadiran Corporation developed a new battery that solved this problem. The electrolyte spontaneously polymerizes above 100°C which reduces drastically the risk of explosion. [4]

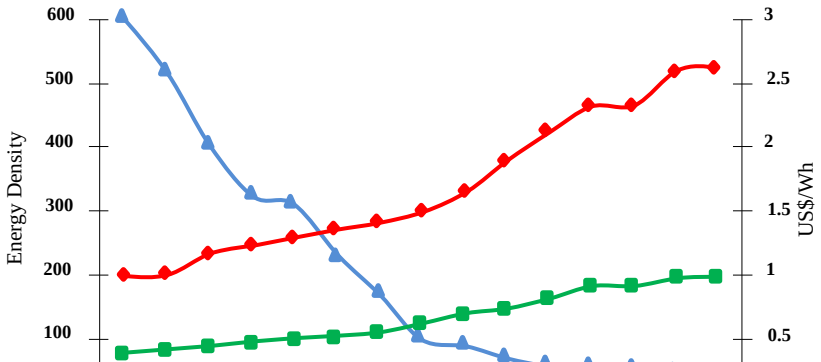

	'91	'92	'93	'94	'95	'96	'97	'98	'99	'00	'01	'02	'03	'04	'05
Wh/l	204	208	250	260	271	281	292	321	343	386	428	471	471	514	514
Wh/kg	88	90	108	113	114	119	123	135	143	159	172	189	189	202	202
US$/Wh	3.17	2.63	2.09	1.75	1.71	1.24	0.95	0.59	0.51	0.42	0.35	0.35	0.33	0.31	0.28

Figure 1. 4. Evolution of energy density and price of Li-ion batteries [5]

The BESS enables controlling the flow of outgoing/incoming active power into the battery and will therefore influence the power system frequency very effectively. [6]
Chile [7] and California [8] are two places where Battery Energy Storage facilities have been installed in recent years. The primary function of the BESS in California is to maintain the critical process loads during outages resulting from external disturbances to the plant. The BESS is designed to supply critical loads of up to 2.5 MW for one hour. This is the required time to safely shutdown the plant. A secondary function of this system is to extend the spinning reserve of the plant. The battery, instead of the generator, supplies the additional energy. This results in a much flatter load demand curve and therefore a higher efficiency of the overall plant. Reference [8] describes the converter and the battery system. PG&E has announced plans to install a second energy storage system in California. [9] The storage system in Chile integrates 20MW of advanced battery energy storage with a 544MW thermal plant. It is the second BESS built by the AES Corporation. The main purpose of this BESS is to increase the capacity of the plants while maintaining system reliability and operational flexibility. The spinning reserve is increased and the efficiency of the plant improved. This system was built and commissioned in only fifteen months and provides very quick operational responses.

1.2 State-of-the-art of battery energy storage for modelling and simulation

To carry out simulations, a suitable battery model needs to be available. This thesis uses the battery model given in Simulink [10], which has got similar functionality to several other models [11, 12]. Even though Simulink offers a high quality model for simulation of the battery dynamics, it still lacks some important modelling capabilities, such as temperature dependency and battery ageing. This is an on-going area of timely research and much more sophisticated models are likely to emerge over the coming years, but the following papers present battery models which may give more advanced alternatives to the model offered by Simulink:

M. Einhorn, F. V. Conte, C. Kral and J. Fleig, "Comparison, Selection, and Parameterization of Electrical Battery Models for Automotive Applications," *Power Electronics, IEEE Transactions On,* vol. 28, pp. 1429-1437, 2013.

T. Huria, M. Ceraolo, J. Gazzarri and R. Jackey, "High fidelity electrical model with thermal dependence for characterization and simulation of high power lithium battery cells," in *Electric Vehicle Conference (IEVC), 2012 IEEE International,* 2012, pp. 1-8.

H. Beltran, M. Swierczynski, N. Aparicio, E. Belenguer, R. Teodorescu and P. Rodriguez, "Lithium ion batteries ageing analysis when used in a PV power plant," in *Industrial Electronics (ISIE), 2012 IEEE International Symposium On,* 2012, pp. 1604-1609.

Nevertheless, for the application pursued in this thesis, the Simulink model was considered to be accurate enough since the influence of Battery ageing and temperature de-

pendency is likely to have little impact as simulation times are barely longer than one minute. Other recent pieces of work where state-of-the-art research on battery modelling and simulation are characterized, are:

L. Gauchía Babé, "Nonlinear dynamic per-unit models for electrochemical energy systems : application to a hardware-in-the-loop hybrid simulation," PhD thesis, Universidad Carlos III de Madrid, Madrid, Spain, 2009.

K. Bao, "Battery charge and discharge control for energy management in EDV and utility integration," MSc thesis, University of Alabama, Tuscaloosa, USA, 2012.

The second major component of the storage system is the DC-DC converter. This converter controls the active power flow between the batteries and the grid. DC-DC converters a commonly used tool for charging batteries as it is easy to control the terminal voltage by adjusting the duty cycle. There is a great deal of well-established research work in this area but some new interpretation of its operation has come to light during the course of this research. This is elucidated in Section 4.3.

The third major element is the voltage source converter, which is the link between the DC-bus and the grid. This converter controls the AC Voltage by regulating the reactive power flow.

1.3 Aim and objectives

The main objectives behind the research reported in this thesis are listed below.

- To develop a BESS model in Matlab/Simulink suitable for interfacing with the model of a power transmission system or a distribution system and that can be easily adjusted to meet future requirements.
- To use the BESS model to investigate the problem of frequency oscillations and its amelioration with a BESS.
- To implement the BESS model in an active distribution system with distributed generation in the form of wind mills, to make the downstream part of the system self-reliant in terms of its energy requirements.

1.4 Publications

The following journal publications have been generated with the outcome of the original research reported in this MSc thesis:

J. Servotte, E. Acha and L. M. Castro, "An Application of BESS to Frequency Control In Power Transmission Systems," Submitted to IEEE Transactions on Power Systems, July 2013

J. Servotte, E. Acha and L. M. Castro, "Assessing the Impact of a BESS in an Active Distribution System with Distributed Wind Turbines," Submitted to IEEE Transactions on Smart Grids, July 2013

1.5 Thesis outline

This thesis consists of four chapters. Chapters 2 and chapter 3 discuss the various elements that make up the BESS. Chapter 2 discusses the main parameters of the batteries, such as Sate-of-Charge, terminal voltage, chemical processes, battery ageing and models. The emphasis in Chapter 3 is on power electronic converters. First, the different types of DC-DC converters and their characteristics are introduced and compared. The second part of chapters deals with VSC and PWM as a method to control the output voltage. Chapter 4 discusses the BESS representation adopted in this work and gives a deeper explanation of the control system. Chapter 5 presents simulation results of two distinct BESS-upgraded power systems. One is in a high voltage transmission system and the other is an active distribution system. The thesis is summarized in Chapter 7.

2 ELECTROCHEMICAL BATTERIES

Arguably, batteries may be considered among the first controlled sources of electricity which were able to store energy. They may be considered to be fuel cells where the fuel is stored inside the cell, hence, the amount of stored energy is limited. Efforts are being made all the time to develop batteries with a higher performance, a higher energy density and a longer battery life. [13]

The most important properties of a battery are: capacity, terminal voltage, State-Of-Health (SOH) and State-Of-Charge (SOC). Different techniques of obtaining these parameters through measurements are explained in [14].

The main characteristics of the most popular battery cells are shown in *Table 2. 1*. This reference also states that the research goals for high-power batteries set in 1977 have been reached, except for the high-energy density cells.

Table 2. 1.Characteristics of selected batteries and comparison with 1977 development goals [13]

Type	Electro-lyte	Energy efficien-cy	Energy density	Power-densities		Cycle life	Operating tempera-tures
				Peak	Sustained		
		(%)	**(Wh kg^{-1})**	**(W kg^{-1})**	**(W kg^{-1})**	**(cycles)**	**(°C)**
Commercial							
Lead-acid	H_2SO_4	75	20-35	120	25	200-2000	-20 to 60
Nickel-cadmium	KOH	60	40-60	300	140	500-2000	-40 to 60
Ni-metal-hydride	KOH	50	60-80	440	220	<3000	10 to 50
Lithium-ion	$LiPF_6$	70	100-200	720	360	500-2000	-20 to 60
Under development							
Sodium-sulphur	β-Al_2O_3	70	120	240	120	2000	300 to 400
Lithium-sulphide	AIN	75	130	200	140	200	430 to 500
Zinc-chlorine	$ZnCl_2$	65	120	100			0
Lithium-polymer	Li- β-Alu	70	200			>1200	-20 to 60
1977 goal cells							
High energy		65	265		55-100	2500	
High power		70	60	280	140	1000	

2.1 Electrochemical principles

Batteries rely on chemical principles to store energy. While discharging, a chemical reaction that converts the chemical energy into electrical energy, in the form of an electric current occurs; this takes place at a certain voltage. In some cases, the process can be reversed, and the batteries able to do so are the so-called secondary batteries. Because of this property, secondary batteries are genuine storage systems, whereas primary batteries can convert their chemical energy into electric energy only once. [15]

2.1.1 Electrochemical cells and battery components

Like fuels cells and ultra-capacitors, batteries are electrochemical systems. However, the difference between them is very significant. For one, the difference lies in the way the reactant is supplied to the system. Batteries are, in contrast to fuel cells, closed systems. So, the amount of energy, that they can deliver, is limited. Conversely, under a constant supply of hydrogen to the anode and oxygen to the cathode, fuel cells can deliver electric energy for an indefinite period of time, assuming the fuel cell remains healthy. [14]

The main difference between batteries and capacitors is the way the energy is stored. In batteries the energy is stored as chemical energy, whereas in capacitors the energy is stored in the form of charges that are placed in an electric field. One of the drawbacks of the small separation between the capacitor electrodes, is the maximum voltage that it can handle, which depends on the dielectric characteristics. [14] Therefore, the energy stored in capacitors and ultra-capacitors is rather limited.

Since there is no need for a constant supply of reactant and the ever increasing levels of stored energy that they can accommodate, the use of bank of batteries for energy storage is becoming more and more popular.

Figure 2.1 shows the main parts of a liquid battery:

A: Valve to evacuate gasses which may be produced during overcharging
B: Battery case
C: Positive and negative terminals
D: Connector between plates to terminal
E: Positive top plate
F: Positive and negative plates
G: Top sealing
H: Negative top plate
I: Plate separating material
J: Plate separator (separates the positive and negative plates)
K: Positive and negative plates

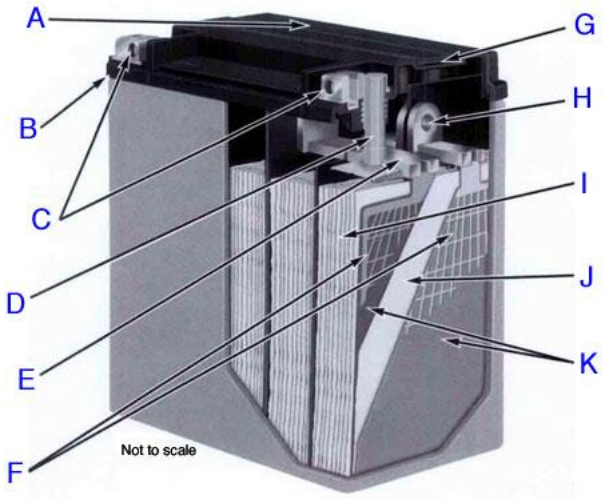

Figure 2.1. Parts of a commercial battery [14]

2.1.2 Chemical reactions during the charging and discharging cycles

When the battery cell is connected to an external load, electrons flow from anode to cathode. This causes the anode to be oxidized and the cathode to be reduced. The electric circuit is closed by the flow of ions in the electrolyte. The positive ions (cations) flow from anode to cathode and the negative ions (anions) in the opposite direction. [16] This operation of discharging is shown in *Figure 2. 2*.

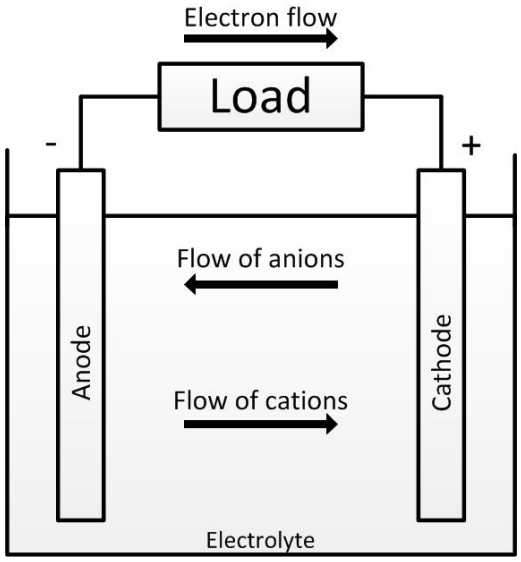

Figure 2. 2. Electrochemical operation of a cell (discharge)

The chemical reactions that take place in a battery during the exchange of power with either a load or a power supply can be illustrated with the example a lead-acid battery. This is a rechargeable system, so the reactions can go in either direction.

In the electrolyte of a lead-acid battery, the following three reactions take place:

$$H_2O \leftrightarrow H^+ + OH^-$$
$$H_2SO_4 \leftrightarrow 2H^+ + SO_4^{2-}$$
$$H_2SO_4 \leftrightarrow H^+ + HSO_4^- \quad (2.1)$$

These reactions involve ionisation of water and sulphuric acid.

The reactions differ for the positive and the negative electrode.

- Positive electrode:

$$PbO_2 + 4H^+ + 2e^- \leftrightarrow Pb^{2+} + 2H_2O \quad (2.2)$$
$$Pb^{2+} + SO_4^{2-} \leftrightarrow PbSO_4 \quad (2.3)$$
Total reaction: $PbO_2 + 4H^+ + 2e^- + SO_4^{2-} \leftrightarrow PbSO_4 + 2H_2O$ (2.4)

- Negative electrode:

$$Pb \leftrightarrow Pb^{2+} + 2e^- \quad (2.5)$$
$$Pb^{2+} + SO_4^{2-} \leftrightarrow PbSO_4 \quad (2.6)$$
Total reaction: $Pb + SO_4^{2-} \leftrightarrow PbSO_4 + 2e^-$ (2.7)

- Overall reaction:

$$Pb + PbO_2 + 2H_2SO_4 \leftrightarrow 2PbSO_4 + 2H_2O \quad (2.8)$$

When the cell discharges, the electrons flow from the anode to the cathode. Charging the cell reverses the process, as illustrated in *Figure 2. 3*.

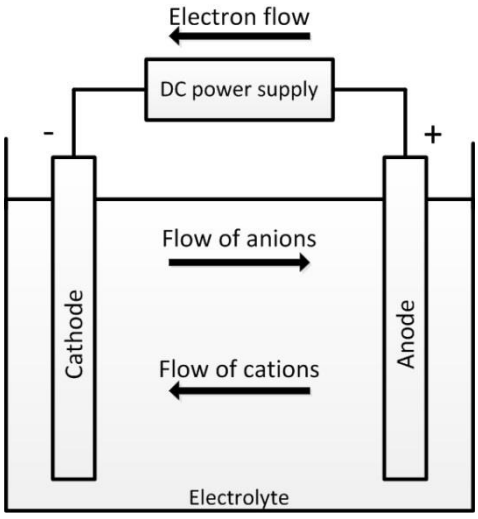

Figure 2. 3. Electrochemical operation of a cell (charge)

2.1.3 Self-discharge

The normal direction in which equations (2.1) to (2.8) apply is in the discharge direction because this is the prevailing stable state. Even when there is no external load connected, there will be some loss of capacity. This phenomenon is called 'self-discharge'. The rate of self-discharging is not constant by any means, it depends on many factors, such as temperature and ageing. [17]
By way of example, the temperature-dependency is shown in *Figure 2. 4.*, which indicates clearly a non-linear behaviour.

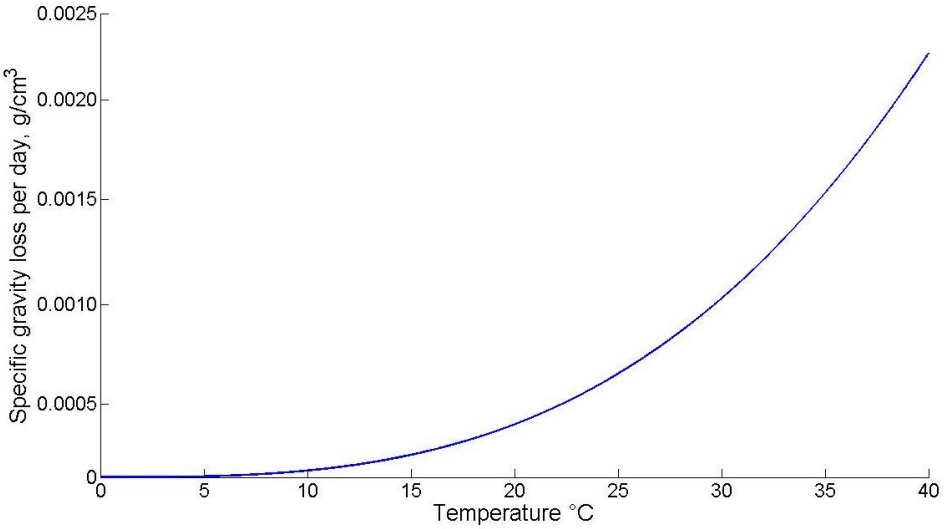

Figure 2. 4. Temperature dependency of self-discharging [17]

The self-discharge rate can be minimized by storing the batteries at lower temperatures. On the other hand, the open-circuit voltage and the capacity of the batteries are affected by temperature; when the temperature is too low, there might be some undesirable effects such as failure of the system due to temporary decrease in battery capacity.

2.2 Battery Parameters

The most accurate approach to model the batteries would be to represent the whole electrochemical response on the external and the internal processes. This approach, however, may be unyielding. Therefore, an approach based on electrical circuit theory is highly popular. This section discusses the main parameters used in the electrical modelling of batteries and the possible techniques to quantify them.

2.2.1 Open-circuit voltage

Open-circuit voltage of the battery is defined as the voltage at its terminals when there is no load or DC source connected to the battery. This equilibrium voltage cannot be exactly measured in most cases, since there is always some self-discharge going on.

One of the parameters that influence the open-circuit voltage is the "Depth of Discharge" (DOD), as shown in *Figure 2. 5*.

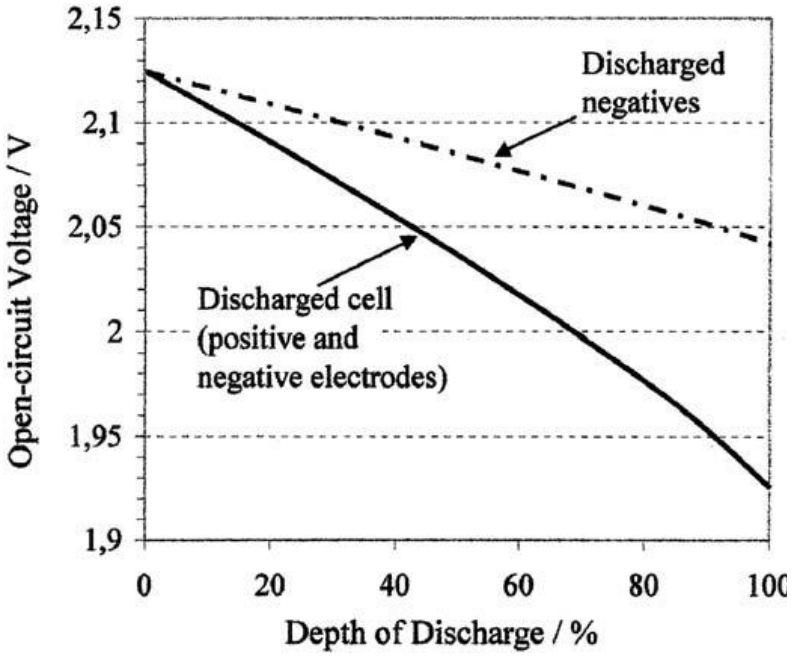

Figure 2. 5. Open circuit voltage as a function of DOD [15]

The open-circuit voltage of lead-acid batteries is used in this figure where the continuous line corresponds to the case when both electrodes are discharged according to Eq. (2.8). The broken line represents the relation when only the negative electrode is discharged according to equation (2.7).
Other factors that influence the open-circuit voltage are the concentration of the electrolytes in the battery (p8.17 in [18]), the system pH, the purity and activity of the cathode material, battery ageing and temperature.

The open-circuit voltage can be used, in some battery systems, as a rough estimation of the SOC (e.g. Lead-acid batteries). [15, 19]

2.2.2 Operating voltage

A key parameter of a battery system is the voltage at which it operates while charging and discharging. The open-circuit voltage represents the equilibrium cell voltage, but during actual use, the operating voltage will differ significantly from this value. This difference is caused by kinetic factors.
The operating voltage has a large influence on the quality of the energy delivered. The power delivered by a source connected to a resistive load is proportional to the square of the voltage; hence, stored energy at a higher voltage is superior to that stored at a lower voltage. [20]
As the operating voltage depends on whether the battery is charged or discharged it is important to discuss these two operating modes of the battery system. One method of presenting this information is in the form of charge and discharge curves, in which the

cell voltage is a function of the SOC. Figure 2. 5 shows the open-circuit voltage as a function of the DOD which for most practical purposes is equivalent to 100% - SOC. [20]

The operating voltage is also influenced by the size of the current density. If the current increases, the voltage decreases, hence, a battery will be able to deliver more energy at lower currents. This is shown in Figure 2. 6.

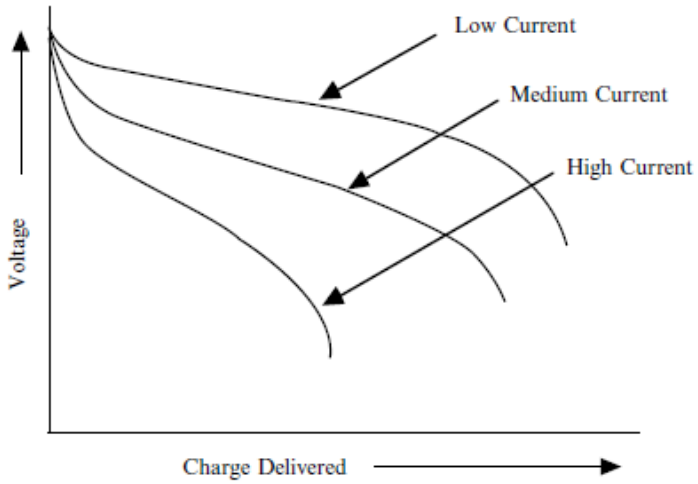

Figure 2. 6. Schematic drawing showing the influence of the current density upon the discharge curve [20]

More detailed information about the charging and discharging characteristics of batteries can be found in [21, 22].

2.2.3 Internal resistance and capacitance

The most commonly used battery models include an internal resistance and one or two RC parallel branches, as shown in *Figure 2. 7.*

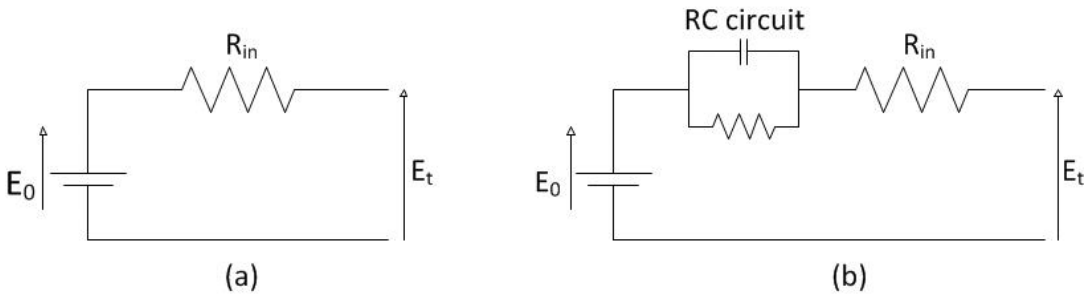

Figure 2. 7. Examples of battery models. (a) is the most basic model, (b) a fuller model

One way to measure these parameters (R_{in}, R and C) is termed the 'Current Interruption Test'. This test is a time domain test in which the (discharging) current is kept stable until the battery reaches a stationary state. Once this has been reached, the load is abruptly interrupted. Notice that this system operates on direct current (DC). After the interruption, the terminal voltage increases until it reaches the open-circuit voltage. The period of returning to the open-circuit voltage can be divided in two parts. At first the

voltage increases vertically and then changes its behaviour to be non-linear, until it reaches the open-circuit voltage. The first part is caused by the ohmic voltage and can be therefore represented by a resistance. The non-linear behaviour may be represented by a chain of capacitors paralleled with a resistance, as shown in *Figure 2. 8*. [14, 23]

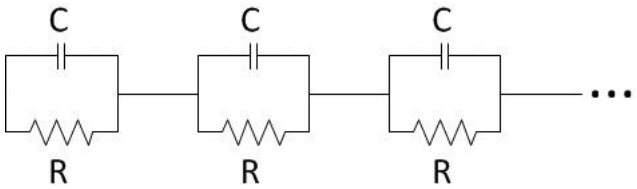

Figure 2. 8. RC chain

This chain simulates the behaviour of the two contact points between the electrolyte and the electrodes. These three parameters (R_{in}, R and C) can be calculated as follows:

$$R_{IN} = \frac{\Delta U_{OHM}}{I} \tag{2.9}$$

$$R = \frac{\Delta U_a}{I} \tag{2.10}$$

$$C = \frac{\tau}{R} \tag{2.11}$$

If this test is carried out with different loads, it is possible to analyse the dependency of the three parameters on current. When this relation is found, an equivalent circuit can be defined as shown in *Figure 2. 7*(b). It is important to keep in mind that E_0, R_{in}, R and C all depend on the SOC and the load current.

This is a straightforward technique to obtain the parameters of the battery, but it has some drawbacks. The first drawback is that it doesn't include all of the battery characteristics, such as the inductive behaviour at higher frequencies and the voltage drop during high load currents. The second drawback is that the precision of the model depends on the point at which the parameters are measured. As discussed, the voltage evolution is not completely linear by any means.

Nonetheless, this technique may still be used quite successfully to model batteries, but it has to be carried out for both the charge and the discharge processes. [14]

2.2.4 Capacity

The capacity of the battery is defined [24] as the electrical charge in units of Ah that can be drawn from the battery:

$$Q_{Ah} = \int_0^t I(t) \cdot dt \tag{2.12}$$

The energy contained in an electrochemical system is the integral of the voltage multiplied by the charge capacity:

$$\text{Energy} = \int E dq \tag{2.13}$$

where E is the output voltage, which is a function of the SOC, the load/charge current and some kinetic parameters and q is the amount of electric charge that can be supplied to the external circuit.

Getting to know the maximum capacity that can be stored in the battery is essential to its good characterization and yet this is not very easy to achieve as the capacity is a function of many parameters, such as temperature, battery health, battery age, etc. [24]

2.2.5 Battery ageing

Battery ageing is the phenomenon which causes the capacity of the battery to reduce most and the internal resistance to increase. Battery ageing is a complex process and it is influenced by many external parameters. The reminder of this section discusses only the most basic points of battery ageing.

One of the major causes of battery ageing in lead-acid batteries is sulphatation. Sulphatation takes place when a battery is kept in a state of low charge for a long time. This causes the lead sulphate, present in the electrodes to form crystals which sink to the bottom of the battery. This process is very difficult to reverse and reduces the concentration of the electrolyte. This concentration affects negatively the voltage and capacity of the battery.

Another phenomenon of battery ageing is corrosion of the electrodes, which increases the internal electric resistance of the battery. Together with corrosion, crystals will be formed on the electrodes, which reduces the battery capacity and reduces the active surface. [14]

Overcharging is a third major cause for capacity reduction. In the case of liquid batteries, gasification may take place. Overcharging means that there is no more lead sulphate on the electrodes to react, as they have already turned into lead or lead oxide. Hydrogen and Oxygen are produced in the positive and negative electrode, respectively. In traditional batteries, these gases leave the battery, causing loss of electrolyte. [14] Due to this phenomenon, batteries may not be suitable for use in closed environments such as mines.

Finally there is a fourth cause for capacity reduction, called ‘Memory effect’. This is not exactly a battery ageing phenomenon, but it can severely reduce capacity. It occurs with nickel-cadmium (Ni-Cd) or nickel-hydride (Ni-MH) batteries when they are partially discharged followed by a charge. By performing this action, some crystals will remain on the cell plate and new crystals will start growing on existing crystals that are already present. Repeating this process will cause the crystals to grow, with the ensuing loss of electrolyte. Hence, the capacity of the battery will drop.
You can find more information about modelling the battery ageing effect in [25].

2.3 Lithium-ion batteries

Since Lithium-ion (Li-ion) batteries were developed, their capacity has almost treble, as indicated in *Figure 2. 9.* You can find more information about this topic in [4].

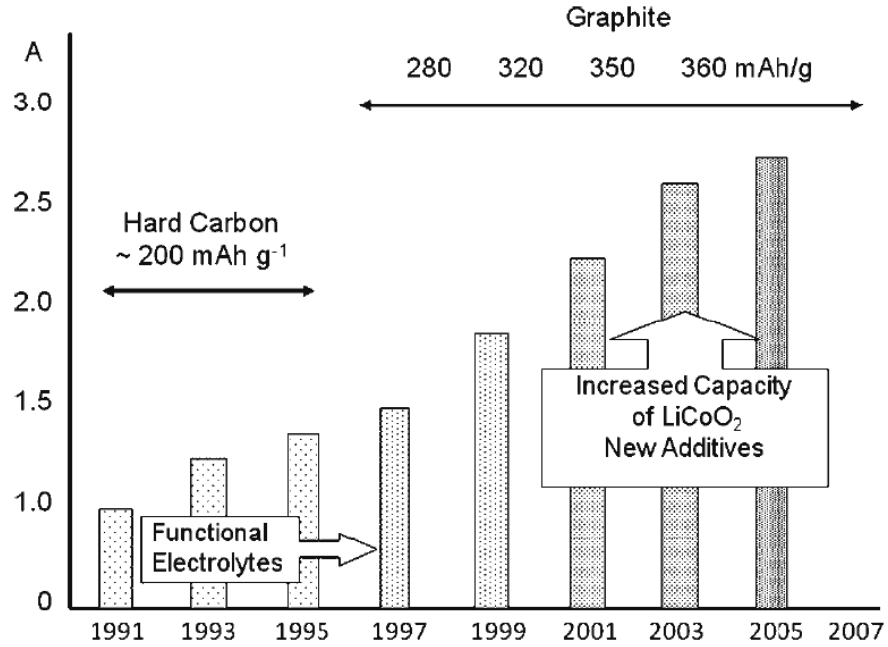

Figure 2. 9. Capacity increase resulting from changes in materials and charging protocol [4]

The higher energy storage capability is a key characteristic of the Li-ion battery system compared to the conventional battery systems. For a given cell size of the Li-ion system, this yields a higher energy density and a higher specific energy. [26] This fact is illustrated in *Figure 2. 10.*

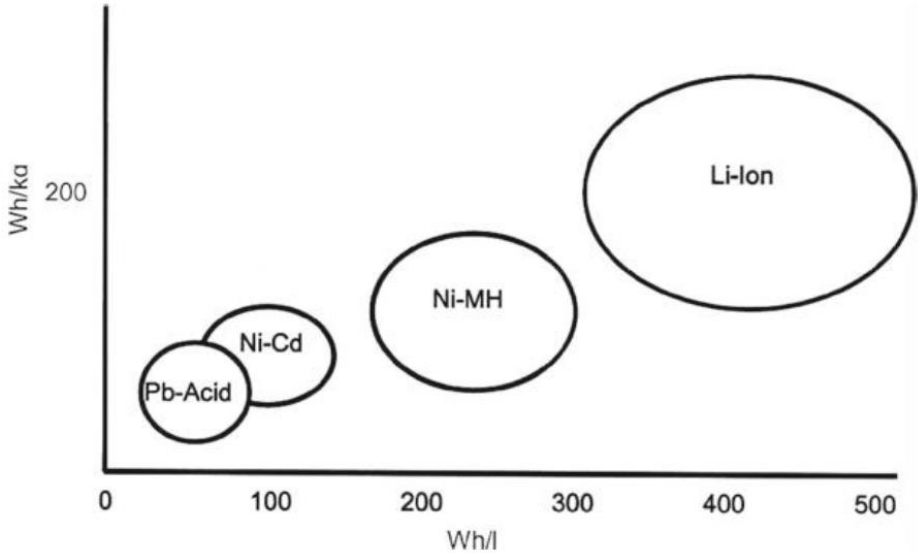

Figure 2. 10. Energy density (Wh/l) and specific energy (Wh/kg) for the major small-sealed rechargeable battery systems [4]

Besides the properties of the Li-ion battery systems, discussed in the previous paragraph, there are also some other trade-offs of Li-ion batteries compared to other systems. They are summarised in *Table 2. 2*.

Table 2. 2. Advantages and disadvantages of Li-ion and Li-ion polymer rechargeable cells [4]

Advantages of Li-ion	Disadvantages of Li-ion
• Chemistry with the highest energy density (Wh/kg) • No memory effect • Good cycle life • High energy efficiency • Good high-rate capability	• Requires protection circuitry for safety and to prevent overcharge and overdischarge • Relatively expensive • Nominal 3h charge • Thermal runaway concerns
Added advantages and disadvantages of Li-ion polymer/laminate cells	
• Flexible footprint • Plasticised electrolyte • Internal bonding of anode, cathode and separator	• Limited high rate capability • Poor low-temperature performance • More expensive

2.3.1 Principle

In a Li-ion cell, both electrodes consist of graphite or other carbon materials. These materials can absorb and emit lithium easily over many cycles. Using a carbon anode, significantly improves the safety, charge rate and ability to recharge many times, but it has the disadvantage of a higher self-discharge rate.[27, 28]

The charging and discharging processes of Li-ion batteries are performed through the transport of Li^+-ions between the anode and cathode. With each ion, there is an electron exchange as a result of doping (when an ion is added) or undoping (extraction). The reactions in this system are quite simple because only Li^+-ions participate in the reactions. For more information about these processes, read [29, 30].

2.3.2 Electrical charge/discharge model (Simulink)

The library of Matlab/Simulink offers a Li-ion battery model. The output voltage of the battery is given by the following equations:

Discharge: $$V_{Batt} = E_0 - R \cdot i - K\frac{Q}{Q-it} \cdot (it + i^*) + A \cdot e^{-B \cdot it} \quad (2.14)$$

Charge: $$V_{Batt} = E_0 - R \cdot i - K\frac{Q}{it-0.1 \cdot Q} \cdot i^* - K\frac{Q}{Q-it} \cdot it + A \cdot e^{-B \cdot it} \quad (2.15)$$

where

V_{Batt} = battery voltage (V)
E_0 = battery constant voltage (V)
K = polarisation constant (V/(Ah)) or polarisation resistance (Ω)
Q = battery capacity (Ah)
it = ∫idt = actual battery charge (Ah)
A = exponential zone amplitude (V)
B = exponential zone time constant inverse $(Ah)^{-1}$
R = internal resistance (Ω)
i = battery current (A)
i^* = filtered current (A)

The designers of this model [10] have made some key assumptions that limit the usefulness of the battery model. Possible improvements to this model could be made to make the assumptions more realistic.

Model assumptions:

- The internal resistance of the battery is independent of the SOC, current or battery health. It is kept constant during the charge and discharge cycles.
- The model's parameters are assumed to be the same for the charging and discharging cycles.
- The temperature has no influence on the model's behaviour.
- The battery has no memory effect.
- The amplitude of the current has no influence on the capacity of the battery.
- The self-discharge rate is assumed to be nil.

Model limitations:

- The minimum open-circuit battery voltage is 0 and the maximum battery voltage is $2 \cdot E_0$.
- The minimum capacity is 0 and the maximum capacity is Q. Therefore the capacity cannot be greater than Q, even if the battery is overcharged.

3 POWER CONVERTERS

Power converters are at the heart of the storage system since they are responsible for controlling the power flow and voltages in the BESS system. The BESS technology employs two power converters, a DC-DC converter and a Pulse-Width Modulated inverter. The former controls the active power flow between the battery and the grid as well as the DC voltage, whereas the latter controls the reactive power injection in order to stabilise the three phase voltage.

3.1 DC-DC converters

DC-DC converters have the purpose to control the average DC output voltage at the desired level in the presence of a fluctuating output load and voltage. Switch-mode DC-DC converters use one or more controlled switches. The control signal of the switches is a pulse train. By changing the pulse width, the average output voltage is kept at the desired level. One of the methods available for controlling the output voltage is switching at a constant frequency. This method is called “Pulse Width Modulation” (PWM) and the time the switch is on, is termed “δ“. [31, 32]

3.1.1 Principles of Pulse Width Modulation

The generated pulse train, which is a saw tooth signal, compared to a reference value, is shown in *Figure 3. 1*. When the reference value is either higher or lower than the instantaneous value of the saw tooth, the output is 1 or 0, respectively. The switch is closed when the output is 1. The switching frequency is controlled by the saw tooth signal and the pulse width is controlled by the reference signal.

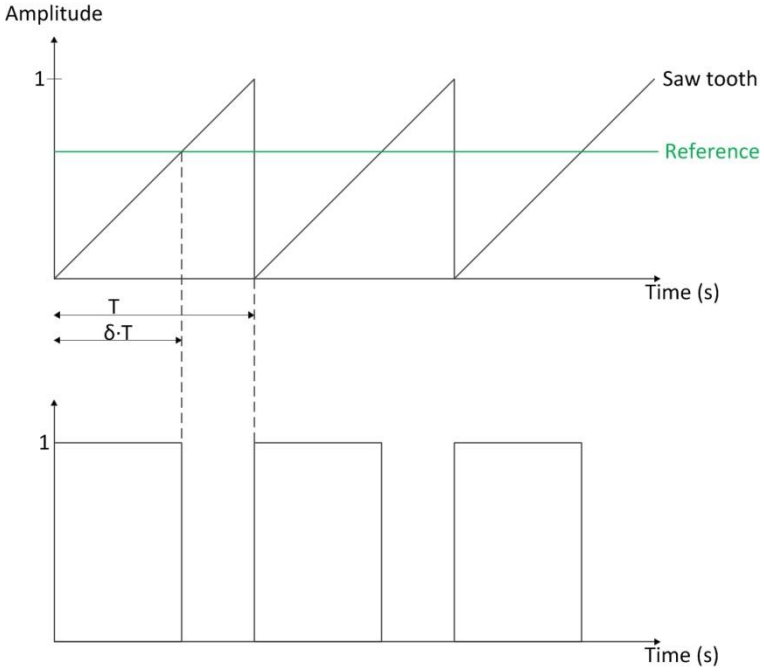

Figure 3. 1. Principles of PWM

3.1.2 Unidirectional vs. Bidirectional converters

Unidirectional converters can only transfer power in one direction. The diode rectifier is an example of this principle. The rectification process converts the current from an AC supply source to a DC form before being supplied to a load. The power can only go from the AC side to the DC side. Other examples are rectifiers consisting of power transistors or thyristors. Possible applications of rectifiers are battery chargers and DC power supplies [33, 34]. The circuit of a three-phase diode rectifier is shown in *Figure 3. 2*.

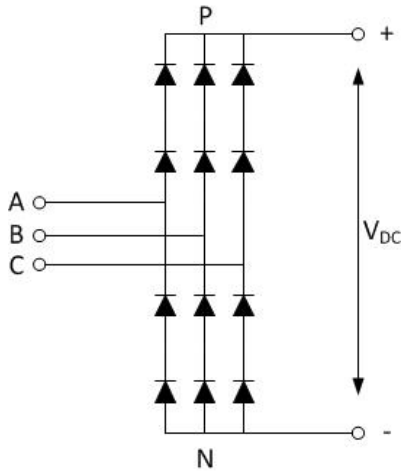

Figure 3. 2. Three-phase diode rectifier [35]

Bidirectional converters have the option of transferring power in both directions. Bidirectional converters use bidirectional switches or multiple unidirectional switches. An example of a bidirectional converter is the bidirectional buck converter. The principles of the buck converter are explained in the section below.

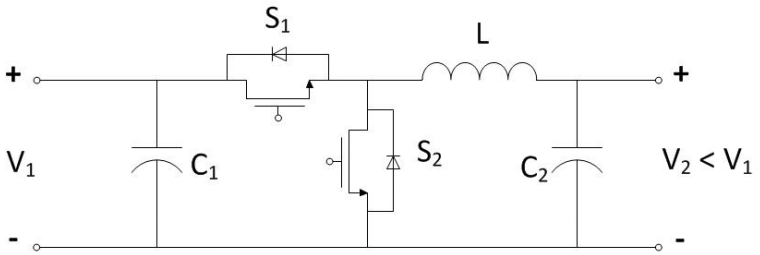

Figure 3. 3. Bidirectional buck converter [36]

In this figure, switch S_1 controls the power flow going from V_1 to V_2. Switch S_2 controls the power flow going from V_2 to V_1. Notice that this configuration does not allow to close S_1 and S_2 at the same time as this would short circuit capacitor C_1, producing terminal damage to the switches and capacitors.

3.1.3 Buck converter

The buck (or Step-Down) converter transforms an input voltage V_1 into an output voltage V_2 which is lower than the input voltage. The basic circuit of the buck converter is shown in *Figure 3. 4.*, where V_1 is the input voltage and V_2 is the output voltage.

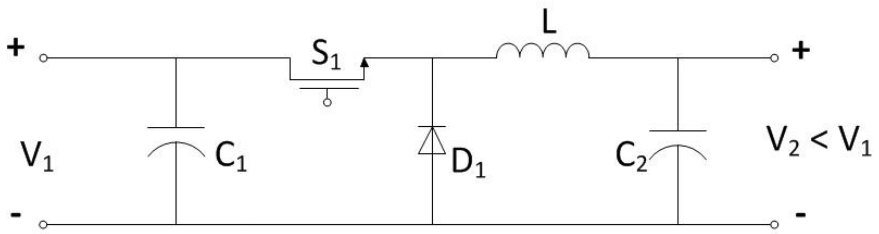

Figure 3. 4. Unidirectional buck converter [37]

The converter in the BESS is used in the continuous mode, which means that the current through the inductance L never drops to zero. Therefore, only the continuous mode will be detailed in this section. More information about the discontinuous mode and the influence of the switches on the controls can be found in [31].

In the continuous mode, there are two sub-modes: the switch is closed or the switch is opened. When the switch is closed and opened, respectively, the circuit diagram is simplified to the representations shown in *Figure 3. 5* (a) and (b).

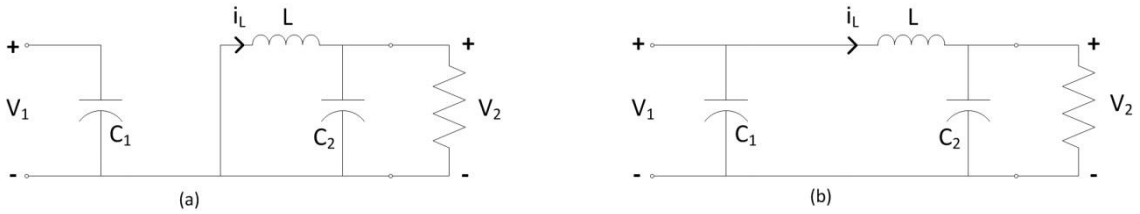

Figure 3. 5. Operating modes of buck converter: (a) switch opened, (b) switch closed

During the time δ·T (closed), the switch conducts the inductor current i_L. As V_1 is larger than V_2, the current i_L increases, governed by equation (3.1):

$$v_L = V_1 - V_2 = L\frac{di_L}{dt} > 0 \tag{3.1}$$

During the time period (1- δ) ·T (opened), the current i_L will not come to zero due to the energy stored in the inductor. The current now flows through diode D_1. The current i_L is now governed by equation (3.2) and will therefore decrease:

$$v_L = 0 - V_2 = L\frac{di_L}{dt} < 0 \tag{3.2}$$

Considering equation (3.1) and (3.2) together and assuming that the capacitor C_2 is very big, the output voltage will have the waveforms shown in *Figure 3. 6.*

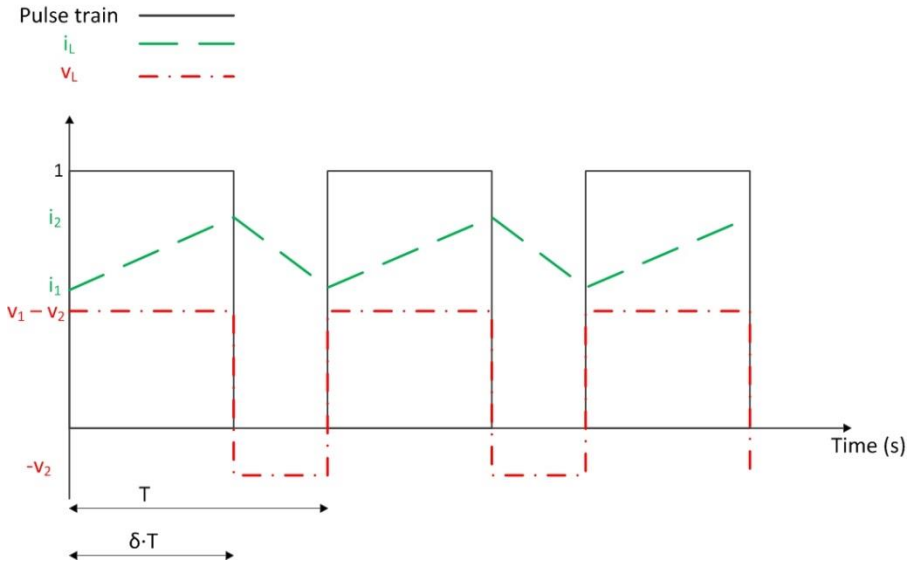

Figure 3. 6. Waveforms in the buck converter

The converter is assumed to operate in periodic steady-state. This means that the absolute value of the change in current during δ·T is the same as the absolute value of the change during (1- δ) ·T:

$$\Delta i^+ = \frac{v_1 - v_2}{L} \cdot \delta \cdot T \tag{3.3}$$

$$\Delta i^- = \frac{-v_2}{L} \cdot (1 - \delta) \cdot T \tag{3.4}$$

$$|\Delta i^+| = |\Delta i^-| \tag{3.5}$$

Combining equations (3.3), (3.4) and (3.5) yields,

$$v_2 = \delta \cdot v_1 \tag{3.6}$$

Equation (3.6) shows that the output voltage v_2 is easily controllable by changing the pulse width. The output voltage is independent of the load. [31, 38, 39]

3.1.4 Buck-boost converter

The principle of a buck-boost converter is similar to that of a buck converter. The main difference is that a buck-boost converter can make the output voltage larger or smaller than the input voltage. *Figure 3. 7.* shows the circuit diagram of a buck-boost converter. Note that the output voltage has a negative polarity with respect to the input voltage. [31]

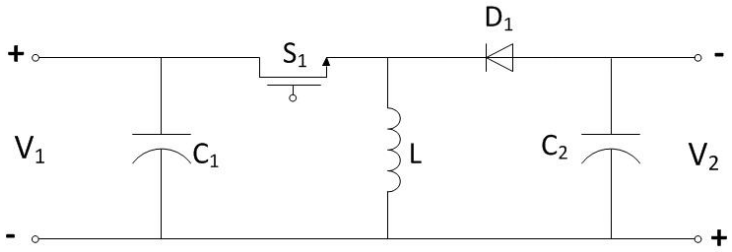

Figure 3. 7. Unidirectional buck-boost converter [31]

While the switch is closed, the current through the inductor increases as the voltage over the inductor is larger than 0:

$$v_L = V_1 = L\frac{di_L}{dt} > 0 \tag{3.7}$$

When the switch is opened, the current through the inductor does not extinguish due to the energy stored in the inductor. Meanwhile the current through the inductor will decrease as the voltage over the inductor is negative:

$$v_L = -V_2 = L\frac{di_L}{dt} < 0 \tag{3.8}$$

The two different operating modes of this converter (switch is opened/closed) are shown in *Figure 3. 8.* [31, 38]

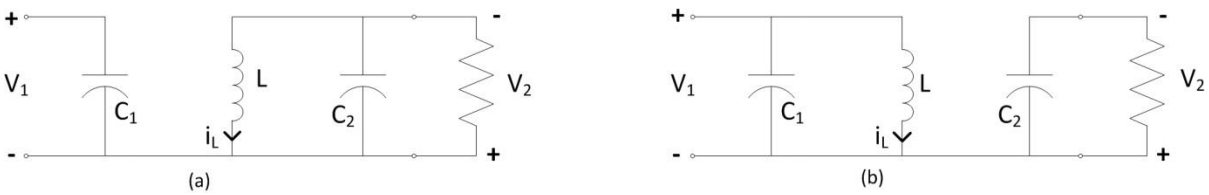

Figure 3. 8. Operating modes of the buck-boost converter: (a) switch opened, (b) switch closed

The converter is assumed to perform in the periodic steady-state. Note that the absolute value of the change in current through the inductor is the same when the switch is closed or opened:

$$\Delta i^{+} = \frac{v_1}{L} \cdot \delta \cdot T \tag{3.9}$$

$$\Delta i^{-} = \frac{-v_2}{L} \cdot (1 - \delta) \cdot T \tag{3.10}$$

$$|\Delta i^{+}| = |\Delta i^{-}| \tag{3.11}$$

Combining equations (3.9), (3.10) and (3.11) yields,

$$v_2 = v_1 \cdot \frac{\delta}{1-\delta} \tag{3.12}$$

The buck-boost converter can work as a boost (step-up) converter or as a buck (step-down) converter, depending on the value of δ:

Buck: $0 < \delta \leq 0.5$
Boost: $0.5 < \delta \leq 1$

3.1.5 Cúk converter

The cúk may be seen as an improved version of the buck-boost converter. Hence, it can also produce an output voltage that is either higher or lower than the input voltage and the output voltage has a negative polarity with respect to the input voltage. The circuit diagram of the cúk converter is shown in *Figure 3. 9*.
The basic function of the capacitor C_2 is to store and transfer the energy from the input to the output of the converter. Similarly to the buck-boost converter, the relationship between the input and the output voltages are governed by equation (3.12).

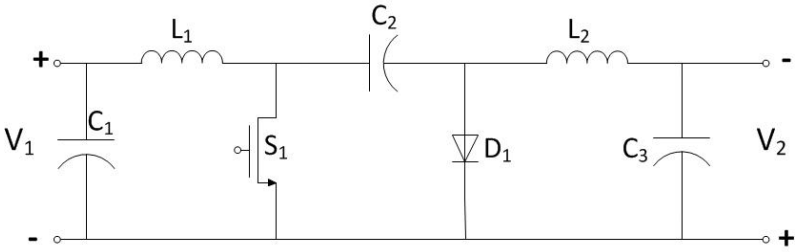

Figure 3. 9. Unidirectional cúk converter

A great advantage of the cúk converter lies on the form of its input and output currents. In the case of a buck-boost converter these currents are highly discontinuous. The cúk converter on the other hand, has a reasonably continuous current profile. This leads to lower external filtering needs.

A significant disadvantage is the need for a larger capacitor C_2 to keep the voltage V_{C2} nearly constant even though it stores and transfers energy from the input to the output. The circuit is also more complicated than the circuit of the buck-boost converter. [31, 38, 39]

3.2 PWM- Controlled Voltage Source Inverter

In order to exchange power between the BESS and the grid a voltage source converter (VSC) is needed. Its primary function is to convert the DC voltage at the output of the DC-DC converter into a three-phase AC voltage. [35] This section addresses PWM-controlled Voltage Source Inverters (VSI). For more information about Current Source Inverters (CSI) and other inverters, the following references [35, 38, 40] are recommended.

3.2.1 Circuit diagram of a single-phase full-bridge inverter

A single-phase full-bridge inverter is shown in *Figure 3. 10*. This inverter comprises two one-leg inverters, which makes it suitable for operation in either unipolar or bipolar switching mode. This is the topic of discussion in the thesis. For cases of half-bridge inverters, the following reference [31] is recommended.

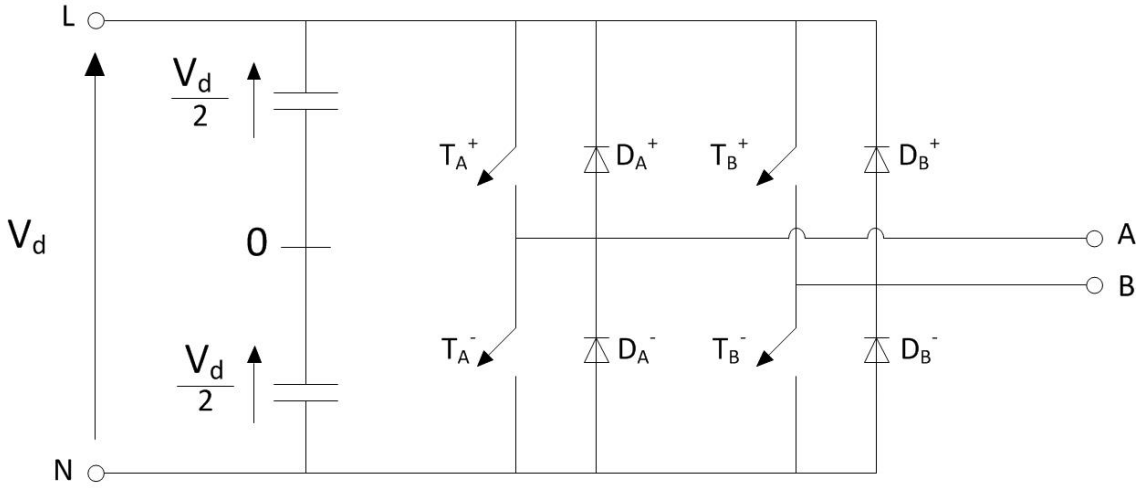

Figure 3. 10. Single-phase full-bridge inverter

The control signals of the switches are realized by a PWM generator. The PWM signal has two main parameters: the frequency modulation ratio m_f and the amplitude modulation ratio m_a. They are defined in equations (3.13) and (3.14)

$$m_a = \frac{\hat{V}_{control}}{\hat{V}_{triangle}} \tag{3.13}$$

$$m_f = \frac{f_{switching}}{f_1} \tag{3.14}$$

where $\hat{V}_{control}$ is the peak amplitude of the control signal and $\hat{V}_{triangle}$ is the amplitude of the triangular signal, which is generally kept constant.
The frequency modulation is calculated as the ratio of the switching frequency $f_{switching}$ and the fundamental frequency of the AC system, f_1. The former is basically the frequency with which the inverter switches are switched. An alternative name for the switching frequency is "carrier frequency". [35]

3.2.2 Harmonic content of the AC-voltage

The harmonic content of the AC-voltage depends on the amplitude and frequency modulation. The use of higher switching frequencies has the significant advantage of filtering harmonic voltages with relative ease. On the other hand, the switching losses in the inverter switches increase rapidly with the increases in the switching frequency f_s.
The influence of the amplitude modulation on the harmonic content is divided into two areas, depending on whether m_a is larger or smaller than 1.

- *Amplitude modulation $m_a \leq 1.0$*

  The harmonic spectrum of the output voltage is shown in *Figure 3. 11*. The harmonics appear as sidebands around the switching frequency and its multiples. In the linear range, the magnitude of the harmonics is independent of m_f. However, it is very important to choose m_f as an odd integer because this results in a harmonic spectrum with odd symmetry as well as in a half-wave symmetry:

  $$f(-t) = -f(t)$$
  $$f(t) = -f(t + \tfrac{1}{2}T_1)$$

  This kind of symmetry has the advantage that the waveform has a harmonic spectrum with no even harmonics. When unipolar switching is performed, the harmonics at the switching frequency and its odd multiples are cancelled out, as presented in *Figure 3. 12*.

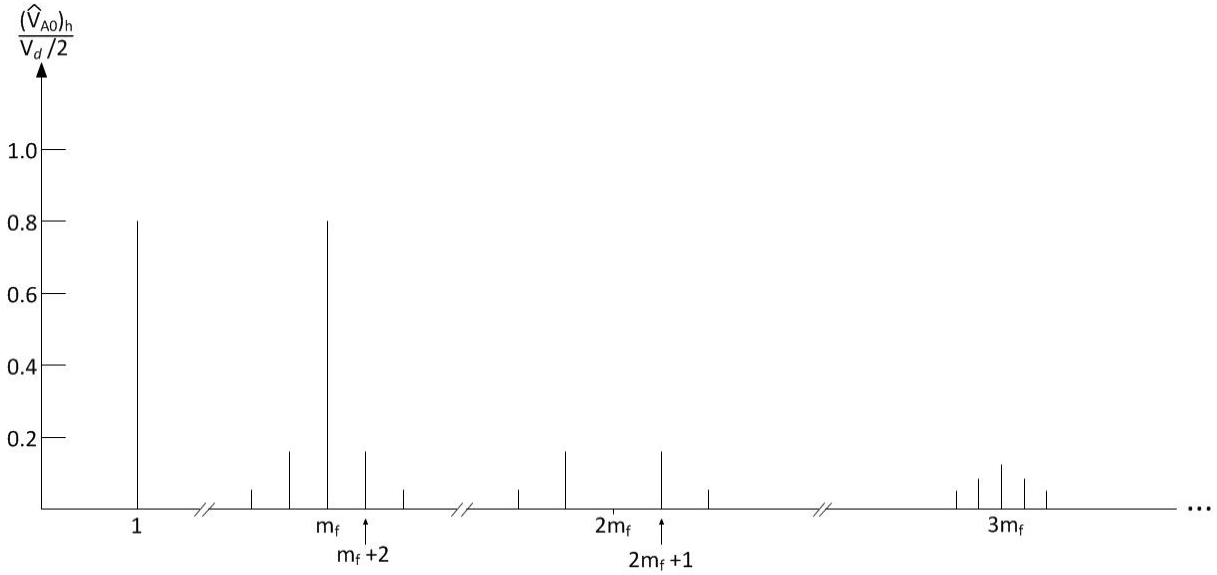

Figure 3. 11. Bipolar switching: Harmonics of f_1 (m_a = 0.8, m_f = 15) [31]

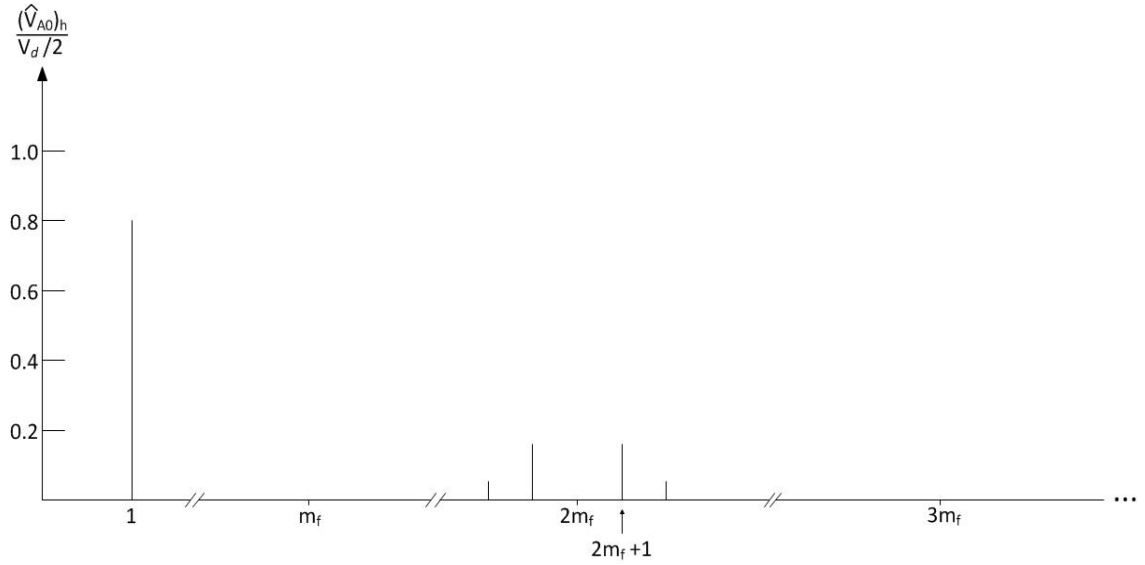

Figure 3. 12. Unipolar switching: Harmonics of f_1 (m_a = 0.8, m_f = 15) [31]

- *Overmodulation (m_a > 1.0)*

  Increasing the amplitude modulation beyond 1.0 is termed "overmodulation". Overmodulation has the advantage that the output voltage can be amplified with respect to the input voltage. However, a major drawback is that the output voltage contains all odd harmonics. The harmonic spectrum of the output voltage is shown in *Figure 3. 13*.

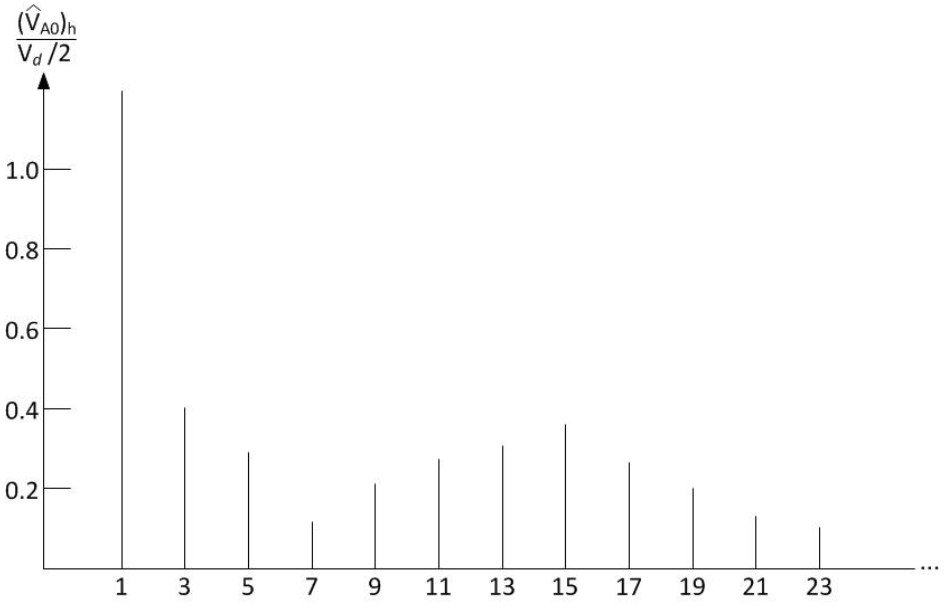

Figure 3. 13. Harmonics due to overmodulation (m_a = 2.5, m_f = 15) [31]

Another drawback of overmodulation is that the magnitude of the fundamental component is not linearly varying with the amplitude modulation ratio as shown in *Figure 3. 14* and, hence, it becomes more difficult to control. At sufficiently large values of m_a, the output voltage turns into a square wave signal. This is the highest attainable output voltage. [31]

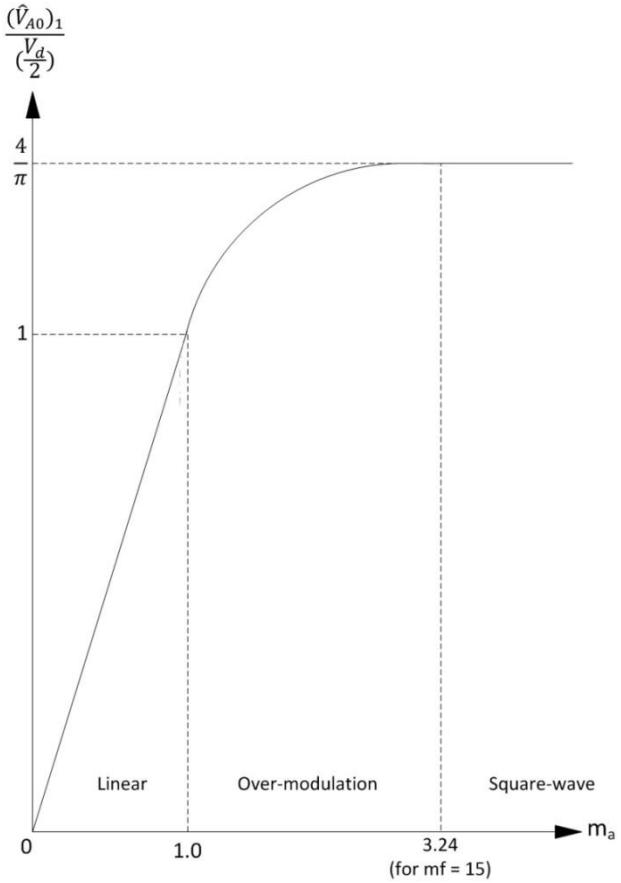

Figure 3. 14. Voltage control by varying m_a [31]

3.2.3 Bipolar switching (single-phase)

Bipolar switching in a full-bridge inverter results in the same output voltage waveform as in the half-bridge inverter. In the former case, the diagonally opposite switches (T_A^+, T_B^-) and (T_A^-, T_B^+) are switching at the same time. The voltage output of inverter leg A is the negative of the voltage output of inverter leg B.

The control signal, triangular signal and the output voltage together with its fundamental frequency waveform are shown in *Figure 3. 15*. [31] In these example figures, m_f equals 15.

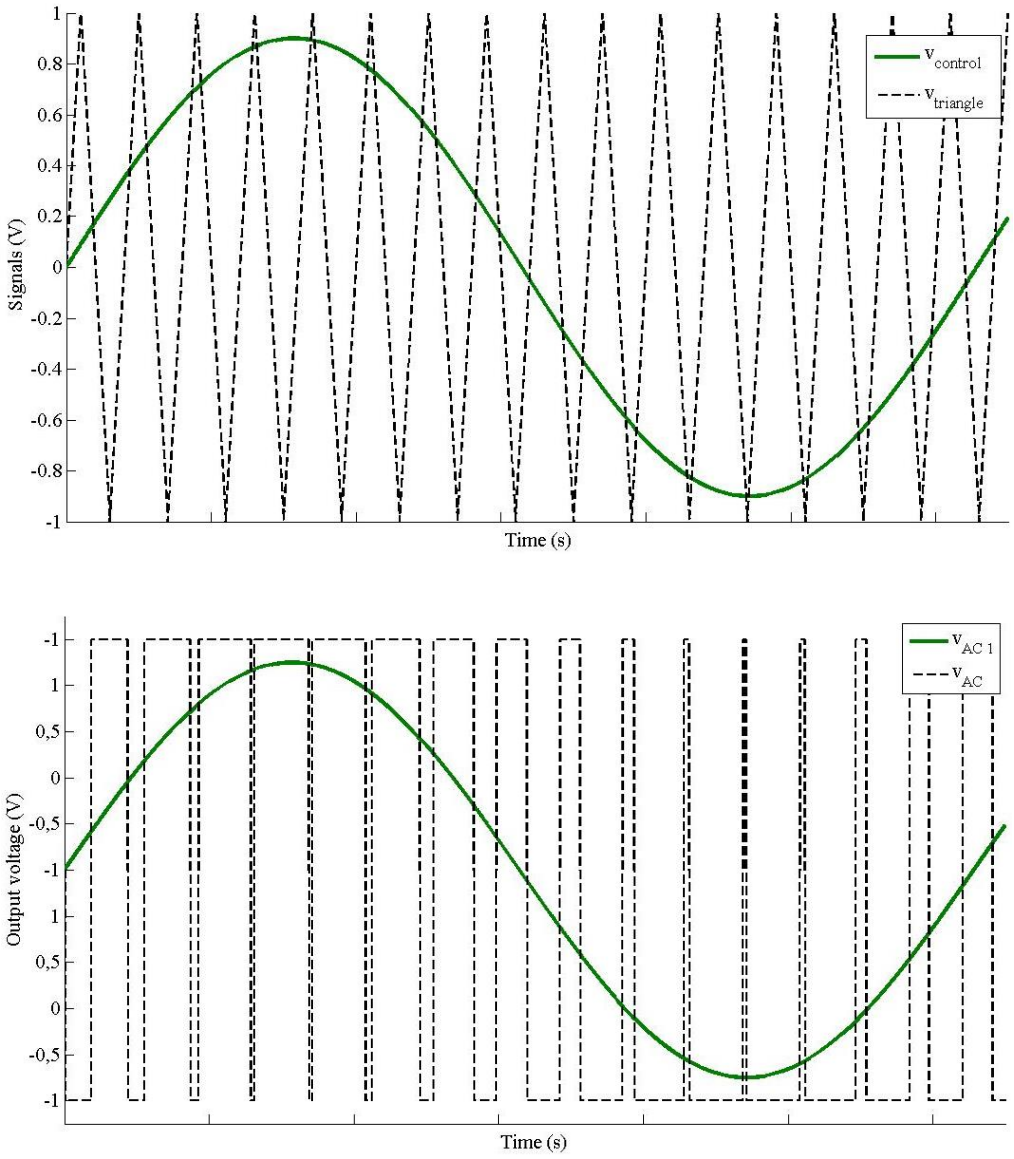

Figure 3. 15. PWM with bipolar voltage switching [31]

The output voltage corresponds to the following equations:

$$v_{out} = V_{dc} \quad \text{for} \quad v_{control} > v_{triangle} \tag{3.15}$$

$$v_{out} = -V_{dc} \quad \text{for} \quad v_{control} < v_{triangle} \tag{3.16}$$

The peak value of the fundamental-frequency component can be obtained from equations (3.17) and (3.18):

$$\hat{V}_{out,1} = m_a V_d \qquad (\text{ma} \leq 1.0) \tag{3.17}$$

$$V_d < \hat{V}_{out,1} < \frac{4}{\pi} V_d \qquad (\text{ma} > 1.0) \tag{3.18}$$

3.2.4 Unipolar switching (single-phase)

Unipolar switching controls the four switches of leg A and B independently by comparing $v_{triangle}$ to $v_{control}$ and $v_{triangle}$ to $-v_{control}$. Refer to *Figure 3. 10* for illustration of a full-bridge inverter.

Comparing $v_{triangle}$ to $v_{control}$ results in the following control signals for leg A:

$$v_{control} > v_{triangle} : T_A^+ \text{ on and } v_{AN} = V_d \tag{3.19}$$

$$v_{control} < v_{triangle} : T_A^- \text{ on and } v_{AN} = 0 \tag{3.20}$$

Comparing $v_{triangle}$ to $-v_{control}$ results in the following control signals for leg B:

$$-v_{control} > v_{triangle} : T_B^+ \text{ on and } v_{BN} = V_d \tag{3.21}$$

$$-v_{control} < v_{triangle} : T_B^- \text{ on and } v_{BN} = 0 \tag{3.22}$$

These signals are shown in *Figure 3. 16.*

The feedback diodes in antiparallel with the switches have the important role to make the foregoing voltages independent of the direction of the load current.
For example, when T_A^+ and T_B^+ are closed at the same time, the output voltage is 0. Depending on the direction of the current, it flows through different switches and diodes:

$$\begin{aligned} &A \rightarrow B: T_A^+ \text{ and } D_B^+ \\ &B \rightarrow A: T_B^+ \text{ and } D_A^+ \end{aligned} \tag{3.23}$$

This type of switching is called unipolar as the output voltage changes between V_d and 0 or $-V_d$ and 0. Conversely, with bipolar switching, the output voltages change between V_d and $-V_d$. [31]

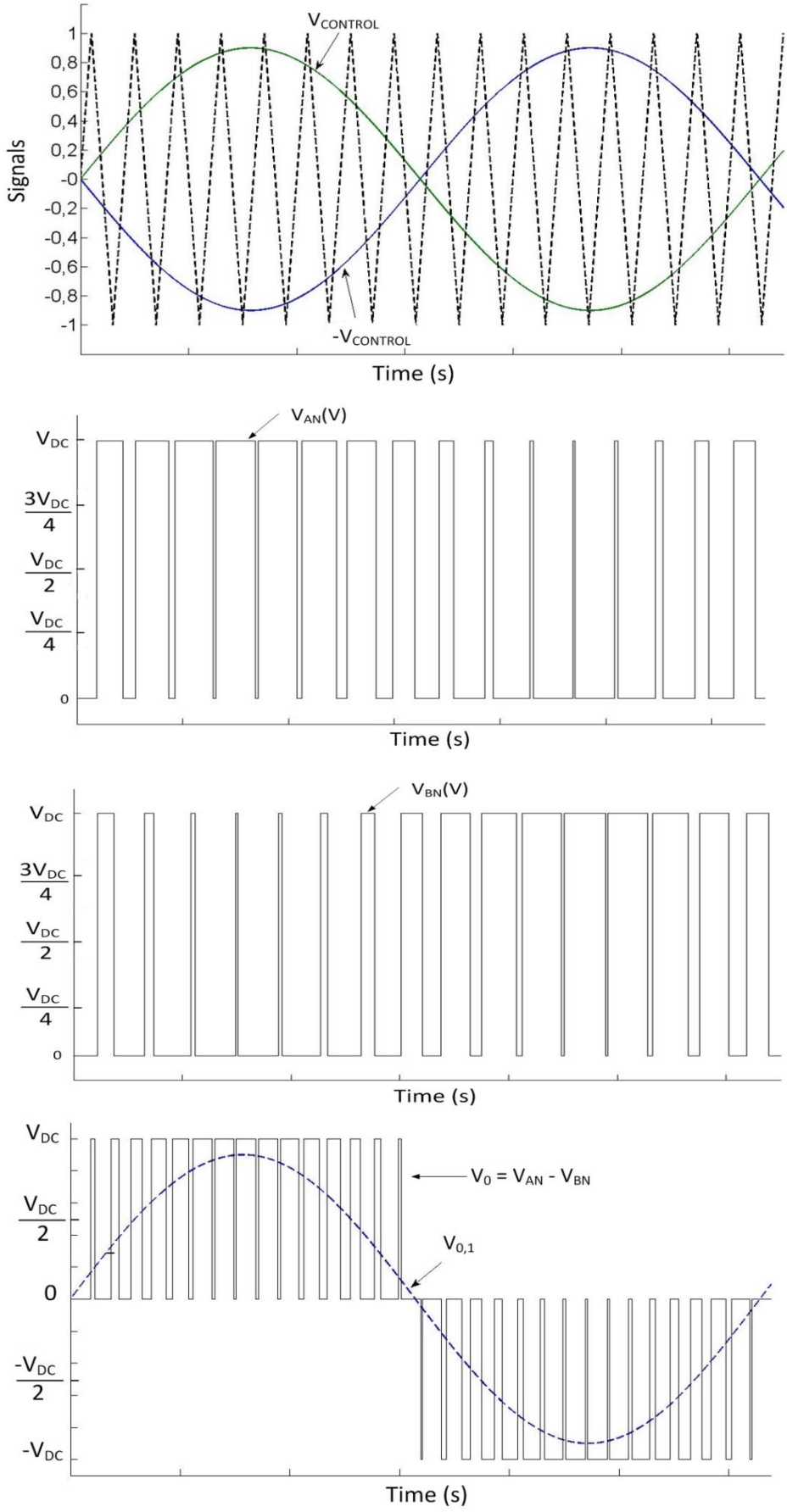

Figure 3. 16. PWM with unipolar voltage switching (single phase) [31]

The unipolar switching has two major advantages over the bipolar switching:

- The switching frequency is "effectively" doubled, so the first harmonics will appear in the sideband of $2m_f$, which means that the harmonics are easier to filter out. The harmonic spectrum shown in *Figure 3. 12* (unipolar) is of a higher quality than the spectrum of *Figure 3. 11* (bipolar).
- The output voltage changes are reduced to V_d. In the case of bipolar switching, the voltage changes are $2V_d$.

3.2.5 Circuit diagram of a three-phase inverter (6 switches)

The most frequently used three-phase inverter circuit consists of three legs as shown in *Figure 3. 17*. The AC output voltage of each leg only depends on the DC voltage and the time the switches are closed. When we assume the switches to be ideal (no transient between opening or closing of the switch and no internal resistance) the output voltage is independent of the direction of the load current. The output AC voltage is also independent of the magnitude of the load current as one of the two switches in a leg is always closed at any instant. [31]

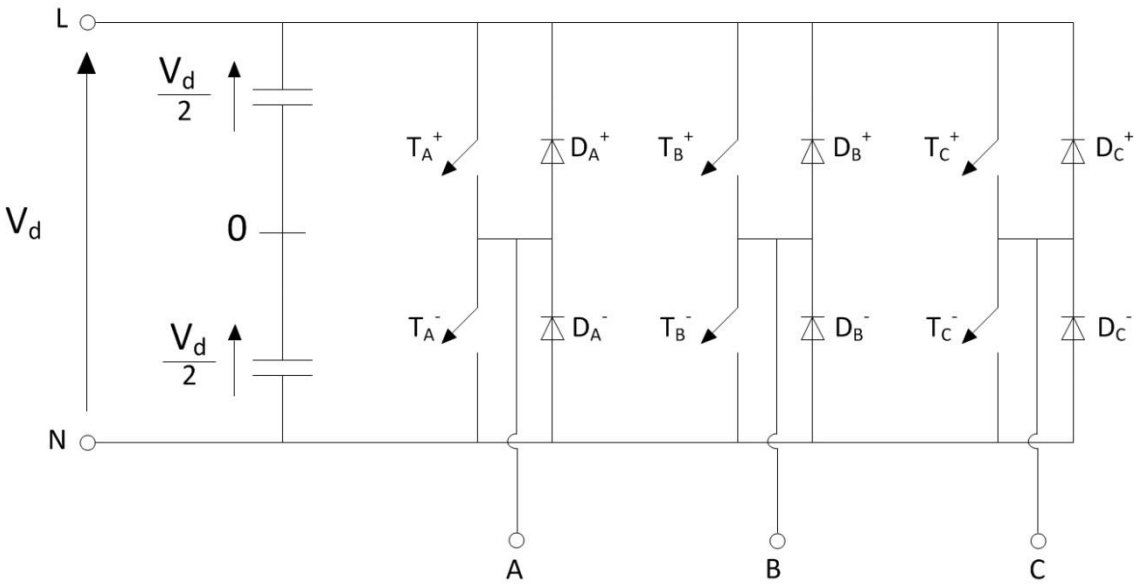

Figure 3. 17. Three phase inverter [31]

3.2.6 Control signals and PWM

The switches are controlled as if the converter consisted of three half-bridge inverters. The three control signals are 120° out of phase, as shown in *Figure 3. 18.*

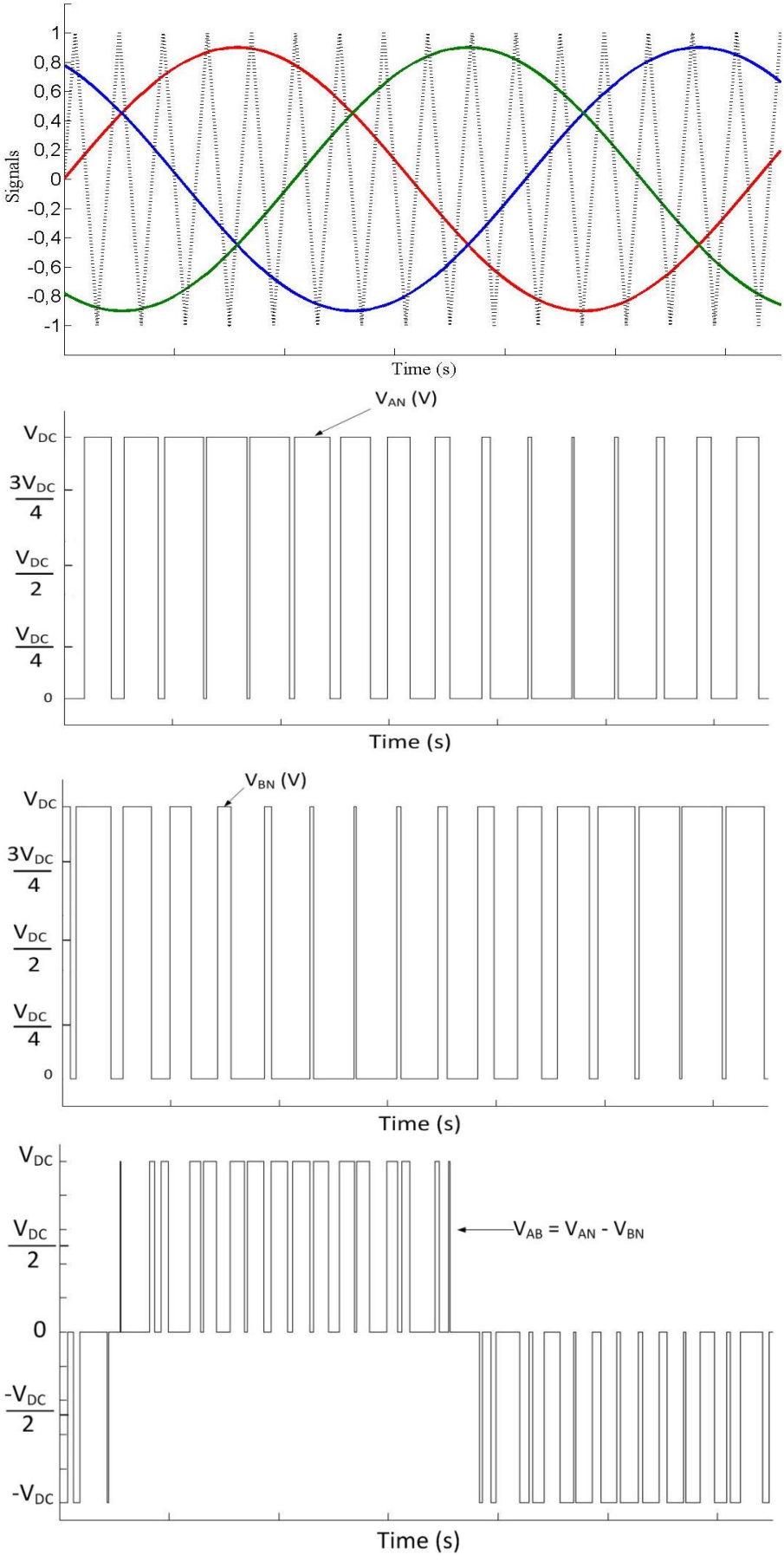

Figure 3. 18. Three-phase PWM waveforms [31]

The average dc components in the output of each leg (v_{AN}, v_{BN}, v_{CN}) are equal. These DC components are cancelled out in the line-to-line voltage. Only the harmonics in the line-to-line voltage are of concern.

Also, the phase difference of the harmonic m_f (and its multiples) in the output voltages of each leg is $m_f \cdot 120°$. This means that if m_f is an odd integer and a multiple of three, the harmonic m_f is suppressed in the line-to-line voltage. This is illustrated in *Figure 3. 19.*

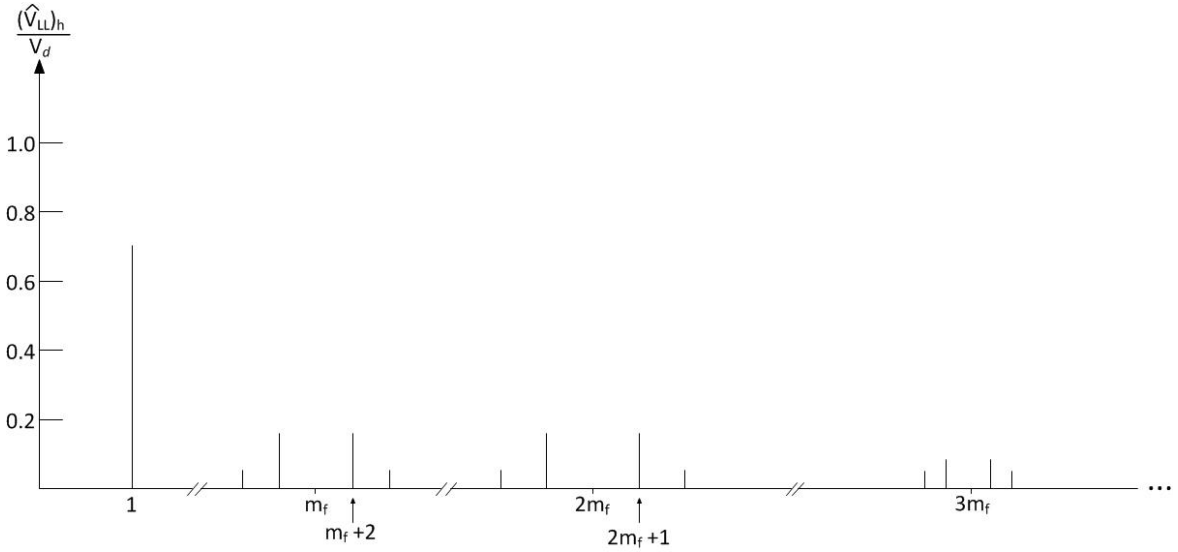

Figure 3. 19. Harmonic spectrum of a three-phase PWM (m_a = 0.8, m_f = 15) [31]

3.2.7 Output voltage modulation

Similar to the single-phase bridge, the output voltage of the three-phase bridge is modulated with m_a. The peak value of the fundamental component in the output voltage v_{AN} equals:

$$(\hat{V}_{AN})_1 = m_a \cdot \frac{V_d}{2} \tag{3.24}$$

The RMS value of the line-to-line voltage at the fundamental frequency can be written as

$$V_{LL,1} = \frac{\sqrt{3}}{\sqrt{2}}(\hat{V}_{AN})_1 = \frac{\sqrt{3}}{2\sqrt{2}} m_a V_d \qquad (m_a \leq 1.0) \tag{3.25}$$

$$\frac{\sqrt{3}}{2\sqrt{2}} V_d < V_{LL,1} \leq \frac{\sqrt{6}}{\pi} V_d \qquad (m_a > 1.0) \tag{3.26}$$

3.2.8 Circuit diagram of a three-phase inverter (12 switches)

An alternative three-phase inverter design consists of three full-bridge inverters, as shown in *Figure 3. 20*. The advantages of this configuration are a higher output voltage and a better harmonic spectrum. However, it exhibits the following drawbacks which have prevented its widespread adoption:

- It employs 12 switches instead of 6 switches.
- It requires a three-phase output transformer with six primary terminals or a separate access for each one of the two three phases.

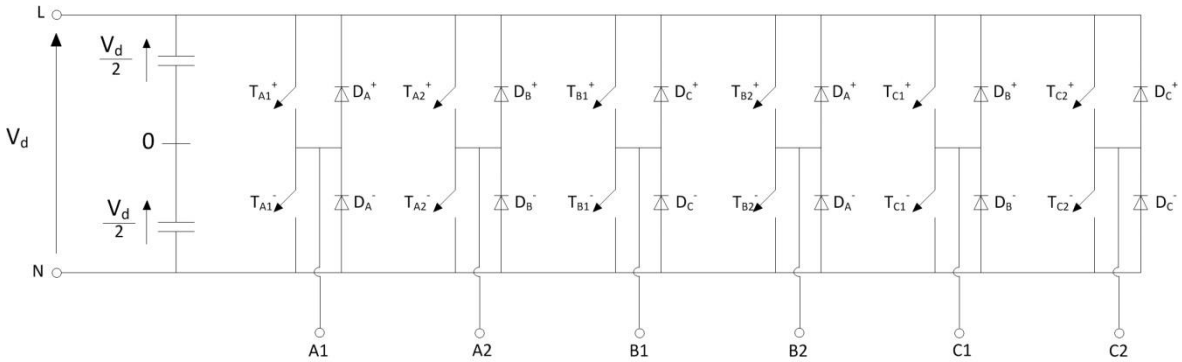

Figure 3. 20. Three-phase inverter with three full-bridge inverters

This set-up gives the possibility to switch from unipolar to bipolar switching and vice versa. When bipolar switching is performed, the results will be similar to the results presented in section 3.2.5. On the other hand when unipolar switching is used the control signals are similar to the signals of the single-phase unipolar controlled inverter, as shown in *Figure 3. 21*.

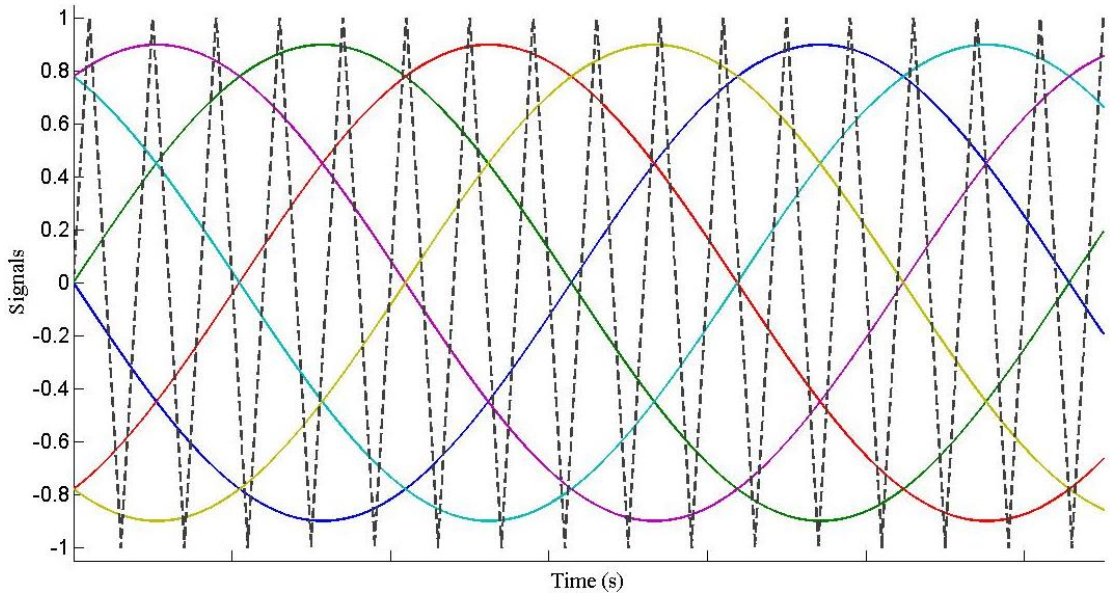

Figure 3. 21. Control signals for unipolar three-phase inverter

This switching scheme results in the line-to-line voltage shown in Figure 3. 22.

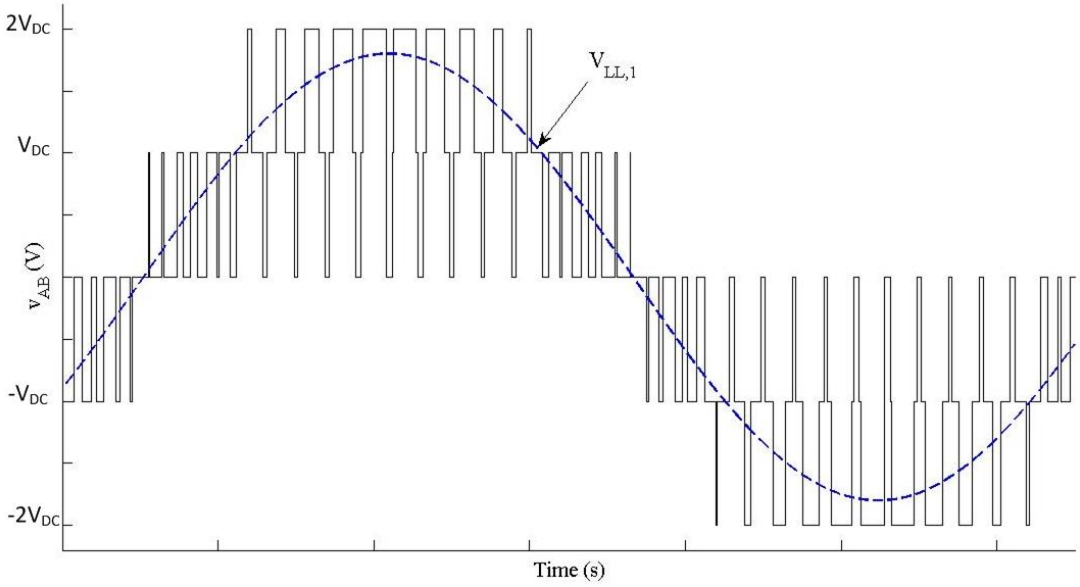

Figure 3. 22. Line-to-line voltage

The switching frequency has, compared to the switching frequency in *Figure 3. 19Figure 3.* ***18***, effectively doubled. This results in a much better harmonic spectrum, as illustrated in *Figure 3. 23*.

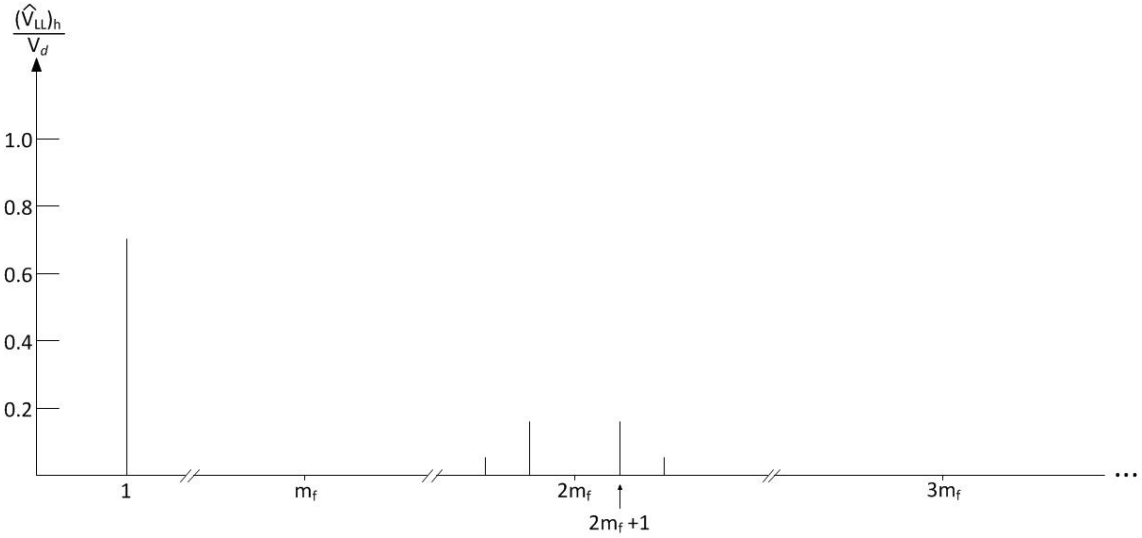

Figure 3. 23. Harmonic spectrum of a three-phase PWM (m_a = 0.8, m_f = 15)

3.2.9 A 48-pulse converter

The DC-AC converter which has been used as part of the BESS implemented in this thesis, is a 48-pulse converter. This converter comprises four 12- pulse full-bridge converters. The output voltage of the four converters is - each time - phase-shifted by 7.5 degrees, which results in a rather clean output voltage and current at the terminals of the BESS. Employing this configuration reduces the complexity of the BESS since no filters are required. The line current and the phase-to-phase voltage of the converter are presented below. For more information about this 48-pulse converter, read [41].

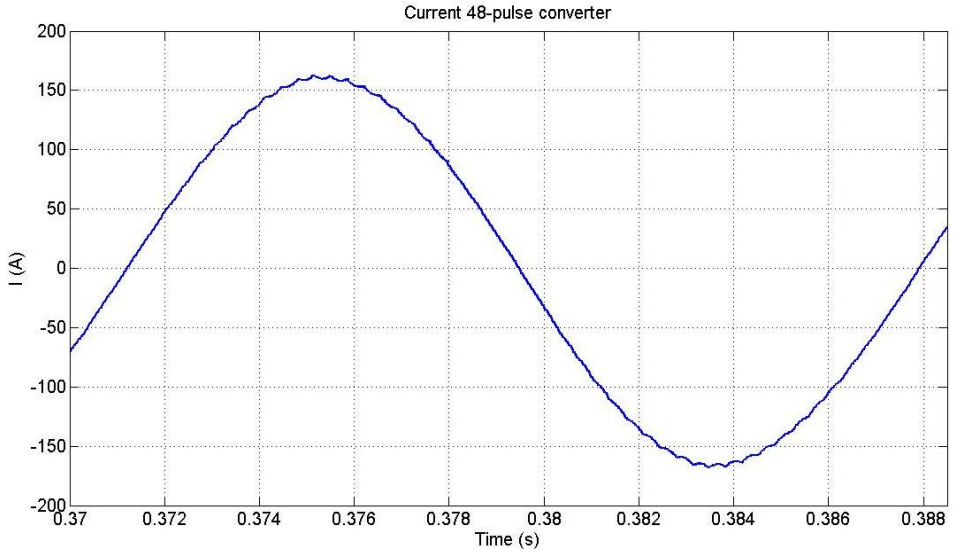

Figure 3. 24. Line current of a 48-Pulse Converter

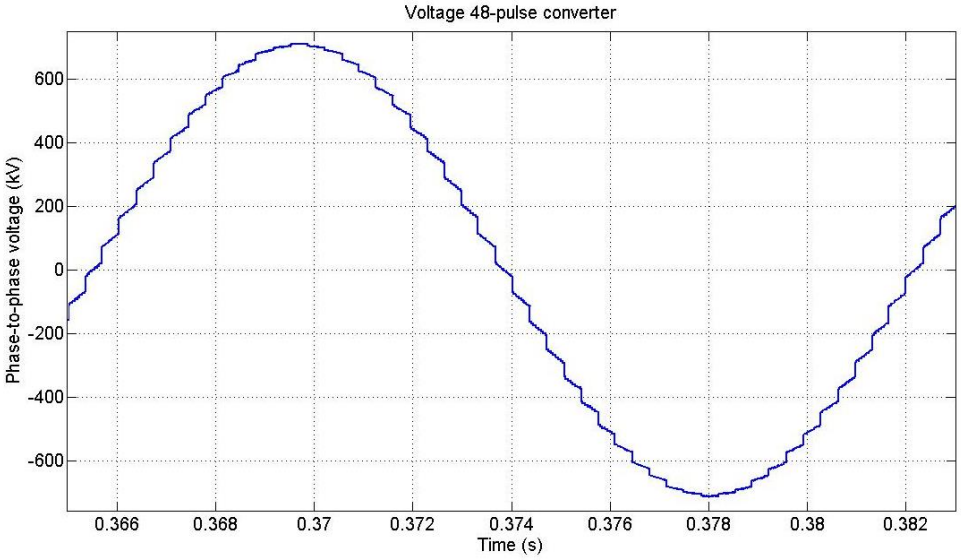

Figure 3. 25. Phase-to-phase voltage of a 48-Pulse Converter

4 BATTERY ENERGY STORAGE SYSTEM

4.1 Introduction

As the deployment of PV and wind generators within the Nordic countries gathers momentum, there is growing interest in searching for measures to ameliorate the problems brought about by intermittent generation. For instance, the MW-level application of battery energy storage systems is a relatively new application on the mitigation of frequency excursions but reports on operational experience in existing installations, is rather encouraging – this has been the case in the Chilean power grid [7] and in California [8]. Nevertheless, the issue of frequency oscillations mitigation still requires a deeper understanding and the voltage control and back-up power applications of BESS remain two crucial areas of research worth investigating because they have the potential to bring about added value to technology deployment. The latter is particularly relevant to distribution systems since it has the potential to turn an active distribution network with renewable generation into a self-reliant network, along the spirit of the Smart Grids philosophy.

Amongst the enabling technologies that make up the Smart Grids drive, energy storage is perhaps the element that until quite recently, it was less well developed. This situation has changed quite substantially over the past few years, with Battery Energy Storage Systems (BESS) becoming a realistic proposition with the availability of reliable and affordable Li-ion batteries – refer to Figure 1.4 for some comparative figures. The BESS's power electronic converters may be as simple as a standard boost converter and a two-level voltage source converter, even though it is anticipated that in future the VSCs employed in BESSs will be of the modular, multi-level kind, with or with no interfacing transformers. The BESS model developed in this research comprises a realistic model of a Li-ion battery pack, a DC-DC converter of the Cuk type and an x-level VSC, which connects to a point of the AC power grid through an interfacing transformer.

4.2 The model

The BESS model developed in this work and aimed at two different applications is carried out in Matlab/Simulink. The BESS basic structure is presented in *Figure 4. 1*.

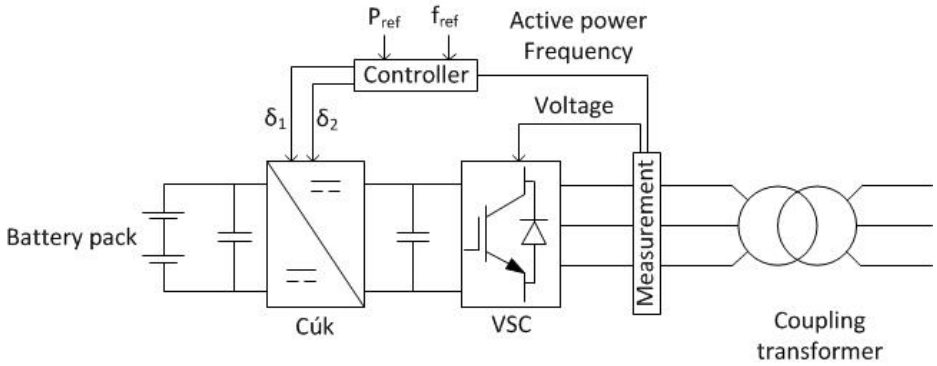

Figure 4. 1. Battery Energy Storage System

This diagram contains three major parts:

- Battery pack: Storage
- DC-DC Converter: Active power control
- Voltage Source Converter: Reactive power control

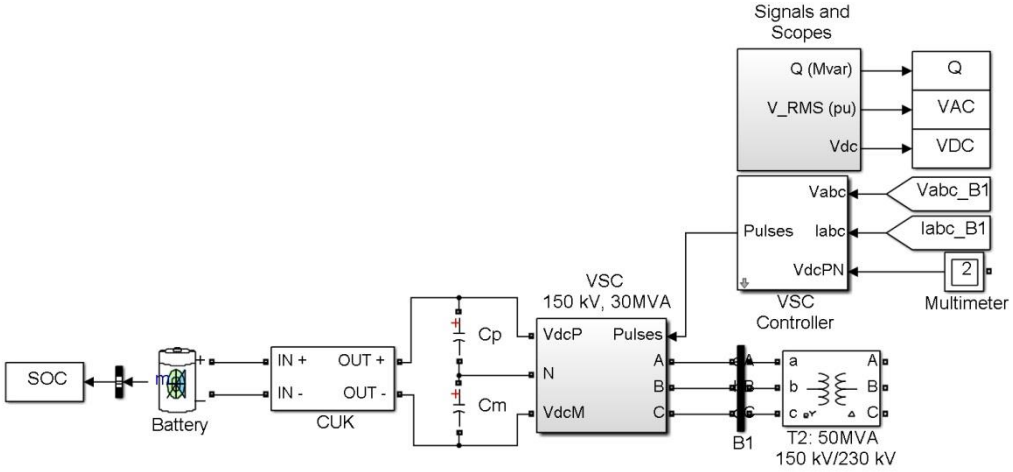

Figure 4. 2. Connection diagram of the BESS in Matlab

These three parts are implemented in Matlab to carry out the simulations with which to assess the impact of the BESS on the power grid. The model implemented in Matlab is presented in *Figure 4. 2*.

The DC-DC converter has been built, as shown in *Figure 4. 3*. It is a bidirectional cúk-converter. The parameters of this converter are:

$C_1 = 750\ \mu F$ $C_2 = 2000\ \mu F$ $C_3 = 7500\ \mu F$
$L_1 = 25\ \mu H$ $L_2 = 20\ \mu H$

Capacitors C_2 and C_3 have been selected to be of large enough capacity. Capacitor C_3 has an important influence on the output voltage ripple of the DC-DC converter. This ripple needs to be as small as possible. Capacitor C_2 needs to have a large capacity to

keep the voltage between the switches constant even as it transfers power between the batteries and the VSC.

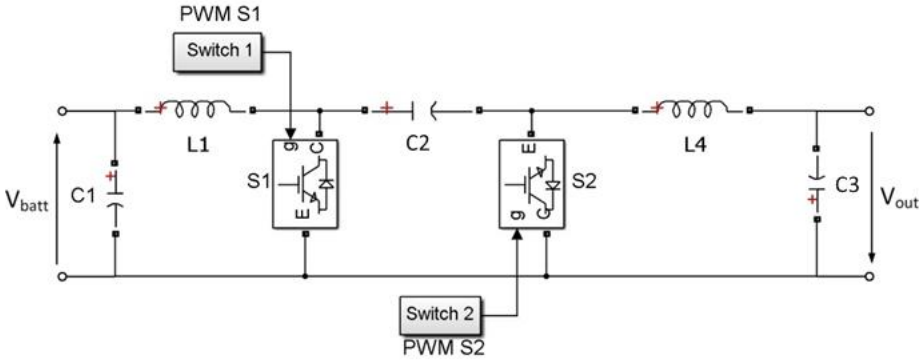

Figure 4. 3. DC-DC Converter BESS

A STATCOM injects/draws reactive power by directly or indirectly controlling the output voltage of the inverter. It is well understood that when the output voltage of the inverter is higher than the grid voltage, reactive power flows from the STATCOM to the grid. The opposite occurs when the inverter output voltage is lower than the grid voltage. The presence of the capacitor on the DC side reduces the voltage ripple on the DC side of the inverter. The main goal of the VSC in the applications of this thesis is to control the AC voltage. [40, 42] The VSC in this BESS implementation is based on an existing VSC model available in the Simulink Examples library (power_statcom_gto48p). When the VSC model is used as a STATCOM, it is set to regulate the DC voltage to indirectly control the output voltage of the inverter and with it the reactive power flow. However, in the BESS application, the DC voltage is tightly controlled by the cúk converter and this option is no longer available for reactive power control. In such a case the VSC model internally changes the control mode to current control mode and it is by this means that the BESS exerts reactive power control. For more information about this VSC model, read [41].

The storage system can exchange active power with the grid. In order to control active power flow between the storage system and the grid, the duty cycles of the switches in the DC-DC converter are adjusted. Switch S_1 controls the power drawn from the battery and switch S_2 controls the power injected into the battery. Of course, the switches can never be closed at the same time. The switches also control the terminal voltage of the battery. When the terminal voltage is higher or lower than the internal voltage of the battery, the converter injects or draws power from the battery, respectively. The power flow control of the DC-DC converter exerts control in two different ways:

- Frequency control mode: this will be used in the case of the transmission system application.

- Active power flow control mode: this will be used in the case of the active distribution system.

Controller Cúk

The control system of the DC-DC converter is split into three major stages:

- Determination of the operating mode and impact of the BESS
- Calculation of the target output voltage
- Calculation of the duty cycles δ_1 and δ_2.

In the first stage, the error is calculated by comparing the actual frequency (or active power flow) with respect to a target value, with the impact of the BESS being proportional to the error incurred. If the error is lower than a pre-defined threshold, the impact of the BESS is kept to zero. This is to prevent the batteries from constantly charging and discharging at an unhealthy rate and in quite an unnecessary manner.

In the second stage, the target output voltage is calculated. When performing simulations, the initial status of the system is its steady-state. The BESS is initialised in such a way that this status is not perturbed. If frequency changes take place in the system, the target output voltage will be adjusted, according to the following relationship:

$$V_{out} = V_{init} + k \cdot (f_{ref} - f_{actual}) \tag{4.1}$$

where f_{ref} and f_{actual} stand for the target frequency and the actual frequency, respectively. For frequencies lower or higher than the target frequency, k takes positive or negative values to control δ_1 and δ_2, respectively. The value of k is a function of the rated power of the BESS; in this work for a BESS of 22 MW, the value of k has been taken as 2000. Note that the frequency is expressed in p.u.

In the third stage the duty cycles δ_1 and δ_2 are calculated and these values are transformed into a PWM signal. The value of δ is calculated using equation (4.2)

$$\delta_n = \frac{V_{out,n}}{V_{batt} + V_{out,n}} \qquad \text{with n = 1 or 2} \tag{4.2}$$

4.3 Primary frequency regulation

As it is well-known, synchronous generators regulate frequency by adjusting the amount of power being injected into the system. When a load change takes place, the generator reacts to this change with ensuing changes in frequency. In the case of a load increment, the electrical power delivered by the generator will exceed the mechanical power delivered by the turbine. This difference in power will be made up by the rotating mass (inertia) of the generator [43, 44]. Hence, the generator will slow down as its kinetic energy

decreases. The Load Frequency Control (LFC) will regulate the power delivered by the turbine by changing the statism of the controller. [45]

The relationship between the power and the frequency is expressed by equation (4.3):

$$P_{gen} - P_0 = -\frac{P_R}{R} \cdot \Delta f \tag{4.3}$$

where P_{gen} stands for the power generated following the disturbance,
P_0 stands for the power generated before the disturbance,
P_R stands for the nominal generated power,
$R = \frac{\Delta f}{\Delta P}$ stands for the statism of the generator and
$\Delta f = f - f_0$ stands for the change in frequency caused by the change in load.
The statism of the generator is adjusted in order to return to the nominal frequency [45]. This regulation is shown in *Figure 4. 4*.

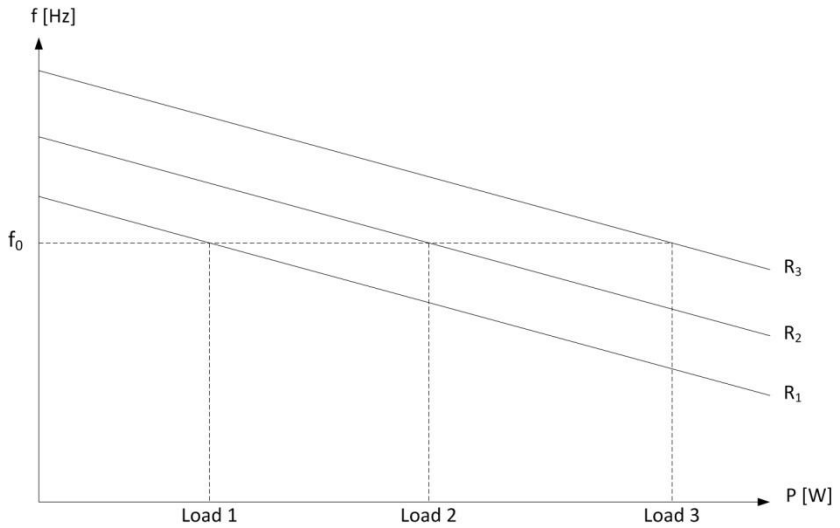

Figure 4. 4. Speed-changer settings [45]

It is interesting to notice that the BESS observes similar operating characteristics as the synchronous generator but it has no rotating parts. However, the lack of rotating parts in a battery results in a much quicker speed of response of the BESS compared to a synchronous generator. The ability of the BESS to provide frequency regulation is presented in this thesis in chapter 5.

The energy stored in the battery has the characteristics of inertia by acting as a stored kinetic energy. The State of Charge (SOC) of the battery will decrease when the load exceeds the power delivered by the synchronous generators in the system.

To further emphasize the operational resemblance between the BESS and the synchronous generator, an analogy between a BESS and a hydro power generator is presented in *Figure 4. 5*. The governor controls the inlet of water into the turbine (with the reser-

voir being discharged) and the duty cycle controller controls the rate of discharge of the battery. Note that the case of battery charging in this analogy would correspond to the case of hydro pumped storage. The AC Voltage controller is in both cases, a regulated gain.

With reference to *Figure 4. 5*, the following analogies exist at the output of the Reservoir and Battery blocks: the volumetric flow rate Q is akin to current I and pressure P is akin to voltage. Likewise, at the output of the Turbine and DC-DC Converter blocks: torque and speed are akin to power and voltage, respectively.

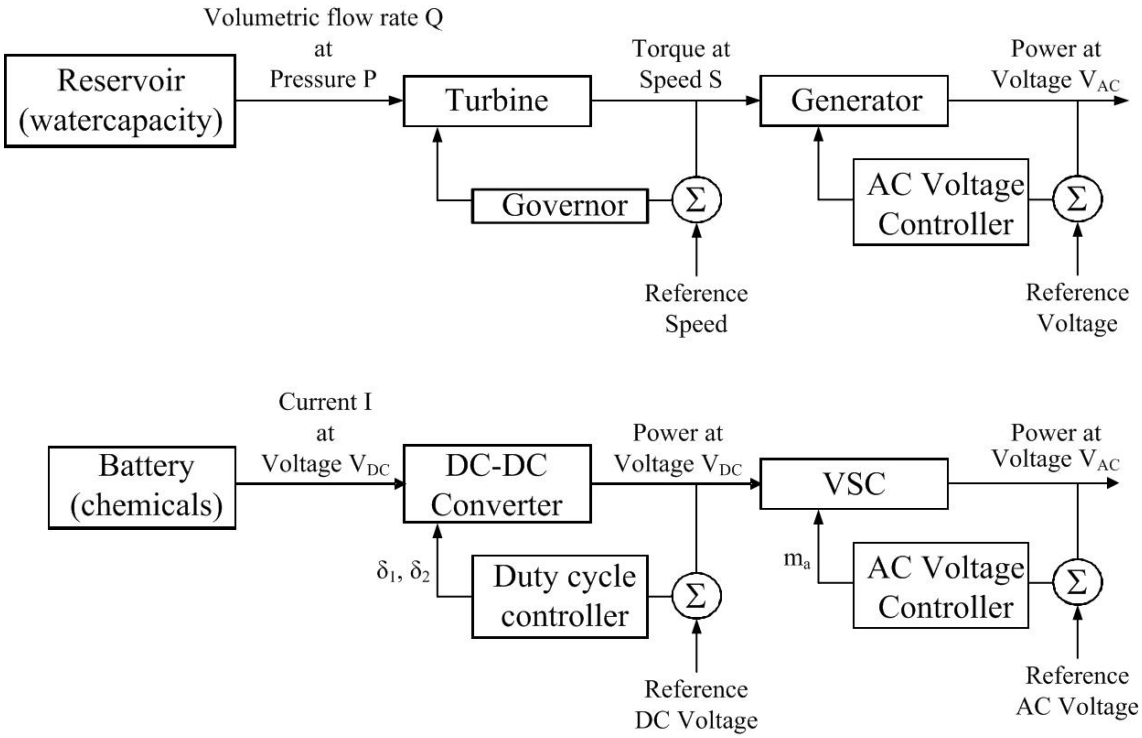

Figure 4. 5. Comparison between hydraulic energy storage and BESS

4.4 Potential applications in power grids

Two possible applications of BESS in electrical power systems are addressed in this thesis. The BESS is capable of injecting or drawing active power at key points of the grid. The first application is in the realm of high-voltage transmission systems by using the test power network given by Prahba Kundur [46]. Two changes in the load around the nominal, are assumed to take place. The impact of the BESS on the synchronous generators' frequency is investigated.

The second application of the BESS pursued in this thesis is related to power flow improvement in an active distribution system which contains distributed generation in the form of windmills. Five windmills are placed at different points of the distribution system. It is shown that a BESS placed at the PCC has the potential for "decoupling" a large part of the active grid from the distribution utility company, in terms of both active and reactive power.

5 SIMULATION RESULTS

Potential applications of the BESS technology are just beginning to emerge. In this chapter the results of two such applications are presented, namely, frequency support in a high-voltage transmission system and a network decoupling scheme in an active distribution system. In the former application, the high-voltage transmission system developed by Prahba Kundur (*Figure 5. 1*), is used for testing the feasibility of the BESS. Two situations are being observed:

- The load at bus 7 is increased by 50MW
- The load at bus 7 is decreased by 50MW

In the realm of active distribution with wind generation, the goal is to store the energy produced by the wind generators in the BESS when the load is lower than production and to make the stored energy available when the opposite situation occurs. As a separate test case, a BESS is assumed connected at a point of common coupling and the self-sufficiency of a portion of the active distribution network is investigated.

5.1 High Voltage Transmission System

The transmission power grid used to test the impact of the BESS can be found in [46]. This grid comprises two areas, linked by a double circuit transmission line. In order to show the prowess of the BESS, the original system has been slightly modified; the active power drawn by the load connected to node 7 has been increased/decreased and the BESS is connected at node 6 through a 230/150kV transformer.

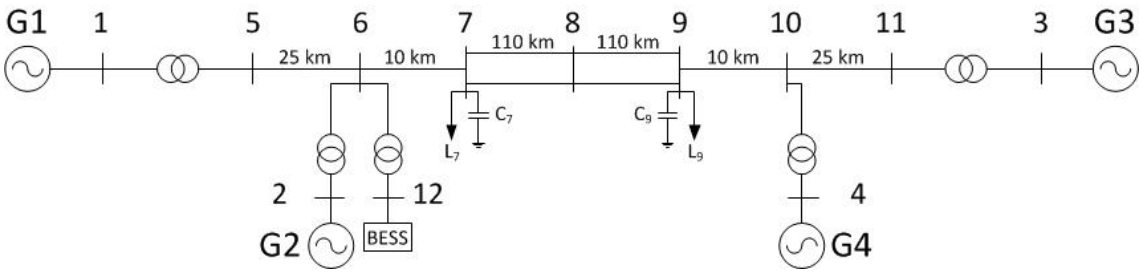

Figure 5. 1. A simple two-area system [46]

Each area comprises two synchronous generators each rated at 900 MVA and 20kV. The parameters of these generators are given in *Table 5. 1*. They are in per unit on the rated MVA base and kV base.

Table 5. 1. Parameters synchronous generators [46]

$X_d = 1.8$	$X_q = 1.7$	$X_l = 0.2$	$T_{d0}' = 8.0$ s	$T_{q0}' = 0.4$ s
$X_d' = 0.3$	$X_q' = 0.55$	$R_a = 0.0025$	$T_{d0}'' = 0.03$ s	$T_{q0}'' = 0.05$ s
$X_d'' = 0.25$	$X_q'' = 0.25$	$\psi_{T1} = 0.9$	H = 6.5 (for G1 and G2)	
$A_{Sat} = 0.015$	$B_{Sat} = 9.6$	$K_D = 0$	H = 1.8 (for G3 and G4)	

The step-up transformers have an impedance of 0+0.15j per unit on a 900 MVA base and a 20/230 kV base. Their off-nominal tap ratio is 1.0.

The transmission system nominal voltage is 230 kV. The parameters of the lines in per unit, on 100 MVA, 230 kV base, are:

$r = 0.0001$ p.u./km $\quad x_L = 0.001$ p.u./km $\quad b_C = 0.00175$ p.u./km

The synchronous generators are loaded as follows:

G1: P = 700 MW, Q = 161 MVAr
G2: P = 502 MW, Q = 266 MVAr
G3: P = 719 MW, Q = 134 MVAr
G4: P = 700 MW, Q = 209 MVAr

The loads in buses 7 and 9 are as follows:

Bus 7: $P_L = 967$ MW, $Q_L = 350$ MVAr
Bus 9: $P_L = 1767$ MW, $Q_L = 100$ MVAr

The shunt capacitive compensation at the same buses are as follows:
Bus 7: $Q_C = 200$ MVAr
Bus 9: $Q_C = 350$ MVAr

Additional modifications to the original system

The shunt capacitors supply reactive power to provide voltage support. These parameters are also adjusted to reflect changes in the load to ensure a working system. For example, when the load increases, the injected reactive power of the shunt capacitors is also increased to ensure that the system remains stable.

5.1.1 Increment of load in bus 7, by 50 MW

Frequency regulation

The key point in this application is frequency regulation improvement using the BESS. The load is increased by 50 MW after two seconds of simulation. The effect of adding this load with and with no BESS is contrasted by comparing *Figure 5. 2* to *Figure 5. 3* and *Figure 5. 4*. The frequency of the generator, which cannot change instantly because of the inertia of the generator, is shown in these figures. It is noticed that the frequency takes about 13 seconds to reach its lowest point. With no BESS the frequency drops to 0.9845 p.u. (*Figure 5. 2*) and with a 22 MW BESS, it only drops to 0.9886 p.u. (*Figure 5. 3*) As expected, the frequency drop also reduces,

$$\frac{(1-0.9845)-(1-0.9886)}{(1-0.9845)} \text{ x } 100 = 26.45\%$$

Further to the action of the BESS, the synchronous generator frequency regulator also influences the system frequency. The frequency returns to its reference value of 1.0 p.u. by adjusting the power contributed by the turbine. It follows that the frequency rises again. After about 34.5 seconds the frequency reaches the reference value, but with no BESS, the frequency exhibits a marked overshoot. At this point, the impact of the BESS is of paramount importance; it damps the frequency oscillations very effectively. More specifically, with no BESS, the frequency keeps rising until it reaches 1.0023 p.u. and with the BESS in place it limits the overshoot to 0.01%.

The rated power of the BESS (22 MW) is similar to the state-of-the-art BESS installations in California and Chile. At this point in the thesis and purely for theoretical reasons, the contribution of an 80 MW BESS is explored and a preliminary result is presented in *Figure 5. 4*. It is quite encouraging to observe that the frequency drop is much smaller and the ensuing frequency oscillations are effectively cancelled out.

The BESS's contribution to ameliorate frequency deviations from the nominal, termed *impact* in this work, is presented in *Figure 5. 6*. During the most severe part of the frequency drop, the BESS's impact is maximum. The impact is proportional to the deviation of the frequency with respect to the reference value. It is observed in *Figure 5. 6* that the impact of the BESS decreases a great deal after the generator has reached its nominal value, after 36 seconds, with its action directed at cancelling out the ensuing frequency oscillations.

Voltage regulation

Figure 5. 7 shows the RMS voltage at node 6 with and with no BESS. When the change in load occurs, the voltage tends to rise slightly in this case (normally the voltage would drop because of load increases), but the increased voltage support of the shunt capaci-

tors at node 7 prevails. The RMS voltage in the case study with BESS observes a similar behaviour (not shown). When the rotor speed departs from the reference value, some ripple is visible in the RMS voltage at the BESS terminals (*Figure 5. 8*). Quite apart from the presence of the ripple, the voltage remains with little change, even at the point of load change. The BESS voltage is mostly a scaled down reflection of the voltage at node 6, except for three small dents in the latter part of the simulation, as shown in *Figure 5. 8*. The small dents seem to correspond to instant in time when the BESS absorbs reactive power from the network for short periods of time (*Figure 5. 10*).

Active and reactive power flow of the BESS

The active power and reactive power injected by the BESS are shown in *Figure 5. 9* and *Figure 5. 10*, respectively. After the load is increased, the outgoing power increases very rapidly. It takes about two seconds to reach its nominal value of 22MW, as shown in *Figure 5. 9*. When the frequency oscillates around the reference value (*Figure 5. 5*) at around 38s, 45s and 53s, the active power changes direction very quickly (*Figure 5. 9*). In two instances the BESS draws small amounts of active power from the grid, these correspond to the two small overshoots in *Figure 5. 5* where the rotor speed is higher than the reference value. Along with the decreasing amplitudes of the frequency oscillations, the changes in active power flow also tend to reduce.

One possible improvement to the overall system would be the implementation of a secondary frequency regulation in the generator. In such a case, the generator would slowly take over the contribution of the BESS when the steady state is achieved.

Immediately after the change in load, the voltage rise observed in *Figure 5. 7* and *Figure 5. 8* is accompanied by a peak in the reactive power injected by the BESS, as shown in *Figure 5. 10*. This is followed by some voltage ripple and the BESS acts to counteract it; this resulting, in turn, in some ripple in the reactive power injected by the BESS. The three inverted peaks towards the end of the simulation result from the BESS's attempt to damp out the frequency oscillations around the nominal value (*Figure 5. 5*). The BESS changes from discharging to charging status and this brings similar effects in reactive power (*Figure 5. 10*) and voltage (*Figure 5. 8*).

Duty cycles and output voltage in the cúk converter

The BESS duty cycles and its power flows are strongly interrelated. This is illustrated in *Figure 5. 11* where the increase in outgoing active power is clearly related to the duty cycle of switch S_1. It is appreciated from this result that, a stable outgoing power flow is due to the stable value of the duty cycle of switch S_1. A change of the power flow direction is associated with the duty cycle of switch S_2 (*Figure 5. 12*) where the three peaks in the second part of the simulation are caused by changes in power flow.

The instantaneous DC voltage of the VSC (*Figure 5. 13*) encapsulates all of the effects so far discussed: the peak at the moment of the load change, the ripple when the fre-

quency deviates from the reference value and the three reversed peaks towards the end of the simulations.

BESS Operating Mode and State of Charge

The operating mode of the BESS is shown in *Figure 5. 14*, where it indicates whether the batteries are charging or discharging. When the frequency deviation with respect to the reference value is smaller than 0.01%, the impact of the BESS is kept to zero, to safeguard the battery. It is well known that excessive charging/discharging of the battery reduces its useful life.

The State of Charge (*Figure 5. 15*) goes down as the BESS contributes active power to the grid. During the first two seconds of simulation, the SOC is kept constant as the frequency deviation is extremely small. When the BESS works at its maximum output point, the batteries are linearly drained. Three small changes in the active power flow are also visible in the State of Charge curve of the battery pack, which is slightly charged at times corresponding to positive excursions of rotor speed, with respect to the reference value (*Figure 5. 5*).

Rotor speed ω_m

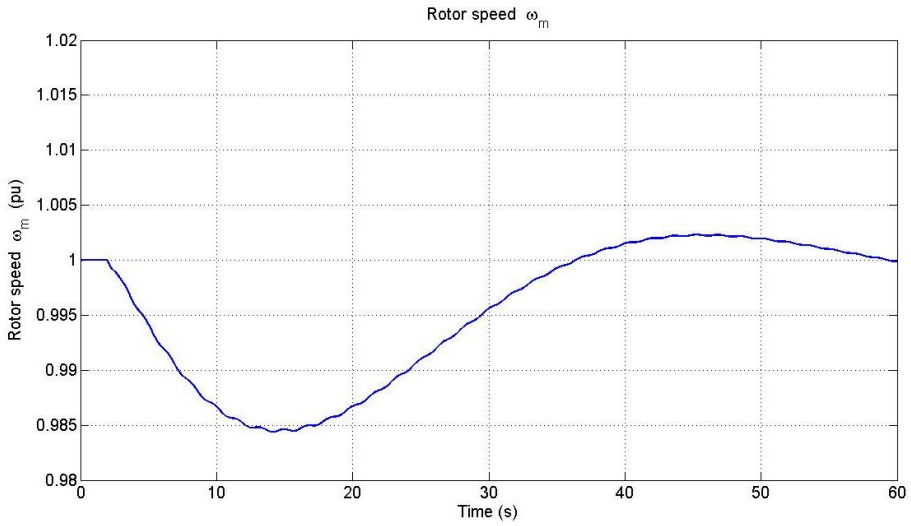

Figure 5. 2. Rotor speed when load is increased (no BESS)

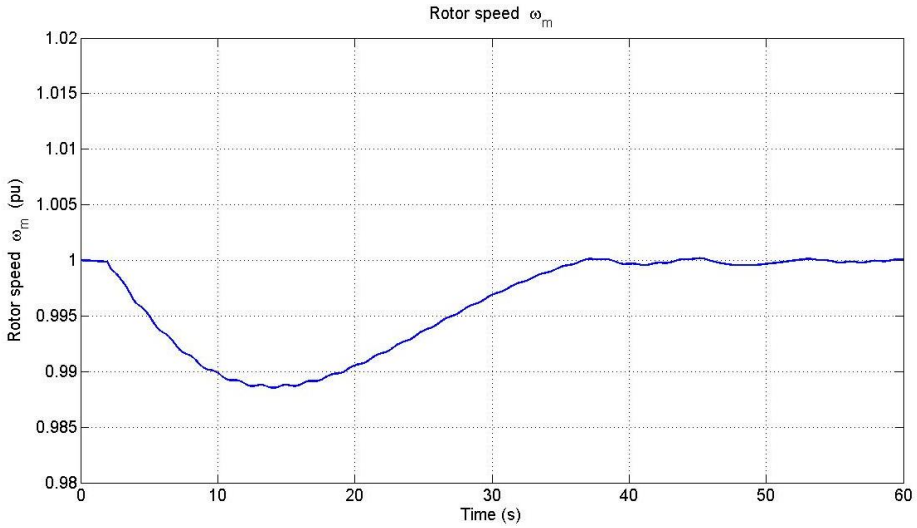

Figure 5. 3. Rotor speed when load is increased (with 22MW BESS)

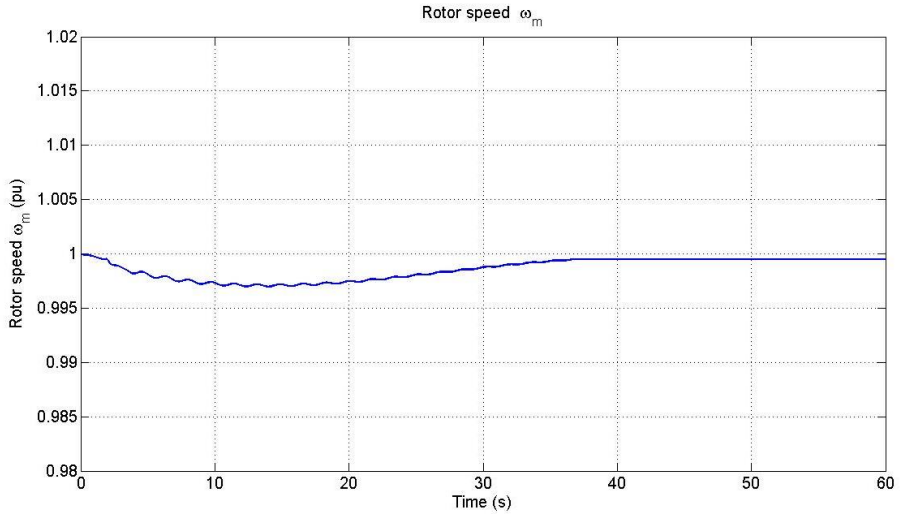

Figure 5. 4. Rotor speed when load is increased (with 80MW BESS)

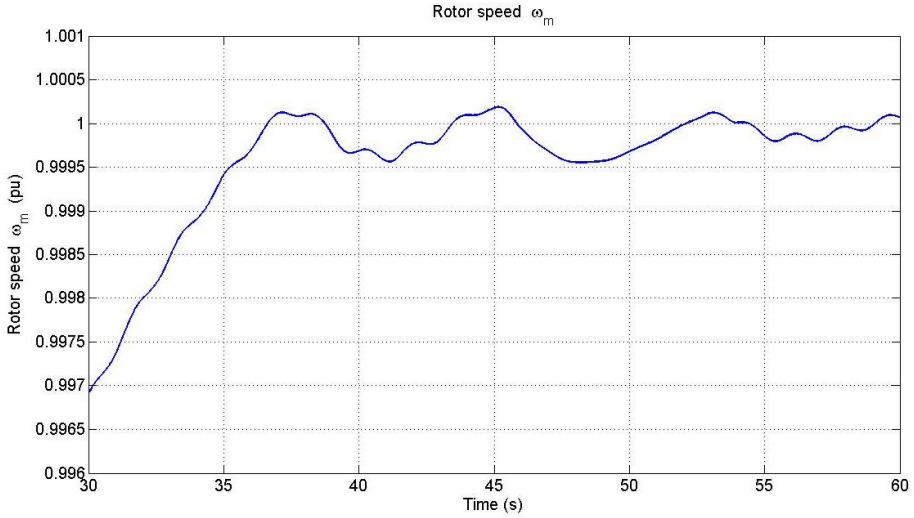

Figure 5. 5 Zoom of rotor speed (with 22MW BESS)

With 22 MW BESS connected

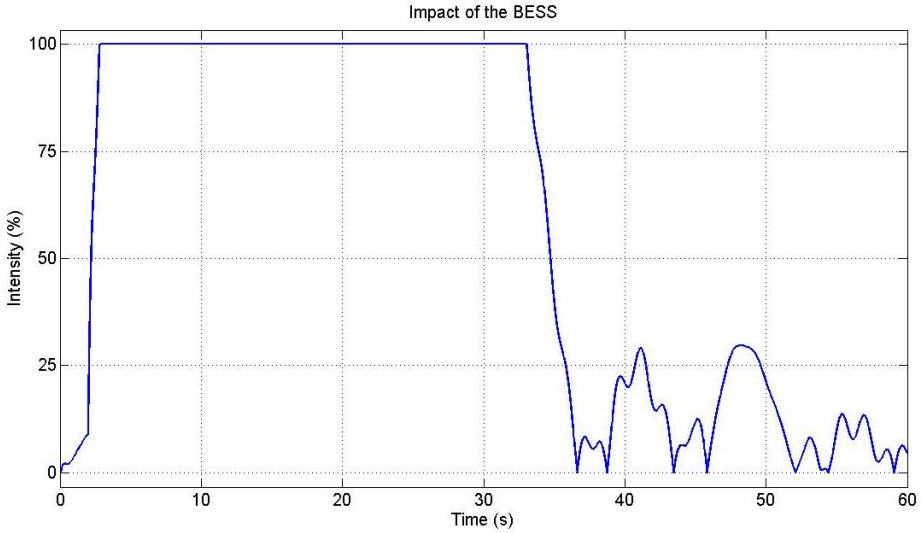

Figure 5. 6. Impact of the BESS when load is increased

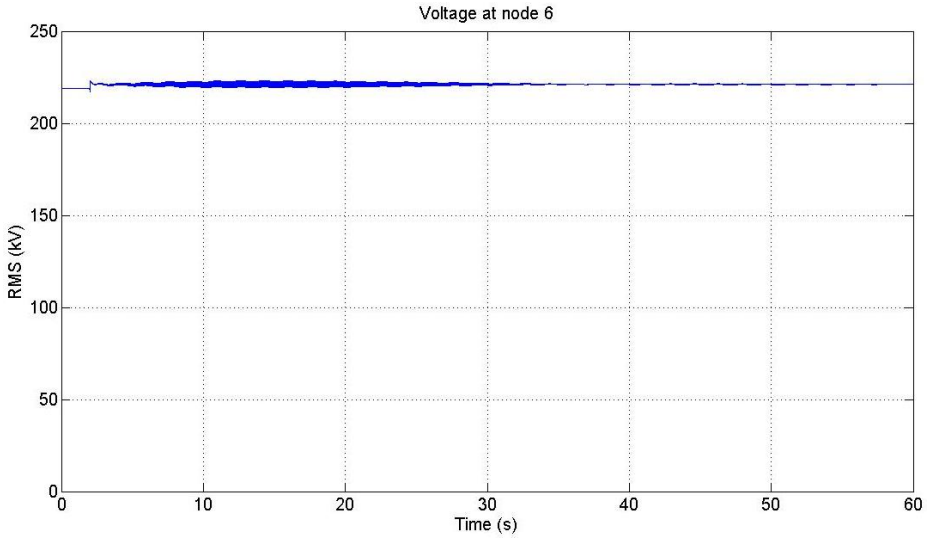

Figure 5. 7. Voltage at node 6 when load is increased (no BESS)

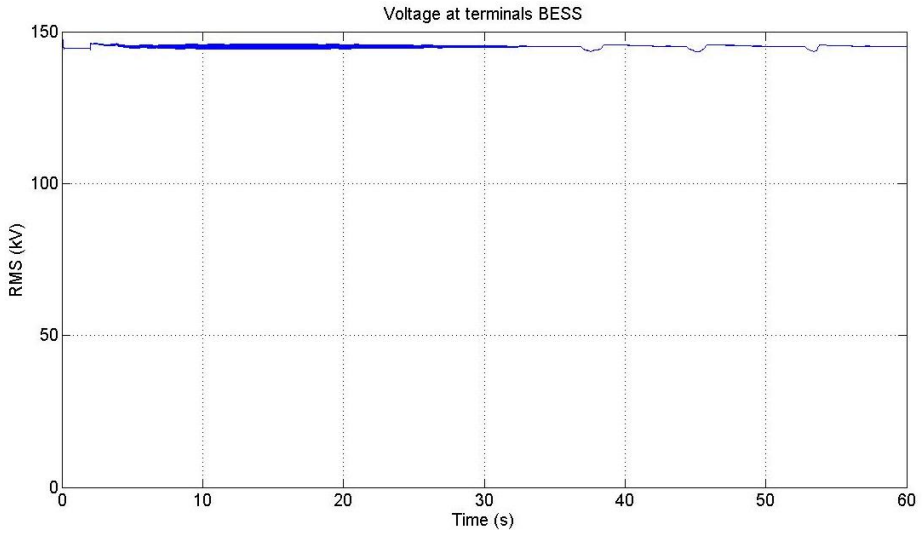

Figure 5. 8. Voltage at the BESS terminals when load is increased

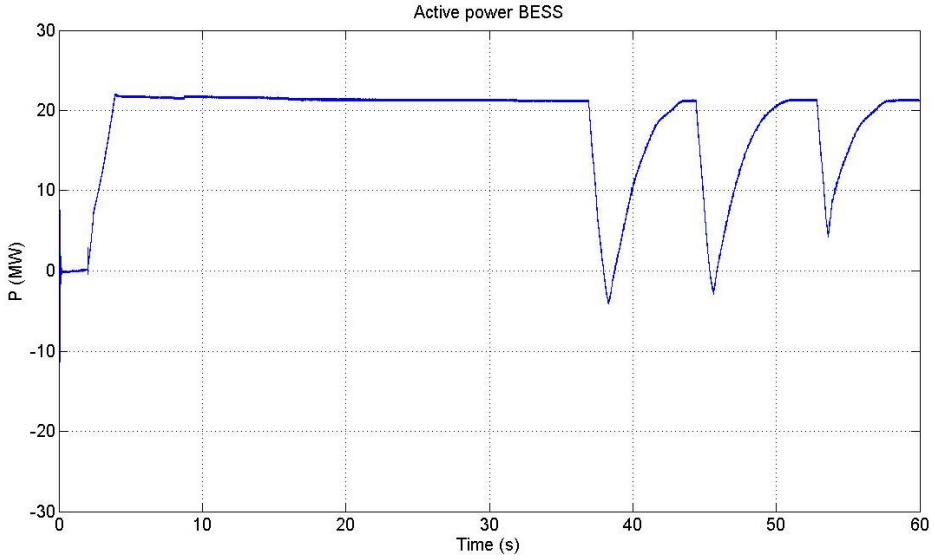

Figure 5. 9. Active power injected by the BESS when load is increased

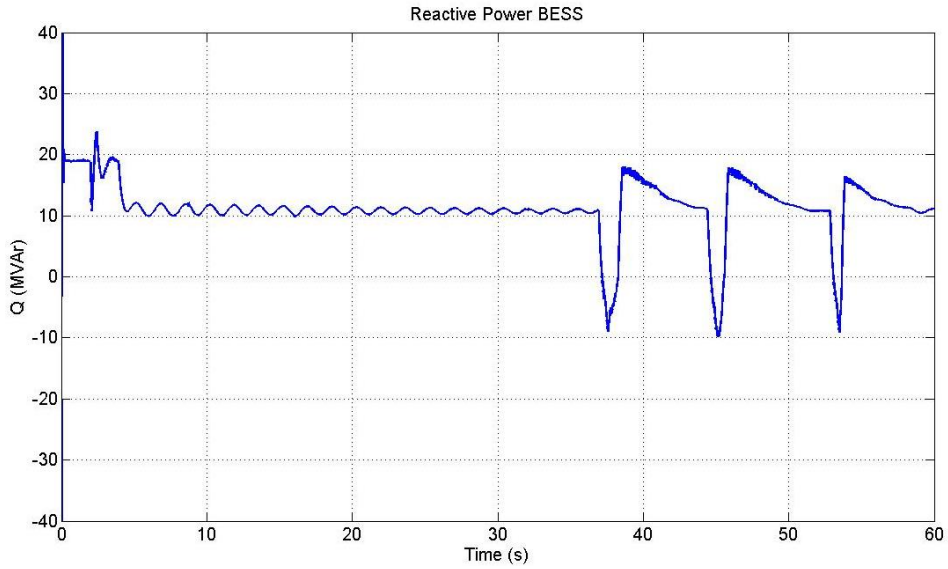

Figure 5. 10. Reactive power injected by the BESS when load is increased

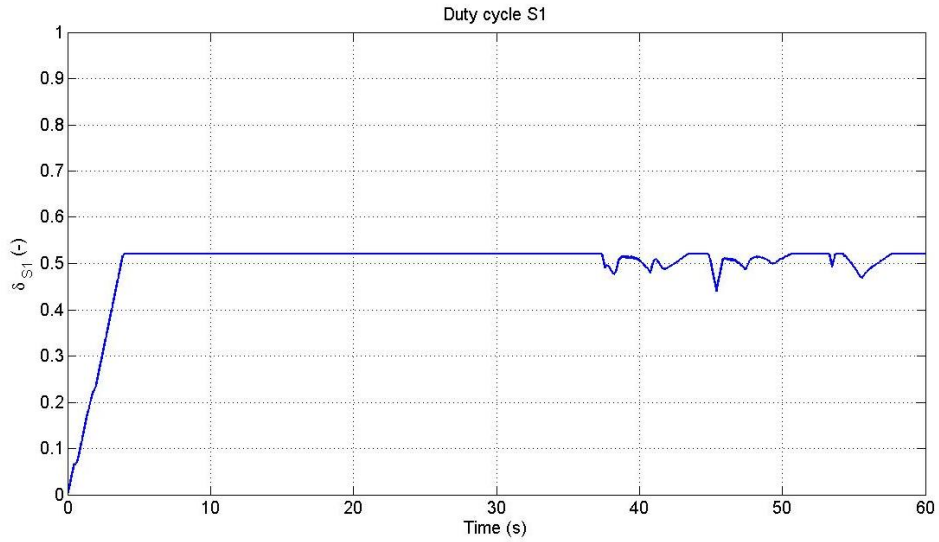

Figure 5. 11. Duty cycle of S_1 when load is increased

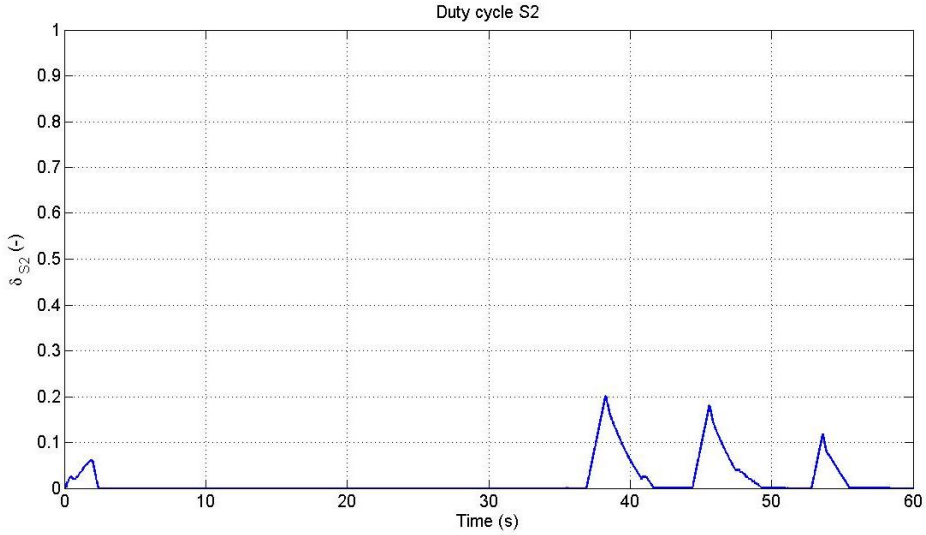

Figure 5. 12. Duty cycle of S_2 when load is increased

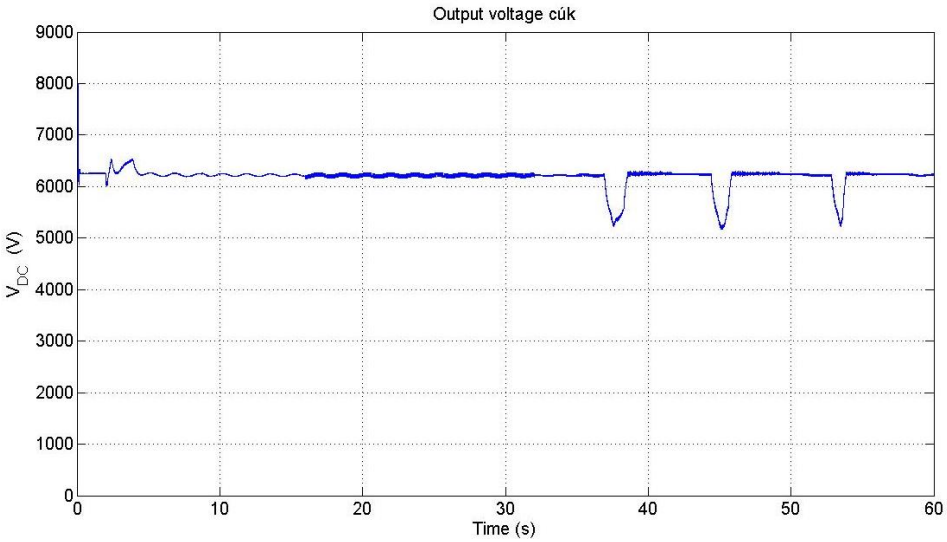

Figure 5. 13. Output voltage DC-DC converter when load is increased

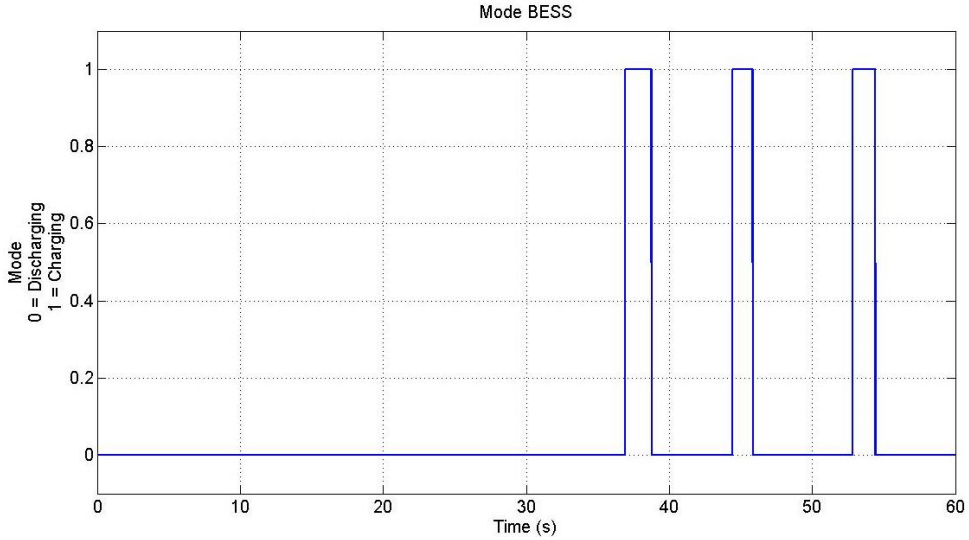

Figure 5. 14. Mode of the BESS when load is increased

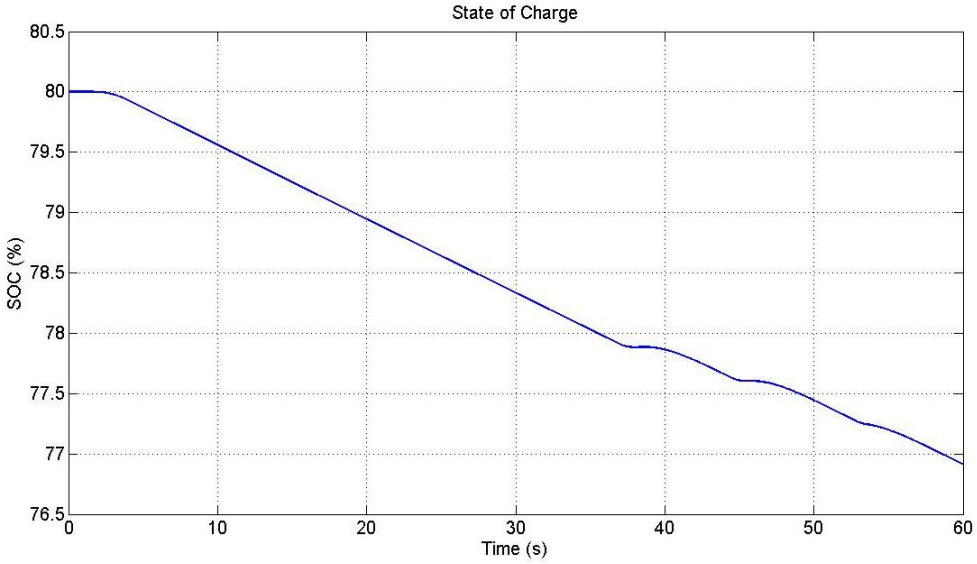

Figure 5. 15. State of Charge of the batteries when load is increased

5.1.2 Decrement of load in bus 7, by 50 MW

Frequency regulation

The second case study that is simulated in the high voltage transmission system is a decrement of load. This load change is also performed after two seconds of simulation. The effect of this disturbance is in both cases (with and with no BESS) instantly visible (*Figure 5. 16* and *Figure 5. 17*). The response in this case is almost an inverted response to the case of load increase (*Figure 5. 2* and *Figure 5. 3*). Instead of a frequency drop, the frequency will now tend to rise as the mechanical power input is higher than the electrical power output. The frequency rises up to 1.0155 p.u. and reaches this peak after about 13 seconds. The BESS is capable of reducing this peak to 1.01 p.u. This is an improvement of

$$\frac{(1.0155-1)-(1.01-1)}{(1.0155-1)} = 0.3548 = 35.48\%$$

The frequency returns to the reference value of 1.0 p.u. by adjusting the power injected by the turbine at about 34.5 seconds. With no BESS, the reversed overshoot reaches the same magnitude as in the case of load increase. In contrast, the BESS reduces the frequency overshoot to a mere 0.04% (*Figure 5. 17*). In this case, the frequency rises slowly, after having gone slightly negative at about 34.5s, reaching at 60s the nominal value. The BESS certainly damps the oscillations instantaneously.

The impact of the BESS is presented in *Figure 5. 19*. The first part of the impact is about the same as in the case of load increase. However, the second part is flatter. The reason is because the frequency is not oscillating as in the case of load increase.

Voltage regulation

The voltage at node 6 with BESS and with no BESS are shown in *Figure 5. 18* and *Figure 5. 20*, respectively. The BESS is connected to the power grid with a coupling transformer. When the disturbance occurs, the voltage tends to drop at first and then some ripple is observed. When the rotor speed differs from the reference value, the voltage ripple appears. The ripple increases with the deviation; otherwise the voltage remains very stable. The voltage ripple with the BESS connected is smaller because of an improved frequency regulation. The voltage at the terminals of the BESS is mainly a scaled-down reflection of the voltage at node 6.

Active and reactive power flow of the BESS

The active power and reactive power absorbed by the BESS are shown in *Figure 5. 22* and *Figure 5. 23*, respectively. Following the load decrease, the BESS absorbs 22 MW of power very quickly. It takes about two seconds to reach the intended value. The absorbed power in the first part of the response (just as the rotor speed goes below the

nominal speed *Figure 5. 17*), is quite stable. This is shown in the impact of the BESS (*Figure 5. 19*). After this the impact of the BESS diminishes quickly to zero, increases again up to 25% and then decreases gradually. Power flow absorption increases rapidly up to its nominal value, i.e. 22 MW. In order to support the system frequency, the BESS draws as much power from the grid as it possibly can. This is so up to about 37s when the rotor speed drops below the nominal speed and there is less need to absorb power from the grid by the battery.

The BESS controls the voltage at node 6 by injecting/drawing reactive power at the node. Following the load change, there is a peak in the reactive power flow of the BESS (*Figure 5. 23*), and this is followed by some ripple, which is associated with the ripple observed in the voltage at the BESS terminals (*Figure 5. 21*). The reverse peak at 38 seconds serves to stabilise the voltage at node 6 when the active power flow changes. Notice that there is a small voltage perturbation in the RMS voltage at precisely this point (*Figure 5. 21*).

Duty cycles and output voltage in the cúk converter

The duty cycles and the power flow are strongly related to each other. The increase of absorbed active power is clearly reflected in the duty cycle of switch S_2 (*Figure 5. 25*). Also the stable power flow is due to the stable value of the duty cycle of switch S_2. The change of direction of the power flow is also appreciated from the duty cycle of switch S_1 (*Figure 5. 24*). This δ increases very quickly when the absorbed power needs to be decreased.

The DC voltage of the VSC (*Figure 5. 26*) shows all the previous mentioned items: the (small) peak at the moment of load change, the ripple when the frequency deviates from the reference value and the change (at about 38s) when the power flow reversal takes place.

BESS Operating Mode and State of Charge

The operating mode of the BESS (*Figure 5. 27*) shows whether the batteries are being charged or discharged. When the deviation of the frequency with respect to the reference value is smaller than 0.01%, the impact of the BESS reduces to zero to safeguard the battery. It is well-known that charging and discharging of the battery at a sustained high rate reduces the battery life.

The State of Charge of the batteries (*Figure 5. 28*) increases linearly as the BESS absorbs active power from the grid. During the first two seconds, the SOC is kept constant as the deviation of the frequency is very small and the impact of the BESS is reduced to a minimum. The dip in the power flow is also visible in the State of Charge.

Rotor speed ω_m

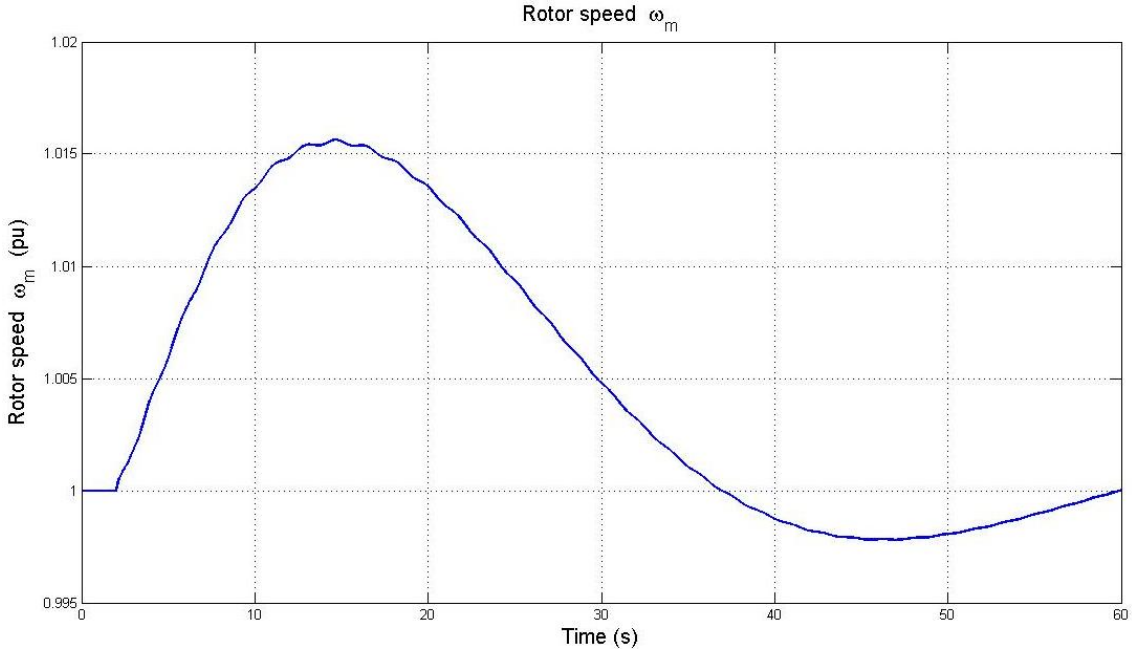

Figure 5. 16. Rotor speed when load is decreased (no BESS)

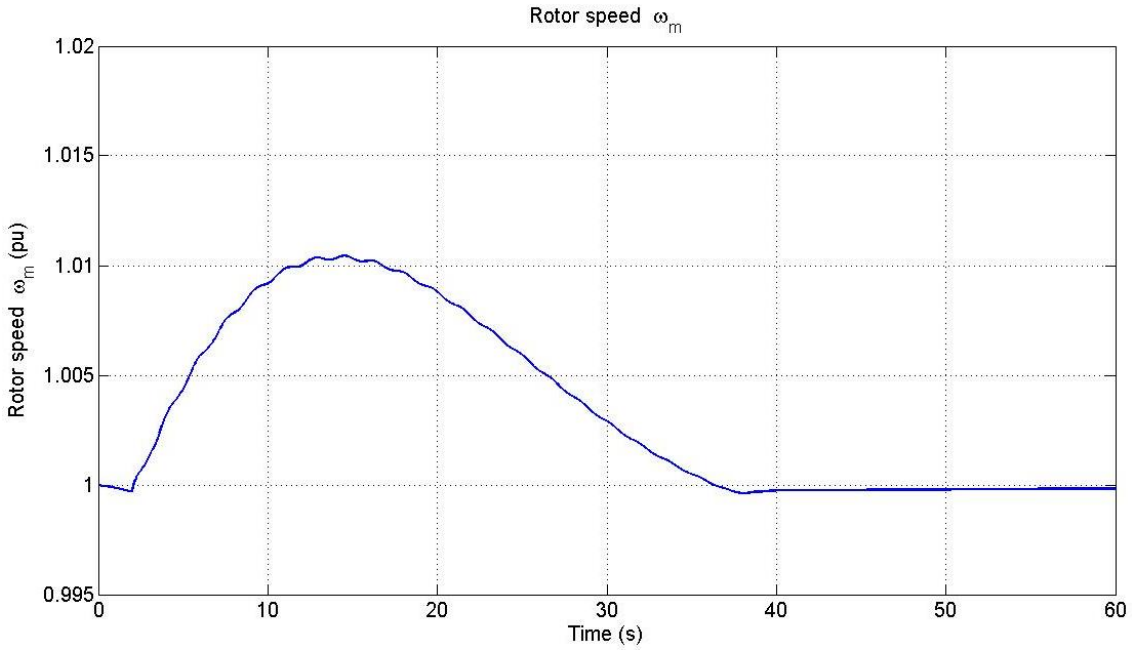

Figure 5. 17. Rotor speed when load is decreased (with BESS)

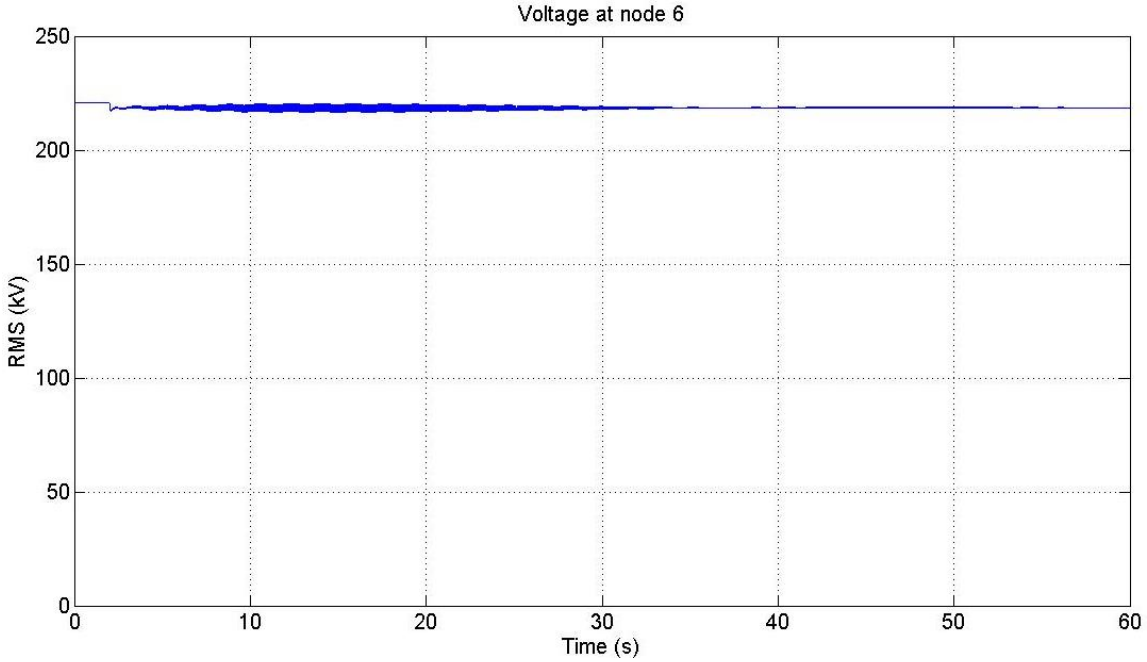

Figure 5. 18. Voltage at node 6 when load is decreased (no BESS)

With 22 MW BESS connected

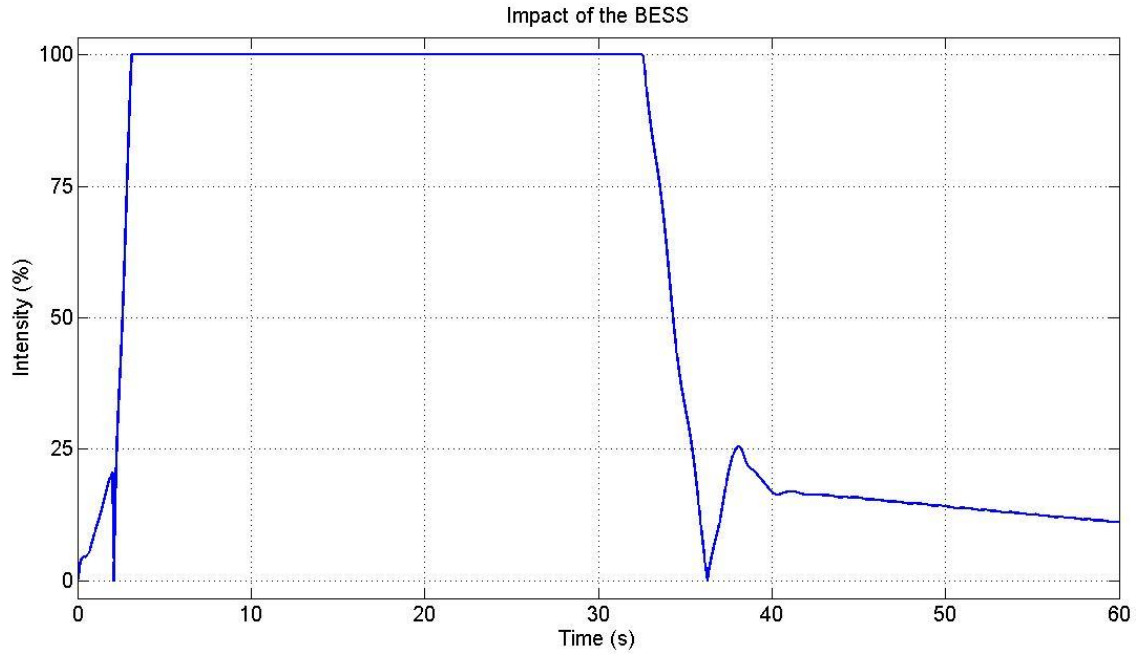

Figure 5. 19. Impact of the BESS when load is decreased

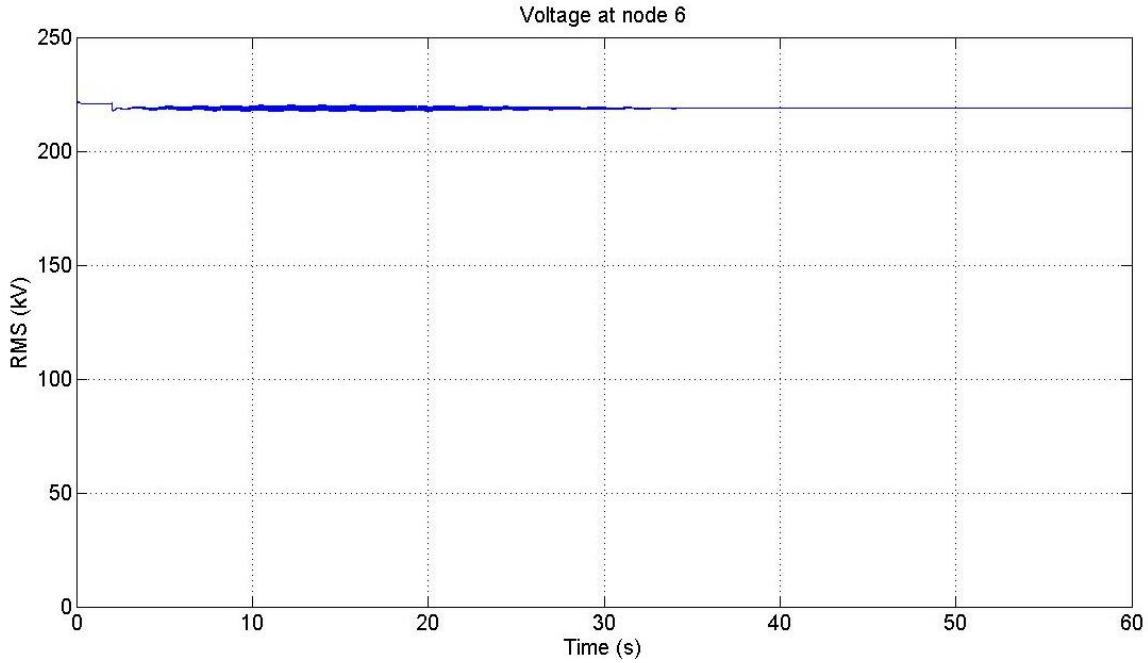

Figure 5. 20. Voltage at node 6 when load is decreased (with BESS)

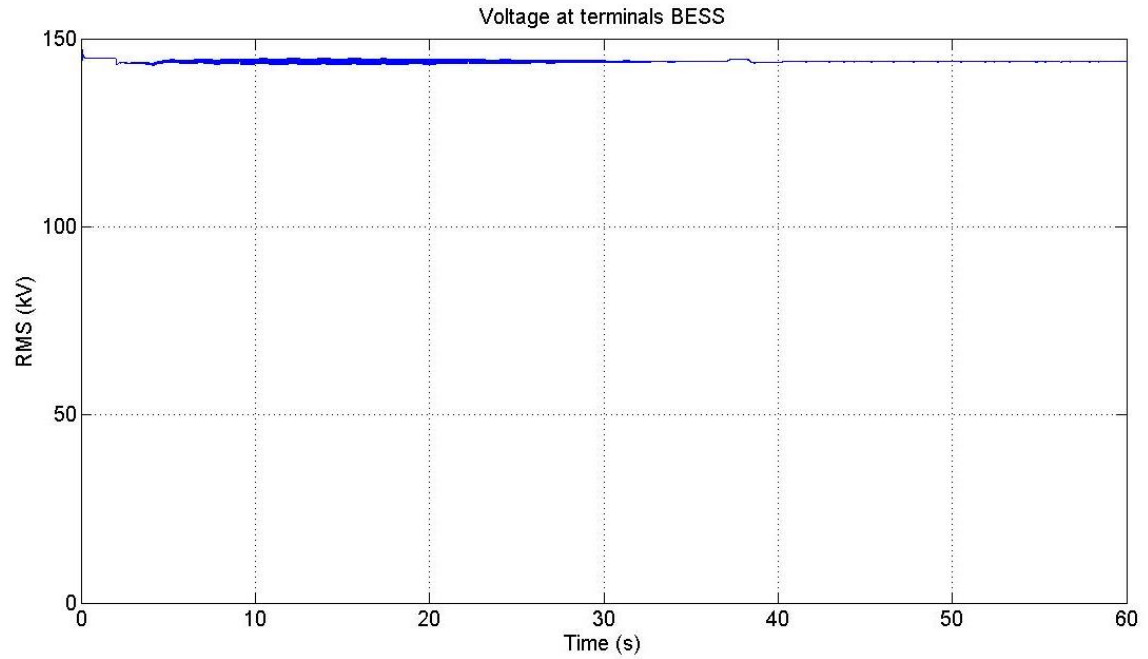

Figure 5. 21. Voltage at the BESS terminals when load is decreased

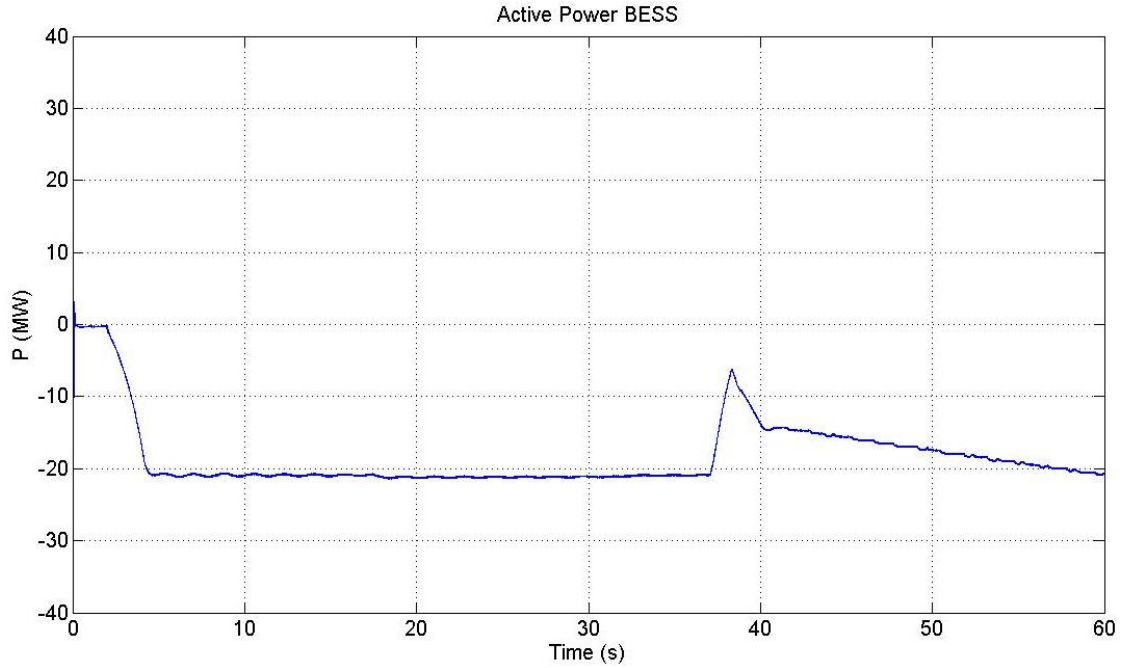

Figure 5. 22. Active power injected by the BESS when load is decreased

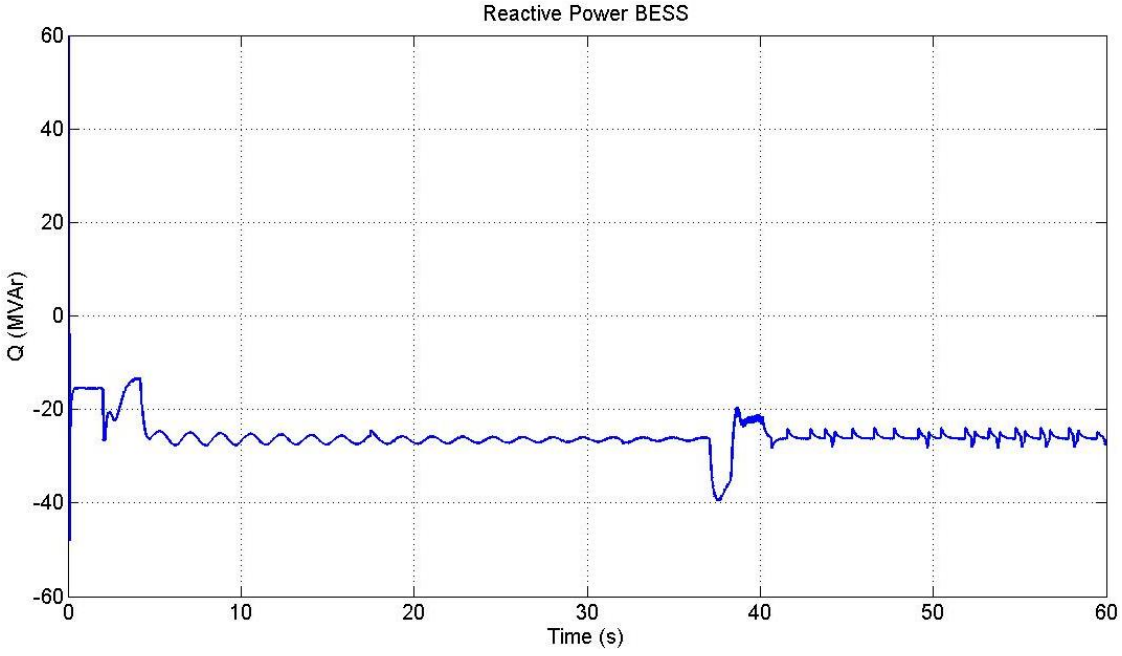

Figure 5. 23. Reactive power injected by the BESS when load is decreased

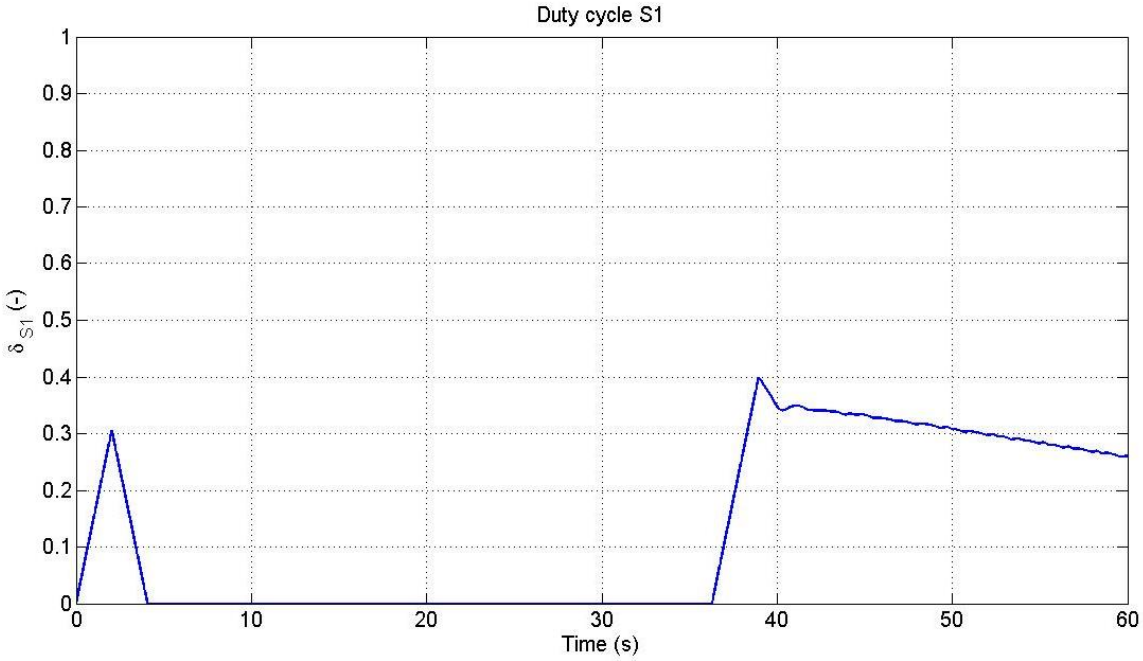

Figure 5. 24. Duty cycle of S_1 when load is decreased

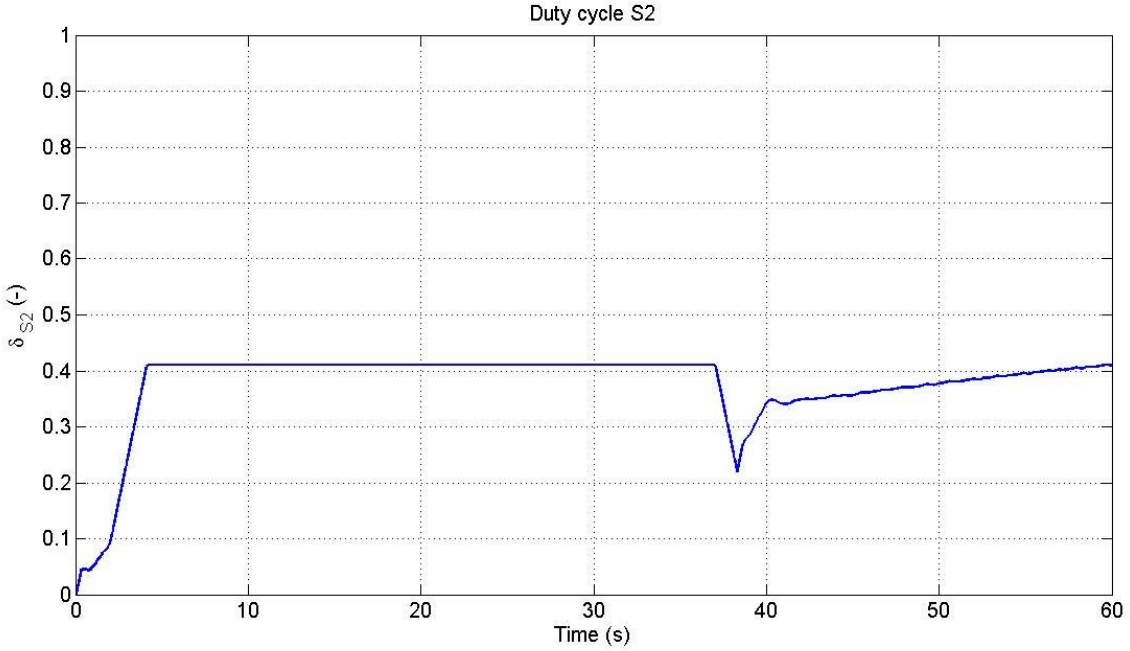

Figure 5. 25. Duty cycle of S_2 when load is decreased

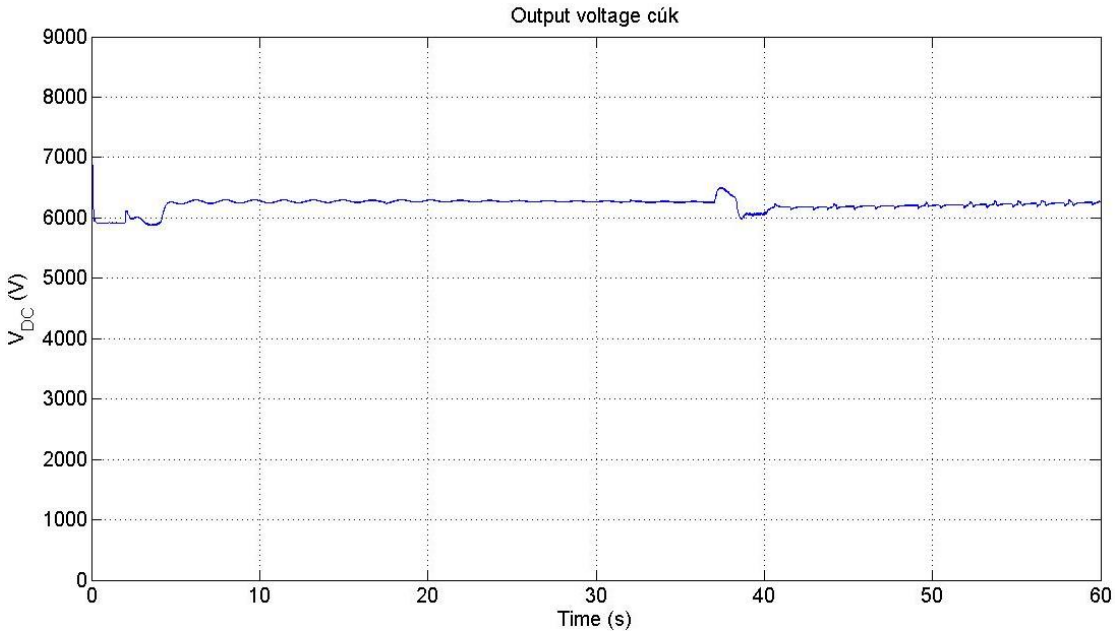

Figure 5. 26. Output voltage DC-DC converter when load is decreased

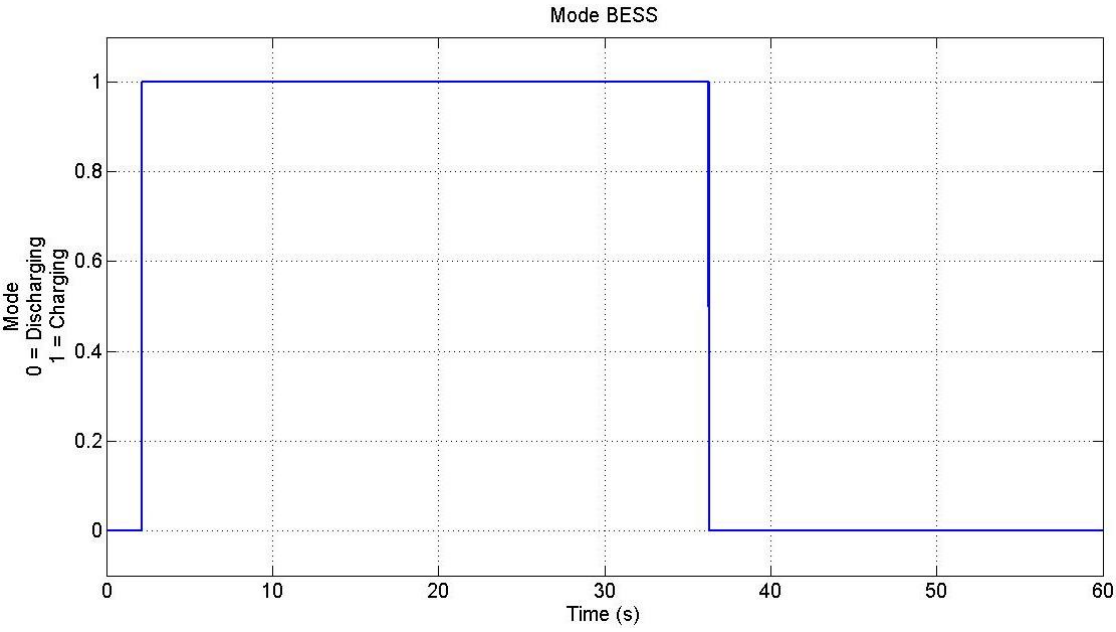

Figure 5. 27. Mode of the BESS when load is decreased

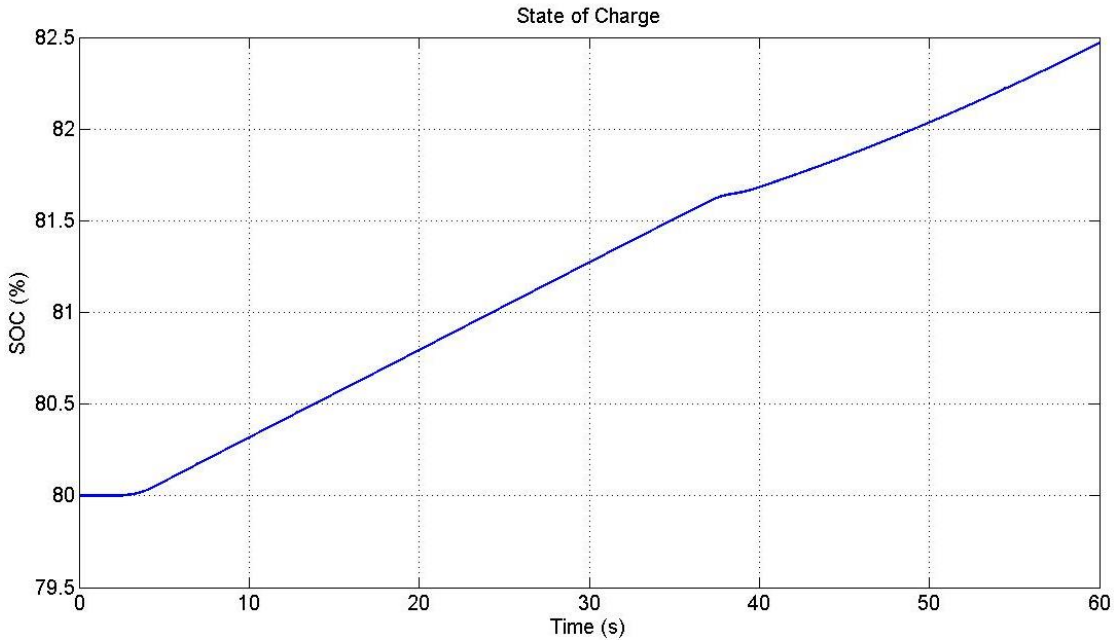

Figure 5. 28. State of Charge of the batteries when load is decreased

5.2 Active distribution system

The second application of BESS in this thesis deals with power flow control in an active distribution system [47]. The system is presented in *Figure 5. 29.* A BESS with a rated power of 5 MVA is connected at node 8. In the simulation, the infeed substation, referred to its 11-kV side, is represented by a three-phase voltage source rated at 11kV. The portion of the network between the utility in-feed point and PCC will be referred to as upstream network and the portion of the network between PCC and nodes 15, 16 and 17 will be referred to as downstream network.

The main goal of the exercise presented in this section is to explore the ability of the BESS to make the distribution system downstream the PCC to be self-sufficient, by relaying only in the active power injected by the windmills and in the energy storage and reactive power capabilities of the BESS.

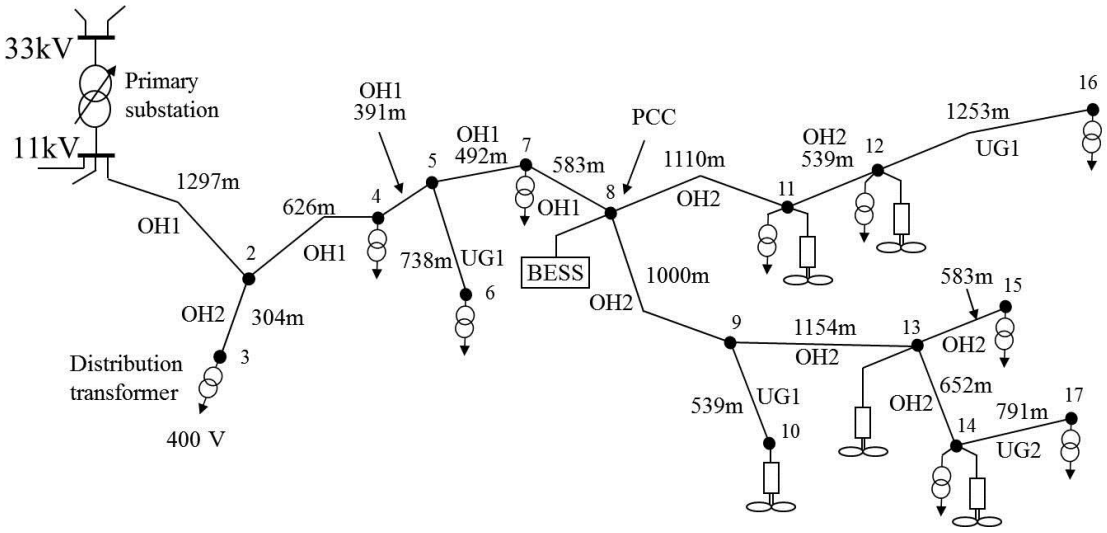

Figure 5. 29. Distribution system [47]

The different types of cables in this system are presented in *Table 5. 2.*

Table 5. 2. Parameters distribution lines [42]

Code	Type	R (Ω/km)	X (Ω/km)	Rating (A)
OH1	50 AAC	0.550	0.372	219
OH2	100 AAC	0.277	0.351	345
UG1	185 AL	0.164	0.085	255
UG2	95 AL	0.320	0.087	170

Five windmills, each of a rated capacity of 550 kW, are assumed connected, one per node, at nodes 10, 11, 12, 13 and 14. Because of the distance between windmills, the wind speed will not be the same at all the locations. A wind profile has been established

for turbine 1 for a period of 24 hours with wind speeds measurements assumed to have been taken every hour. This profile is shown in *Figure 5. 30*. Note that in this wind speed profile, the average wind speed during the night is approximately two times higher than during the day and that it drops to zero at around midday. The wind speed at other turbines sites has been taken to vary around the wind pattern established for turbine 1, according to information given in *Table 5. 3*.

Table 5. 3. Relative wind speeds at each turbine

Turbine	Variations with respect to turbine 1
Turbine 2	+5%
Turbine 3	+10%
Turbine 4	-5%
Turbine 5	-10%

The generators used to convert the mechanical power into electrical power are induction generators. The transformers, used to connect the generators to the system, have an impedance of 0.001+0.025j per unit on a 630 kVA base and a 11kV/ 575V base. The parameters of the induction generators are presented below:

Type	Squirrel-cage
Nominal power	S_{nom} = 650 MVA
Nominal output voltage	$V_{LL,nom}$ = 575 V
Frequency	60 Hz
Stator impedance (pu)	$\mathbf{Z}_{stator}$ = 0.004843 + 01248j
Rotor impedance (pu)	$\mathbf{Z}_{rotor}$ = 0.004377 + 0.1791j
Mutual inductance (pu)	L_m = 6.77
Inertia constant	H(s) = 5.04
Friction factor	F(pu) = 0.01
Pole pairs	p = 3

The loads for the system are given in *Table 5. 4.*

Table 5. 4. Loads in the distribution system

Bus	P (kW)	Q (kVAr)
3	238	71
4	159	48
6	340	102
7	178	53
11	458	137
12	221	66
14	97	29
15	386	116
16	161	48
17	64	19

Note that the torque profile (*Figure 5. 31*) and the power generation profile (*Figure 5. 32*) exhibit similar patterns to the wind speed profile; except that the turbine's cut in speed has taken to be 4.5 m/s, below which the turbine produces no torque and the electrical generator produces no power.

It is important to clarify that the actual simulation time associated with the electrical power profile shown in *Figure 5. 32*, is not a true 24 hours simulation time; with the simulation tool being used, this simulation task would be unyielding. Instead, since the wind speed is assumed to change only every hour, as a result of measurements taken every hour; two full minutes of simulation at the beginning of a torque change gives enough information to be able to extrapolate the simulation results with no error.

Two different experiments have been conducted; in the first one, the VSC is set to regulate voltage at PCC and in the second one the aim is to maintain not only active power flow exchange at near zero in branch 7-8 but also reactive power flow. The former case includes active power flow and voltage magnitude control whereas in the latter case it is for active and reactive power flow control.

5.2.1 Active power and voltage regulation mode

Active and reactive power and rotor speed of turbine 1

The injected active power (*Figure 5. 32*) is almost a scaled-up reflection of the rotor speed (*Figure 5. 33*). Every time the wind speed changes, a transient occurs in the rotor speed. As expected, the injected active power and the rotor speed are zero when the torque on the rotor drops to zero. On the other hand, it is observed that the generator keeps on consuming reactive power (*Figure 5. 32*) even though the turbine is not turning. This reactive power consumption is necessary to keep the induction generator in the

fluxed state and this is correctly picked up by the simulation. It is likely that disconnection of the induction generator during periods of low winds would not pose a risk to its operation and this would prevent the consumption of reactive power, a situation that would require some investigation.

Power through branch 7-8 and RMS voltage at PCC

The active and reactive power through the branch connecting the PCC with the upstream part of the distribution system (branch 7-8 in *Figure 5. 29*), are presented in *Figure 5. 34* and *Figure 5. 36* for cases with no BESS and with BESS, respectively. In the case with no BESS, the active and reactive power flow changes are quite large. At the peak of the available wind resource, the downstream system contributes about 1.25 MW to the upstream system. Conversely, when no wind resource is available, the downstream system draws about 1.4 MW. On the other hand, the downstream system always draws reactive power from the upstream system; at the time of maximum wind power generation, it draws 2.4 MVAr, and at the time of no wind power generation, its reactive power requirements decrease to 0.9 MVAr. These changes in active and reactive powers are reflected on the voltage (*Figure 5. 35*). It is observed that during the day-hours there is less local energy available and the voltage at PCC is at its lowest, i.e. 10.53 kV. At night there is more wind resource available and sufficient power is generated to fulfil the local demand and to export the remaining generated power to the upstream network, hence, the downstream network, as seen from PCC, turns into an "unloaded network". The overall effect is that the voltage raises to about 10.82 kV. When the variations in wind speed are small, the RMS voltage is quite stable.

When the BESS is assumed to be connected at PCC, the active power flow at branch 7-8 in *Figure 5. 29*, is very close to zero, as shown in *Figure 5. 36*. The reason is that the active power injected by the BESS (*Figure 5. 37*) follows a similar pattern to the active power flow in *Figure 5. 34*, thus performing the roll of an excellent active power balancer. The reactive power deviates from zero since the VSC is set to control the voltage at PCC and not the reactive power injection - these are mutually exclusive control actions. As shown in *Figure 5.37*, the BESS produces between 2.2 and 2 MVAr and, hence, some reactive power is exported to the upstream network for most of the time but this is accentuated during the day-time when up to 1 MVAr flows upstream branch 7-8. Owing to the much smaller changes in active and reactive power due to the BESS, the voltage at PCC remains much more stable and closer to the reference voltage value of 11kV.

Duty cycles and output voltage in the cúk converter

The duty cycles of the two switches (*Figure 5. 39* and *Figure 5. 40*) are strongly related to the active power flow between the BESS and the distribution system. The duty cycle of switch S_1 rises above 0.5 at the moment the injected active power changes direction, at around 7 and 8 hours. It tends to decrease below 0.5 when the injected active power

again changes direction. The duty cycle of switch S_2 is an inverted scaled-down reflection of the active power injected by the BESS, with maximum and minimum values of 0.25 and 0.075, respectively.

The output voltage of the DC-DC converter remains very stable. The little fluctuations observed in *Figure 5. 41*, are related to reactive power injections. When the injected reactive power goes down, the DC voltage follows suit.

Power flow turbine 1, wind speed, torque and rotor speed

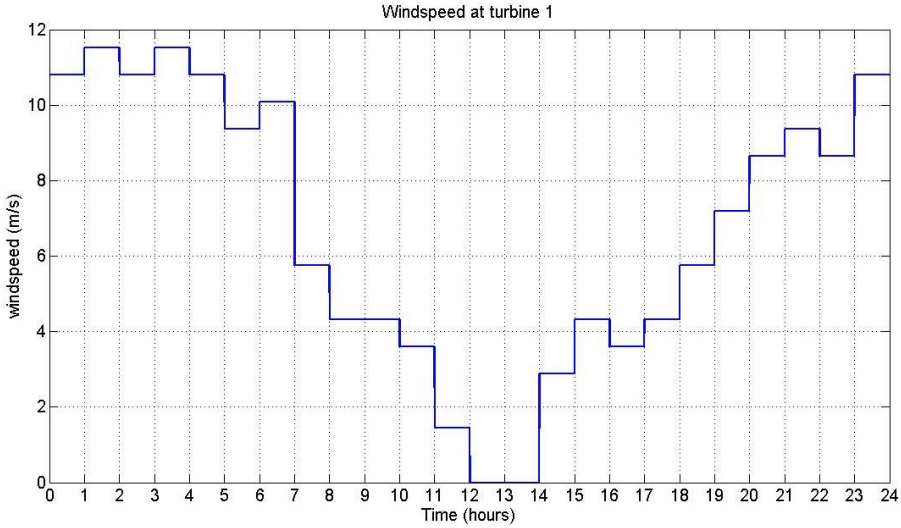

Figure 5. 30. Windspeed at turbine 1

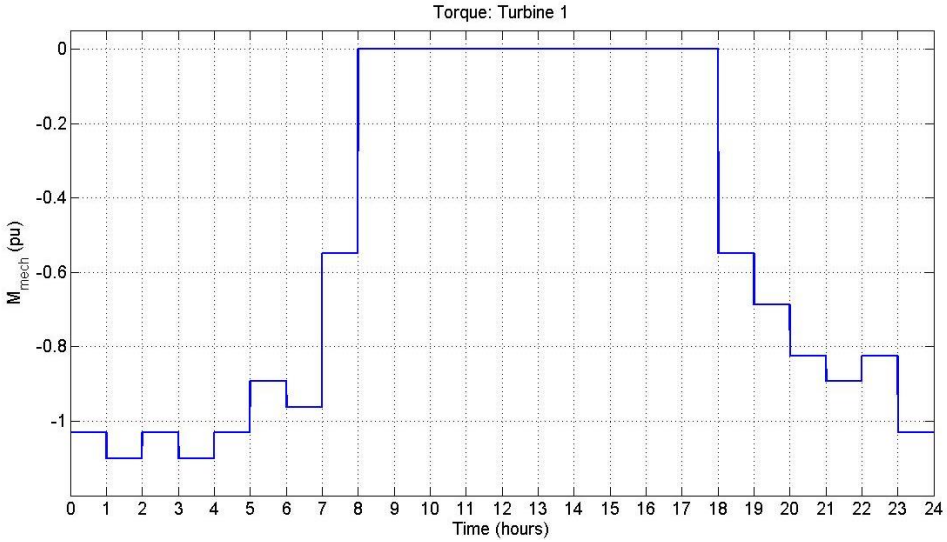

Figure 5. 31. Torque on the rotor of turbine 1

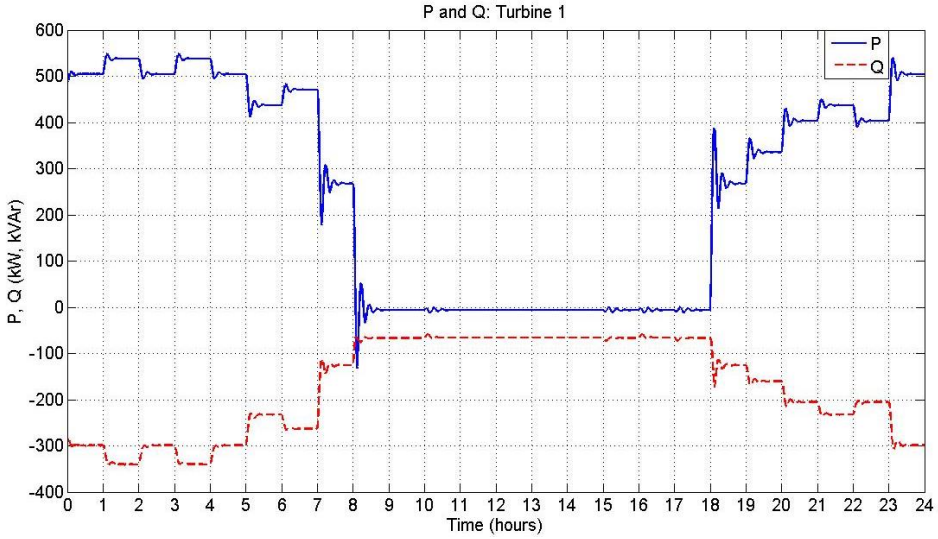

Figure 5. 32. Active and reactive power injected by turbine 1

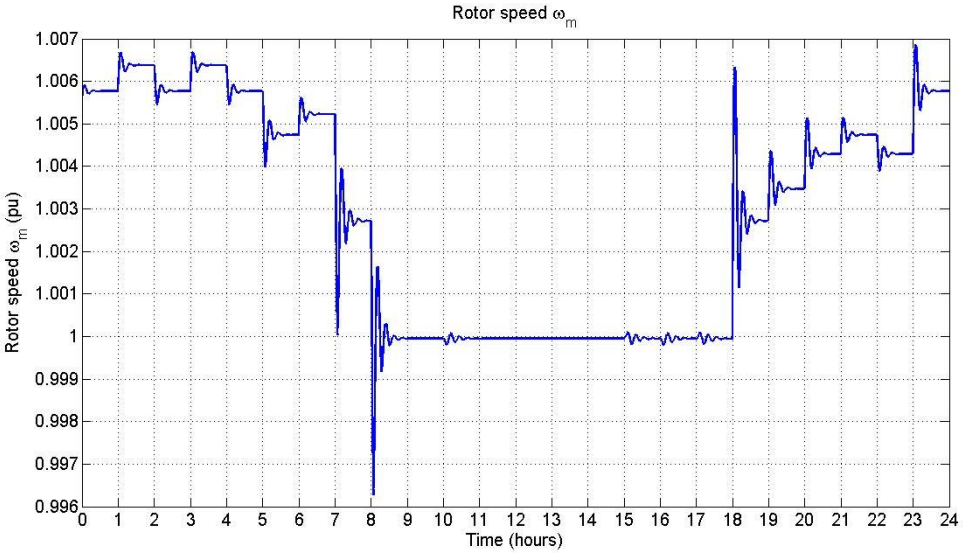

Figure 5. 33. Rotor speed of turbine 1 in p.u.

No BESS

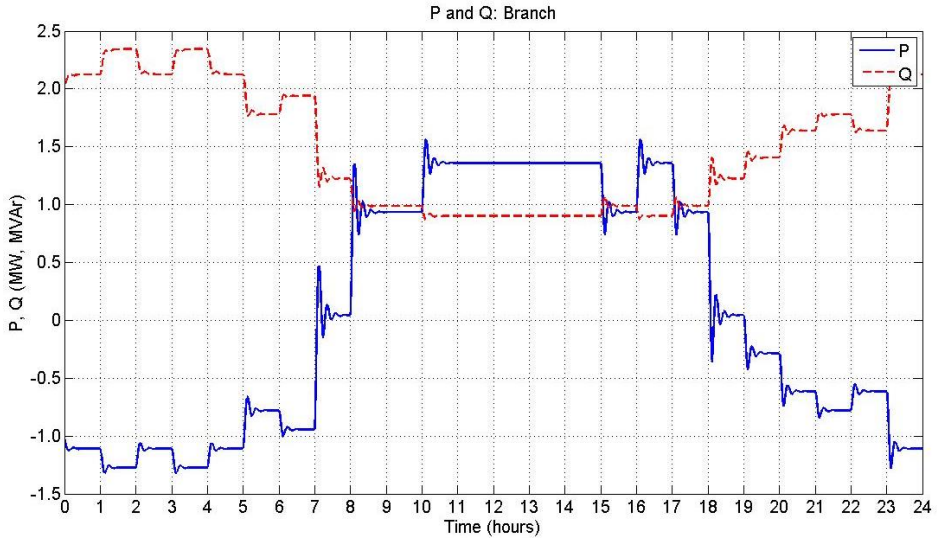

Figure 5. 34. Active and reactive power through branch at PCC (no BESS)

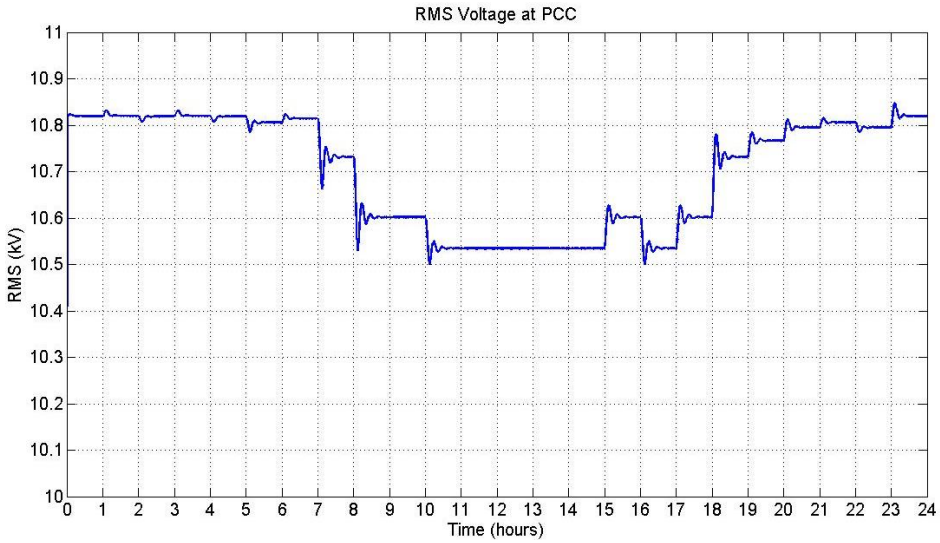

Figure 5. 35. RMS Voltage at PCC (no BESS)

With BESS

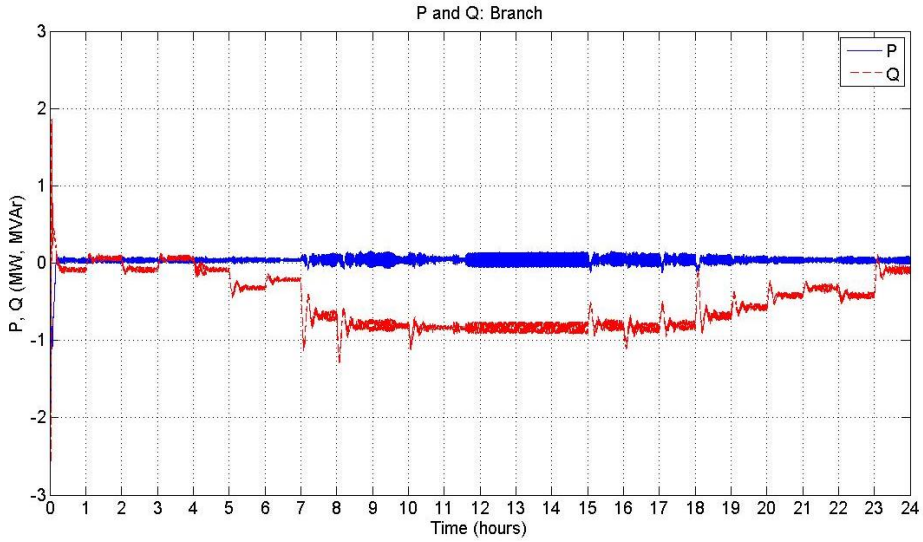

Figure 5. 36. Active and reactive power through branch at PCC (with BESS)

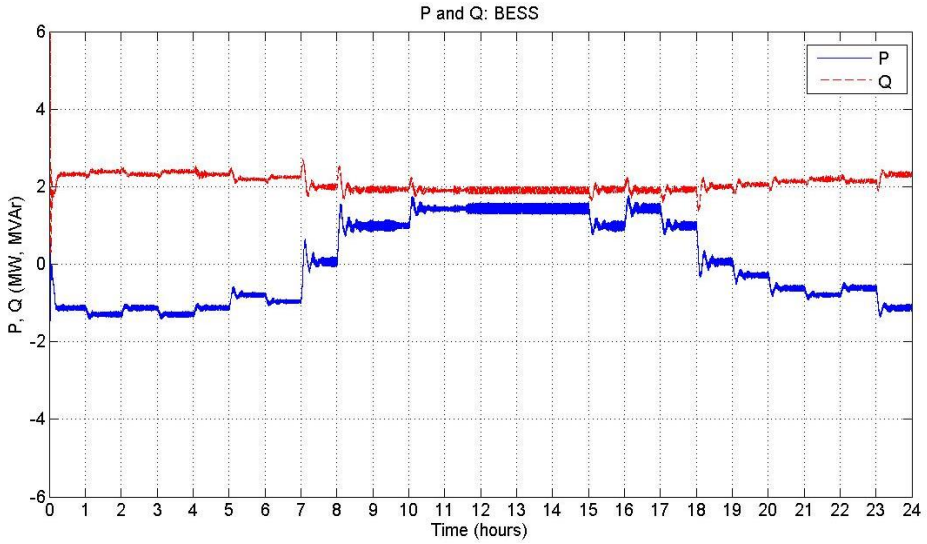

Figure 5. 37. Active and reactive power injected by the BESS

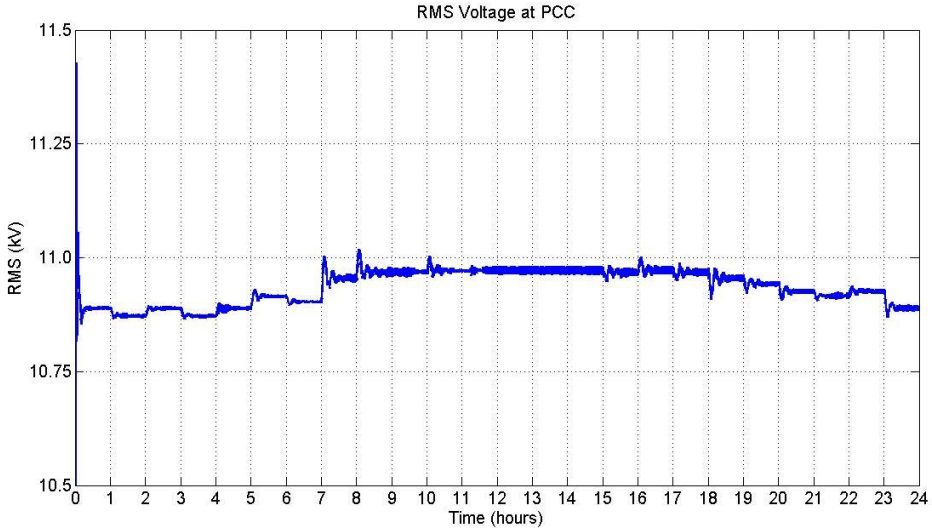

Figure 5. 38. RMS Voltage at PCC (with BESS)

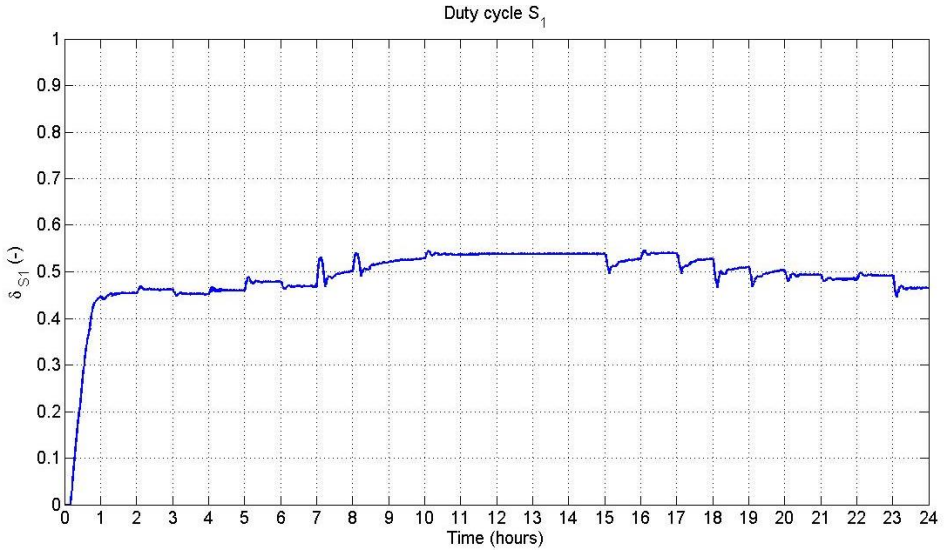

Figure 5. 39. Duty cycle of switch S_1

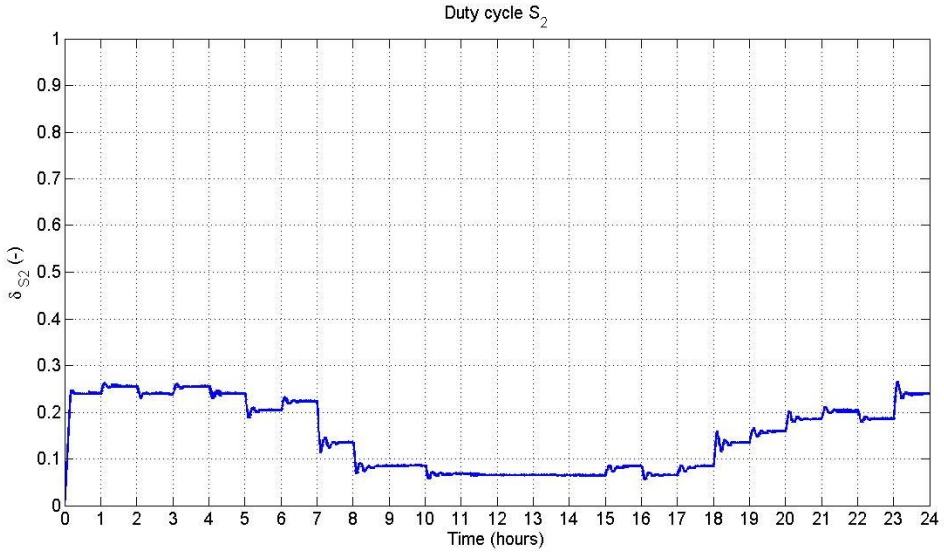

Figure 5. 40. Duty cycle of switch S_2

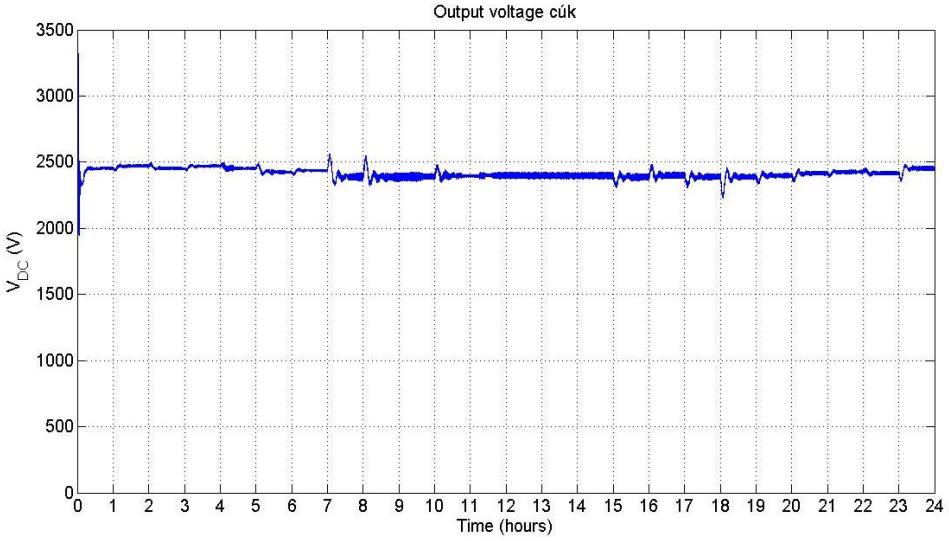

Figure 5. 41. Output voltage DC-DC converter

5.2.2 Active and reactive power regulation mode

The simulations in this case only covers a time lapse of 15 hours, from midnight until 3 pm since the wind profile from noon to midnight is largely a mirroring situation of the profile from midnight to noon. Hence, in these simulations only the first 15 hours are presented. Information of wind profile, torque and turbines is presented in section 5.2.1.

Power flow through branch 7-8 and RMS voltage at PCC

The VSC controls the reactive power flow through the branch at near-zero values, as observed in *Figure 5. 42*. The cúk converter also controls active power flow through this branch very well but it should be observed from this figure that some spikes do occur, noticeably around the 7^{th} hour. This is a point in time when the wind speed drops drastically and some overshoots in the response of the BESS, shown in *Figure 5. 43*, cause a peak in the active power flow, particularly at the 7^{th} hour. This peak alerts us to the critical importance of keeping the downstream part of the grid tied to the upstream part of the network. In case of large changes in the wind, it helps to stabilise the voltage in the downstream network. It should be stated that operation of the downstream network in islanding mode would not be possible as it is. It would necessitate the installation of energy dissipating resistors and a mechanism for load shedding for the islanding mode to be possible.

The output voltage, shown in *Figure 5. 44*, remains even flatter than in the case of the voltage regulation (*Figure 5. 38*). The reason for this is the reactive power flow control which is very effective. Except for the peak at the 7^{th} hour, the BESS is able to annihilate the varying influence of the wind speed on the voltage profile at PCC.

Output voltage in the cúk converter

The output voltage of the cúk converter follows a similar behaviour to the case, presented in *Figure 5. 41* for the case of reactive power injected by the BESS. When the injected reactive power drops, the DC voltage follows suit, particularly around the 7^{th} hour.

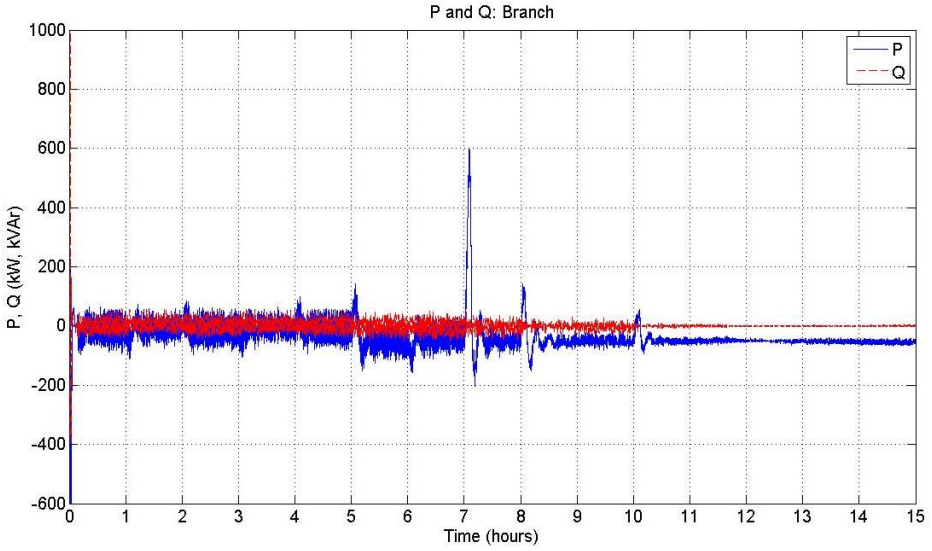

Figure 5. 42. Active and reactive power through branch at PCC (with BESS)

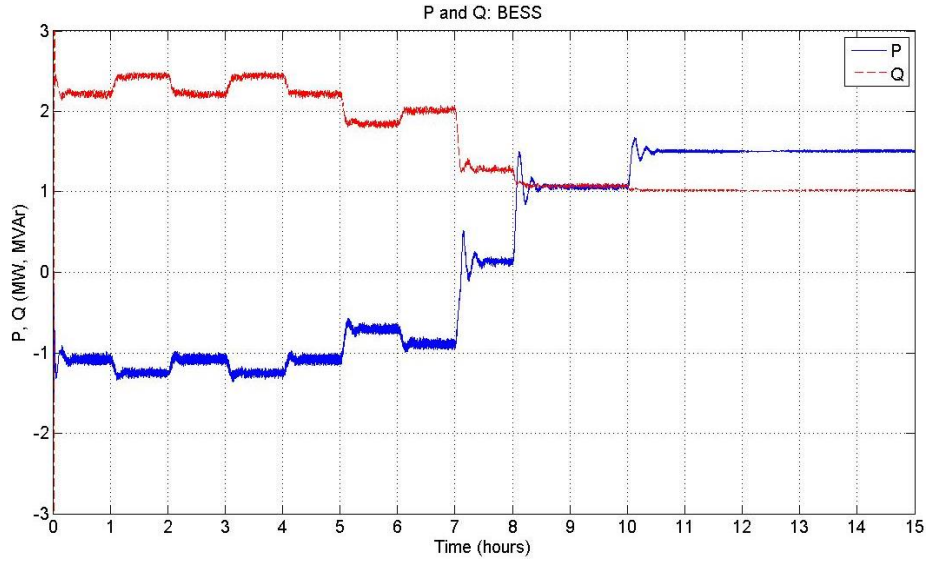

Figure 5. 43. Active and reactive power injected by the BESS

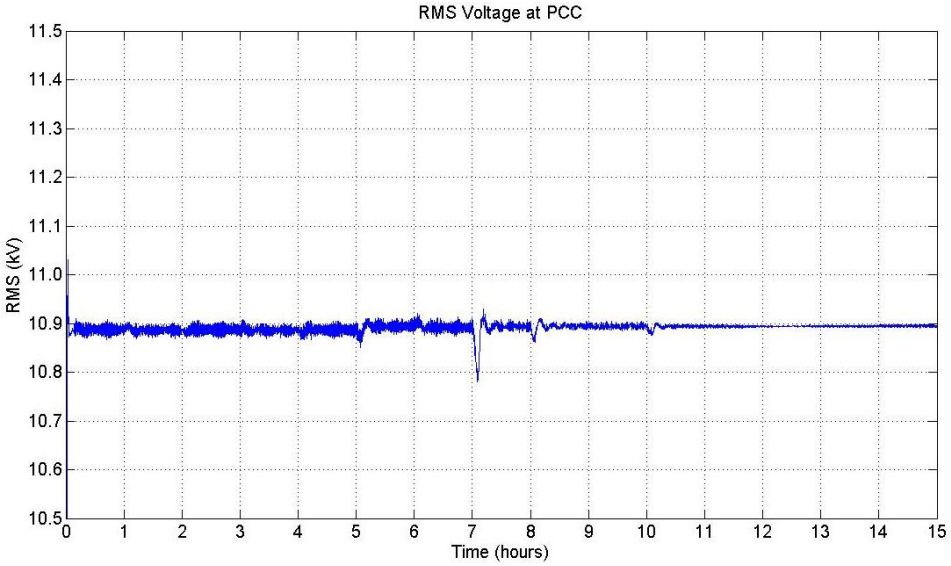

Figure 5. 44. RMS Voltage at PCC (with BESS)

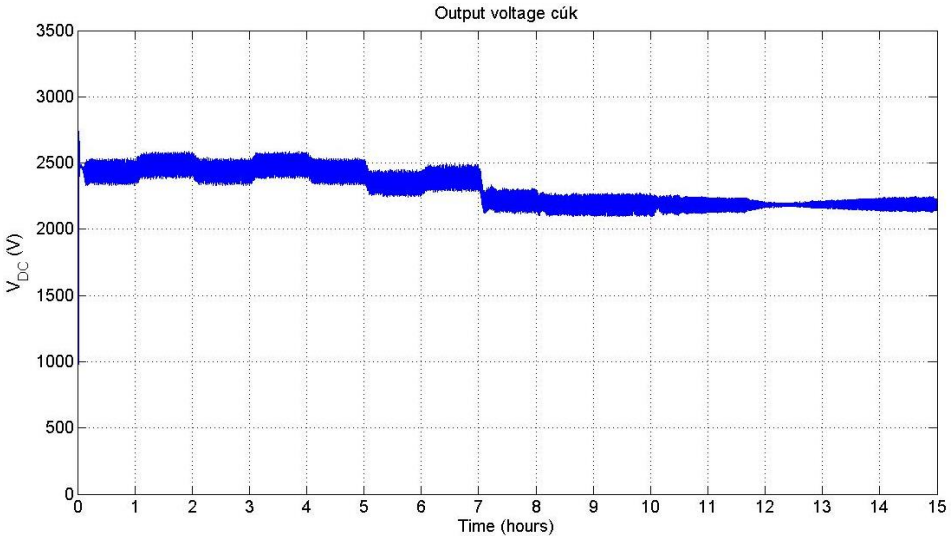

Figure 5. 45. Output voltage DC-DC converter

5.3 The use of MATLAB/Simulink (and its limitations)

Simulink is a popular tool for simulations and it is widely known in academic circles and industry. The library of Simulink provides for a wide range of applications (hydraulics, electrical systems, electronics, control systems, fuzzy logic, aerospace, power system, etc.). Simulink is a user-friendly tool since it shows clearly the representation of the models and how the different elements in a simulation interact with each other. It includes a large number of solution methods for applications, speed and accuracy. However, Simulink is not suitable for every single application. A case in point is the study of large scale power systems, for which Simulink becomes inefficient. The calculation times tend to become prohibitively expensive when the simulation system expands. When the sample time is increased to reduce the simulation time, numerical instabilities have been experienced. For a simulation time of 24 hours for the distribution system, for example, it would have taken six months to complete the full simulation with time steps of 1μs (assuming that the calculation time increases linearly with the simulation time and taking into account that it took 190s to calculate 1s of simulation time). It is likely that more advance integration methods are available in an industry-version of Simulink or that more sophisticated integration methods may become available in academic versions.

6 SUMMARY

This chapter summarizes the major objectives and the results of this thesis. It also puts forward recommendations for future research on this topic.

6.1 Final conclusions

The main objective of this thesis was to investigate the impact of a BESS in a wide range of credible operational situations. The BESS controllers can be set to either support the system frequency or to regulate the active power flow at a key branch of the network. The impact of the frequency support mode is tested in a high voltage transmission system designed by Prahba Kundur [46]. The results show significant improvements in frequency stability which are strongly linked to the size of BESS. Although 80 MW BESS are not currently installed anywhere, this has been tested, purely for theoretical reasons. The result shows a rather small frequency deviation and an almost perfect damping of frequency oscillations.
A second control mode of the BESS controls active power flow through a branch. This control mode has been tested in a modified 11kV distribution system [47]. In this case study, five windmills were distributed across the 11kV-distribution system and the impact of a BESS, installed at the PCC, has been assessed. The objective in this application was to keep the power flow through the branch as low and constant as possible in order to make the sub-grid self-reliant in terms of active power. The major goal of the VSC is to support the voltage at the PCC, and therefore, the reactive power flow in branch 7-8 is not zero. The active power flow, on the other hand, shows a significant improvement. Where the active power flow changes direction (from about -1.25 up to about 1.40 MW) when no BESS is installed, the BESS manages to keep the power flow very close to zero at every point in time of the simulation.

6.2 Recommendations for future work

No attempts have been made to optimize the controller of the BESS in this research, other than improved responses carried out through experimentation. It is expected that adjusting the control parameters in an optimal or semi-optimal manner would result in even better results, such as minimizing the active power flow peaks shown in *Figure 5. 9*. When optimizing the BESS size and design, it would be necessary to implement energy dissipating resistors and a mechanism for load shedding, in order to permit the downstream network to operate in an islanding mode.

A second possible improvement of the BESS in the case study of the high voltage transmission system of Prahba Kundur, would be the implementation of small, distributed storage systems instead of the one large storage system. It is noticed that the active power flow of the BESS does not drop to zero after reaching the steady state. A possible improvement in the model would be the implementation of a secondary frequency regulation of the generators which would reduce the impact of the BESS after reaching the steady state.

Concerning the active distribution system, the simulation results could be made more realistic by using a load profile instead of a constant load and by switching of the turbines when the wind speed goes below or above the cut-in or cut-off speeds, respectively.

At the level of the individual elements of the BESS, the switching-based converter models are a realistic representation but the multi-level VSC model using GTO valves should be replaced by a modular multi-level VSC model using IGBT valves. The battery model should incorporate its temperature dependency and functions to take account of battery ageing and other environmental factors such as extreme weather conditions.

7 REFERENCES

[1] A. Ter-Gazarian, *Energy Storage for Power Systems, 2nd Edition.* Institution of Engineering and Technology, 2011.

[2] F. A. Farret and G. Simões, *Integration of Alternative Sources of Energy*. Wiley, 2006.

[3] A. Chakraborty, S. K. Musunuri, A. K. Srivastava and A. K. Kondabathini, "Integrating STATCOM and Battery Energy Storage System for Power System Transient Stability: A Review and Application," *Advances in Power Electronics*, vol. 2012, pp. 12, 2012.

[4] M. Yoshio, R. J. Brodd and A. Kozawa, *Lithium-Ion Batteries: Science and Technologies.* Springer-Verlag New York, 2009.

[5] (May 8, 2013). *Battery Statistics*. Available: http://batteryuniversity.com/learn/article/battery_statistics.

[6] D. Kottick, M. Blau and D. Edelstein, "Battery energy storage for frequency regulation in an island power system," *Energy Conversion, IEEE Transactions On*, vol. 8, pp. 455-459, 1993.

[7] (May 6, 2013). *AES Combines Advanced Battery-Based Energy Storage with a Traditional Power Plant*. Available: http://www.aesenergystorage.com/news/aes-combines-advanced-battery-based-energy-storage-traditional-power-plant.html.

[8] N. W. Miller, R. S. Zrebiec, G. Hunt and R. W. Deimerico, "Design and commissioning of a 5 MVA, 2.5 MWh battery energy storage system," in *Transmission and Distribution Conference, 1996. Proceedings., 1996 IEEE*, 1996, pp. 339-345.

[9] (June, 3, 2013). *PG&E Operating Second Energy Storage System With NGK Batteries - Bloomberg*. Available: http://www.bloomberg.com/news/2013-05-23/pg-e-operating-second-energy-storage-system-with-ngk-batteries.html.

[10] O. Tremblay, "Experimental Validation of a Battery Dynamic Model for EV Applications," vol. 36, 9, 2009.

[11] C. R. Gould, C. M. Bingham, D. A. Stone and P. Bentley, "New Battery Model and State-of-Health Determination Through Subspace Parameter Estimation and State-Observer Techniques," *Vehicular Technology, IEEE Transactions On*, vol. 58, pp. 3905-3916, 2009.

[12] S. X. Chen, K. J. Tseng and S. S. Choi, "Modeling of lithium-ion battery for energy storage system simulation," in *Power and Energy Engineering Conference, 2009. APPEEC 2009. Asia-Pacific*, 2009, pp. 1-4.

[13] B. Sørensen. "Chapter 33: Battery storage," in *Renewable Energy Conversion, Transmission and Storage*, B. Sørensen, Ed. 2007, .

[14] L. Gauchía Babé, "Nonlinear dynamic per-unit models for electrochemical energy systems : application to a hardware-in-the-loop hybrid simulation," PhD thesis, Universidad Carlos III de Madrid, Madrid, Spain, 2009.

[15] H. A. Kiehne, "Electrochemical energy storage," in *Battery Technology Handbook*, D. Berndt, Ed. CRC Press, 2003, .

[16] D. Linden and T. B. Reddy, "Chapter 2 - electrochemical principles and reactions," in *Handbook of Batteries*, J. Broadhead and H. C. Kuo, Eds. New York: McGraw-Hill, 2002, .

[17] D. Linden and T. B. Reddy, "Chapter 23 - lead-acid batteries," in *Handbook of Batteries*, A. J. Salkind, A. G. Cannone and F. A. Trumbure, Eds. New York: McGraw-Hill, 2002, .

[18] D. Linden and T. B. Reddy, "Chapter 8- zink-carbon batteries," in *Handbook of Batteries*, D. W. McComsey, Ed. New York: McGraw-Hill, 2002, .

[19] H. J. Bergveld, W. S. Kruijt and P. H. L. Notten, "Chapter 3 - A state-of-charge indication algorithm," in *Battery Management Systems: Design by Modelling*, H. J. Bergveld, W. S. Kruijt and P. H. L. Notten, Eds. Springer, 2002, pp. 47-52.

[20] R. Huggins, *Advanced Batteries: Materials Science Aspects.* Springer London, Limited, 2009.

[21] G. E. Products, "Charging," in *Rechargeable Batteries Applications Handbook*, G. E. Products, Ed. Elsevier Science, 1998, pp. 178-201.

[22] G. E. Products, "Discharge characteristics," in *Rechargeable Batteries Applications Handbook*, G. E. Products, Ed. Elsevier Science, 1998, pp. 157-177.

[23] K. Bao, "Battery charge and discharge control for energy management in EDV and utility integration," MSc thesis, University of Alabama, Tuscaloosa, USA, 2012.

[24] R. A. Huggins, *Energy Storage.* Springer, 2010.

[25] G. Pistoia, "Electric and Hybrid Vehicles - Power Sources, Models, Sustainability, Infrastructure and the Market," pp. 217-218, 2010.

[26] H. A. Kiehne, "Lithium batteries," in *Battery Technology Handbook*, W. Jacobi, Ed. CRC Press, 2003, .

[27] K. E. Aifantis, S. A. Hackney and R. V. Kumar, *High Energy Density Lithium Batteries.* Wiley, 2010.

[28] D. F. Warne, "Newnes Electrical Power Engineer's Handbook (2nd Edition)," 2005.

[29] K. Ozawa, *Lithium Ion Rechargeable Batteries.* Wiley, 2009.

[30] D. Linden and T. B. Reddy, "Chapter 35 - lithium-ion batteries," in *Handbook of Batteries*, G. M. Ehrlich, Ed. New York: McGraw-Hill, 2002, .

[31] N. Mohan and T. M. Undeland, *Power Electronics: Converters, Applications, and Design.* Wiley India Pvt. Limited, 2007.

[32] R. W. Erickson and D. Maksimovic, *Fundamentals of Power Electronics.* Springer, 2001.

[33] W. Shepherd, L. Zhang and L. Z. Crowther, *Power Converter Circuits.* Marcel Dekker Incorporated, 2004.

[34] F. L. Luo, H. Ye and M. Rashid, "Chapter 5 - digitally controlled AC/DC rectifiers," in *Digital Power Electronics and Applications*, F. L. Luo, H. Ye and M. Rashid, Eds. San Diego: Academic Press, 2005, pp. 142-161.

[35] B. Wu, *High-Power Converters and AC Drives.* Wiley, 2006.

[36] M. K. Kazimierczuk, *Pulse-Width Modulated DC-DC Power Converters.* Wiley, 2008.

[37] D. Czarkowski, "Chapter 13 - DC-DC converters," in *Power Electronics Handbook (Second Edition)*, M. Rashid, Ed. Burlington: Academic Press, 2007, pp. 245-259.

[38] S. S. Ang and A. Oliva, *Power Switching Converters.* Taylor & Francis Group, 2005.

[39] K. C. Wu, *Switch-Mode Power Converters: Design and Analysis.* Elsevier Science, 2005.

[40] N. G. Hingorani and L. Gyugyi, *Understanding FACTS: Concepts and Technology of Flexible AC Transmission Systems.* Wiley, 2000.

[41] A. K. Sahoo, K. Murugesan and T. Thygarajan, "Modeling and simulation of 48-pulse VSC based STATCOM using simulink's power system blockset," in *Power Electronics, 2006. IICPE 2006. India International Conference On*, 2006, pp. 303-308.

[42] V. K. Sood, *HVDC and FACTS Controllers: Applications of Static Converters in Power Systems.* Springer, 2004.

[43] H. Saadat, *Power System Analysis.* PSA Publishing, 2010.

[44] J. Machowski, J. Bialek and J. Bumby, *Power System Dynamics: Stability and Control.* Wiley, 2011.

[45] A. J. Wood and B. F. Wollenberg, *Power Generation, Operation, and Control.* Wiley, 2012.

[46] P. Kundur, N. J. Balu and M. G. Lauby, *Power System Stability and Control.* New York; Montréal: McGraw-Hill, 1994.

[47] L. Freris and D. Infield, *Renewable Energy in Power Systems.* Wiley, 2008.